SCUOLA INTERNAZIONALE SUPERIORE DI STUDI AVANZATI

DOCTORAL THESIS

Ring Polymers in Entangled Solutions: Complex Structure and Heterogeneous Dynamics

---

Author	*Supervisor*
Negar Nahali	Dr. Angelo Rosa

October 12, 2017

ABSTRACT

Understanding how topological constraints affect the structure and dynamics of polymers in solution is a historical challenge in polymer physics: in particular, it still represents the goal of all modern studies aiming at understanding the behavior of concentrated solutions of ring polymers. Ring polymers represent in fact some of the most puzzling objects in polymer physics: at odds with their linear counterparts they do not swell assuming ideal conformations, but they fold into compact, space-filling conformations. At the same time though, rings maintain a considerable degree of mutual interpenetration in the form of "threading", which is at the basis of their surprisingly rich mechanical and rheological behavior.

In this Thesis, I investigate general and universal properties of ring polymers emerging in concentrated solutions. Notably, I discuss the scaling behavior of structural and dynamical quantities of single rings being surrounded by neighboring polymers exerting volume interactions on each other. Then, I consider important connection between "threadings" in close-by rings and their consequent slowing down. For the systems under analysis, I employ extensive Molecular Dynamics computer simulations in order to provide a detailed description concerning the equilibrium and dynamical properties of ring polymers in solutions of different densities. For systematic comparison, we also discuss the same properties for their linear counterparts.

Contents

List of Tables

List of Figures

ACKNOWLEDGEMENTS

Firstly, I would like to express my sincere gratitude to my advisor, Dr. Angelo Rosa for his continuous support during my PhD and for his limitless patience. I am deeply indebted to all his help. Thanks a lot for all these four years.
I am very grateful to Giuseppe D'Adamo. Giuseppe thanks for all your help, all the time you generously gave to me. Thank you for being such a wonderful polymer physicist and office-mate!
My time in Trieste would have not been an amazing experience without all amazing people that I met and I am thankful.
Eli, it was worth ending up in Trieste only if it was about to meet you. I am immensely grateful for your sister-ship!
Abraham, whom I still don't believe how strange our friendship started and how unconditional it was.
Kevin, Tiago, Simon, thanks for your great company. "all you can eat" Saturdays will be missed so much.
Ana Maria and Andrea, the fruit-breaks are missing girls.
Trieste, thanks for making me who I am now and for all the Capo in B's.
Italy, I never felt homesick in you!
And finally to Masoud, to your truly endless love.

Motivation

Systems observed in soft matter physics are challenging due to their intrinsic many-body nature, the presence of interactions affecting length- and time-scales over several orders of magnitude, possible existence of metastable states, long relaxation times [9] and their intrinsically complex geometry and topology [10]. In particular, materials whose properties are ruled by topology (like, biomaterials, polymers and biopolymers, sediments and emulsions) have received considerable attention recently [10].

Although apparently simple, a notable category of non-trivial systems in which topology plays a crucial role for the structure and dynamics of its single constituents are semi-dilute or concentrated solutions (melt) of unknotted and unconcatenated circular (ring) polymers. As a matter of fact, these systems represent one of the most debated topics in Polymer Physics [11].

Ring polymers differ from their linear counterparts [2, 12] in many respects:

(a) In concentrated solutions, linear polymers behave as (quasi) ideal owing to the "almost" exact compensation of excluded volume effects [2]. On the contrary, ring polymers tend to fold into crumpled, "lattice animal"-like (Fig. 1(b)) conformations which display considerable amount of *threading* events between close-by chains.

(b) Ring polymers lack free ends and, consequently, they do not relax by "standard" reptation-like [2, 12] mechanisms, which are typical of linear chains (Fig. 1(a)).

(c) Recent experiments conducted with highly-purified ring samples have demonstrated that rings do not exhibit apparent rubbery plateaus as in linear polymer solutions, but represent power-law decay of the stress relaxation function (Fig. 1(c)). These results indicate that rings adopt completely different chain relaxation mechanisms from linear polymers.

Aside from their intrinsic experimental as well as theoretical importance, ring polymers play a prominent role as well in biology. In particular, there are the two cases of: (1) the single circular DNA filament which constitutes the chromosome of certain species of bacteria (like, E.coli) [100, 101] and (2) the crumpled conformations of chromosomes inside the nuclei of eukaryotic cells closely resembling compact configurations of ring polymers in melt [102, 23, 16](Fig. 1(d)).

In spite of their indisputable theoretical and practical importance, many aspects of the physics of ring polymers still remain puzzling and largely unexplored. The main

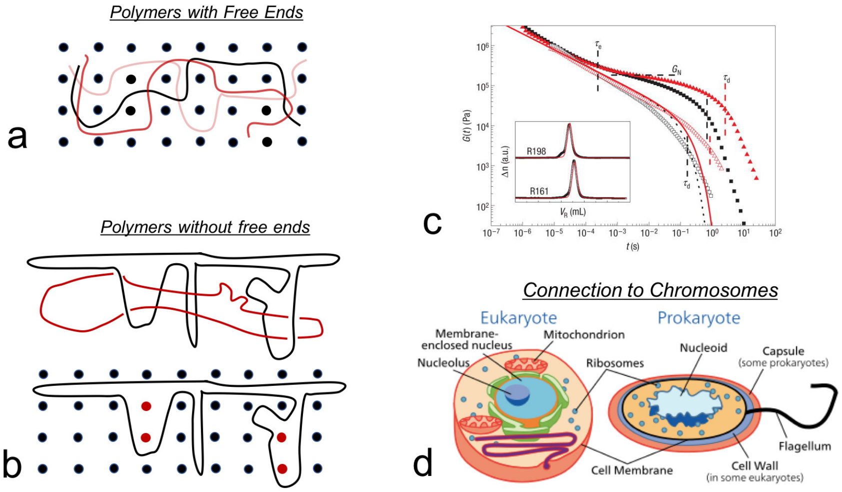

Figure 1: (a) Reptation of a linear chain. Topological constraints due to neighbors (black dots) force the chain to carry out snake-like motion along its contour length (brighter colors show earlier conformations). (b) A ring that is threaded by its neighbors. Its contour can be thought of as encircling points (red) that cannot be crossed until the blue ring has diffused away. (c) Comparison of the stress relaxation moduli $G(t)$ for two polystyrene rings (open triangles and open circles) and their linear counterparts shown with their corresponding filled symbols (See Ref. [1]). (d) Schematic representation of chromosomes in eukaryotes and prokaryotes.

goal of this Thesis is to fill the gap between rings phenomenology and quantitative understanding.

To this purpose, we have resorted to a combination of massive computer simulations alongside with theoretical considerations and analysis.

The Thesis is then structured as follows: after introducing the reader to the relevant concepts and quantities in polymer physics, polymer solutions and melts (Chapter 1), we characterize the effects of topological interactions in ring polymer solutions of different densities (Chapter 2), the role of inter-chain threadings on the long-time relaxation of rings (Chapter 3) and the rheological properties of rings solutions at the micro-scales (Chapter 4).

Chapter 1

Introduction: Physical Aspects of Polymers

1.1 Polymer Physics: Basic Concepts and Theoretical Considerations

In this section, we introduce the reader to the basic concepts in polymer physics and polymer solutions. We will mainly follow the classical textbooks [18, 2]. For ring polymers, where the body of the literature is not as significant as for linear chains, we will review results from the most recently published literature on them.

A polymer (from *polys* meaning *many* and *meros* meaning *part*) is a large molecule composed of multiple repeating units (monomers) typically connected by *covalent bonds*. If the macromolecule contains monomers of only one type is called *homopolymer* [12].

This type of polymer is usually represented as a chain of N repeating sequences. Experimentally the chain length N is large, generally $10^3 \leq N \leq 10^5$. The size of a chain ($\sim 10^3 \mathring{A}$) thus exceeds that of a monomer ($\sim 1\mathring{A}$) by several orders of magnitude.

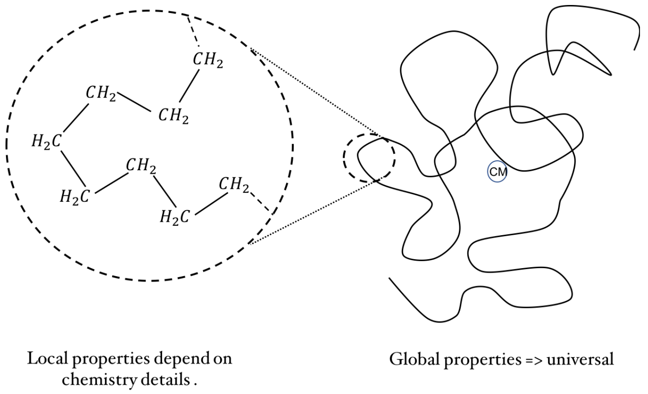

Figure 1.1: Schematic illustration of a polymer. The local properties of the polymer depend on its microscopic degrees of freedom, while the global properties are universal.

Polymers are intrinsically hierarchical (fractal) objects and conformational changes occur on very different scales, ranging from the local scale of a bond to the global scale of the chain (See Fig. 1.1). Factors that influence the conformational properties of a polymer chain are the *microstructure*, which is related to the physical arrangement of the monomers along the chain, and the *architecture*, which is the way, for instance, a branched polymer turns to deviate from a simple linear chain. Polymer architectures may be trivially simple as in the case of linear polymers, or quite complicate as in the cases of branched polymers or polymer networks [19].

1.2 Statics

1.2.1 Single Chain Statistical Treatment

1.2.1.1 Random-Walk Model

There are different models describing the conformation of an ideal (i.e., with no excluded volume) polymer. While each model adds a new constraint for the system, usually on the "short-range" interactions, all of these models neglect "long-range" interactions. In this section, we specify the random walk (RW) model which is widely used due to its great mathematical simplicity.

In order to characterize the $N - body$ system in RW model, consider a chain with a degree of polymerization N where each monomeric link in the backbone has length a. As shown schematically in Fig. 1.2, the end-to-end vector, $\vec{R}_{ee}$ is the sum of the N

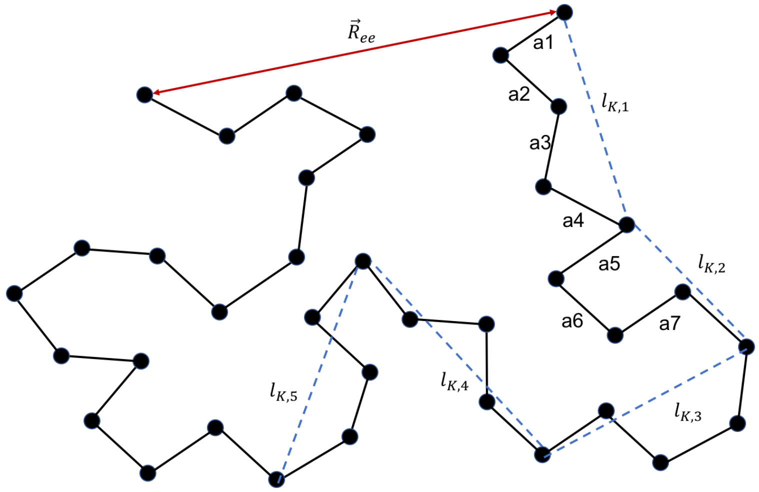

Figure 1.2: Schematic of the dimensions of a polymer chain in the melt. A linear polymer molecule in the melt is accurately described as a random walk and the end-to-end distance of the molecule R_{ee} scales with molecular wight as $R_{ee} \sim N^{1/2}$.

bond vectors along the chain, a_i, which represent the orientation of each monomer unit: $\vec{R}_{ee} = \sum_{i=1}^{N} a_i$. On short length scales, the orientation of monomer segments may be correlated. However, these correlations typically decay very rapidly [12] and there is no correlation between widely separated segments of the chain.

We now consider a simple model where the real polymer chain is broken into N_K segments of length l_K, where l_K is the minimum length scale over which the segments a_i are not correlated. l_K is chosen such that the real and model chain have the same contour length and end-to-end distance: $L = Na = N_K l_K$ and $\vec{R}_{ee} = \sum_{i=1}^{N} a_i = \sum_{i=1}^{N_K} l_{K,i}$. Therefore the real chain is entirely equivalent to the ideal freely jointed chain (See Fig. 1.2, blue dashed lines). If we now consider the average end-to-end distance of such a chain, we have

$$\begin{aligned} R_{ee}^2 &=< \vec{R}_{ee}.\vec{R}_{ee} >=< (\sum_{i=1}^{N_K} l_{K,i}.\sum_{i=1}^{N_K} l_{K,i}) > \\ &=< \sum_{i=1}^{N_K}\sum_{j=1}^{N_K} l_{K,i}.l_{K,j} > \\ &= N_K l_K^2 + < \sum_{i \neq j}^{N_K} l_{K,i}.l_{K,j} > \end{aligned} \tag{1.1}$$

Since the chain is freely jointed, the orientation of different monomers is uncorrelated and the cross terms disappear leaving

$$R_{ee}^2 = N_K l_K^2 \tag{1.2}$$

Finally, noting that $N_K \sim N$ we have,

$$R_{ee} \sim \sqrt{N} \tag{1.3}$$

At the same time, different segments of length l_K (which is known as Kuhn segments) behave as nearly independent and we can write:

$$R_{ee}^2 = N_K l_K^2 = \frac{L}{l_K} l_K^2 = L l_K \tag{1.4}$$

Equation 1.4 gives, in fact, the definition of Kuhn length; that is $l_K = R_{ee}^2/L$.
The above formalism relies on the assumption that the polymer chain is ideal. This is valid only for chains in melt [18, 2]. In fact, in the melt each chain is surrounded by many other chains and interactions between monomers on the same chain are "compensated" from the interaction with the others [18].
The space occupied by the random walk configuration of a polymer chain in the melt is the pervaded volume, $V_p \sim R_{ee}^3 \sim N^{3/2}$. Within a sphere of radius R_{ee} the volume occupied by a single chain is given by $V_c \sim N$. Therefore, the fraction of space filled by a single polymer chain in its own pervaded volume, $V_c/V_p \sim N^{-1/2}$ is small since $N > 100$ for a typical polymeric system. Polymer melts fill space so a consequence of this fact is that many chains must share the same pervaded volume. Therefore, in the melt there are many interactions between chains.
When two chains share the same pervaded volume, they may take on a conformation that severely restricts the movement of the chains in the direction perpendicular to their backbones [18]. Such conformations are referred to as "entanglements". On a fundamental level, entanglements arise due to the simple fact that polymer backbones cannot pass through one another. It is important to note that in the melt, polymers are constantly exploring new space meaning entanglements represent temporary constraints. Many of the physical properties exhibited by polymer melts including viscoelasticity and high viscosities are a result of these type of topological interactions [18]. Before proceeding to discuss some of the physical phenomena resulting

Figure 1.3: The representation of two entangled chains. The entanglement interactions slow the relative movement of center of mass of the chains and even draw them back.

from them, I will briefly explain the entanglement length, N_e which is defined as the average molecular weight between two entanglements. In Fig. 1.3, N_e represents the length of the chain between the two entangled points. It is important to note that for polymer chains to be entangled, it is necessary to have some minimal length [18]. The onset of entanglement is experimentally observed through measurements of viscosity. As discussed above, they restrict the motion of polymer chains and therefore increase the viscosity of the melt.

The ideal chain model is valid for linear polymers in dense polymer melts or blends [2, 18], where the excluded-volume interactions are screened [2], whereas in the melt of ring polymers, the screening is rather not complete (See Chapter. 2).

1.2.1.2 Worm-Like Chain (WLC) Model

A model for ideal polymer chains, which neglects monomer/monomer interactions and only retains chain connectivity, was discussed in 1.2.1.1. The model neglects any type of correlation between neighboring monomers and represents a configuration as a realization of a random walk (RW). It is a reasonable model for a fully-flexible chain without interactions and, to a first approximation, for melts and dense solutions where interactions between monomers are screened [2]. The possibility for two neighboring monomers to overlap or for the RW to allow for immediate return is not realistic. Many biopolymers such as DNA, filamentous (F-) actin or microtubules belong to the class of semiflexible polymers. The biological function of these polymers requires considerable mechanical rigidity. For instance, actin filaments are the main structural elements of the cytoskeleton in which they form a network rigid enough to maintain the shape of the cell and to transmit forces, yet flexible to allow for cell motion and internal reorganization in response to external stimuli. While the behavior of flexible polymers is dominated by entropic forces, semiflexible polymers like most biopolymers additionally have internal energy contributions.

The WLC model treats the conformation of a polymer chain as a continuous entity, describes a polymer chain as a homogenous string of constant bending elasticity. Although entropic and enthalpic contributions are combined in this approach, the extension is limited by the contour length of the polymer. A semiflexible polymer is defined as a chain connected by multiple bonds that have the tendency of staying aligned in a given direction. These polymers lack long-range orientational order along the chain, but on the other hand, there is a length-scale over which the chain orientation is correlated. Semiflexibility describes behavior where the polymer behaves as a rigid rod over short length scales and performs a random-walk over large length scales. The persistence length l_p is defined as the exponential decay length of tangent-tangent correlations along the chain in the bulk, and is equal to the bending rigidity of the chain. In other words, it emerges as the correlation length of the exponential decay of contour tangents in thermal equilibrium, i.e.

$$< \vec{t}(s).\vec{t}(s^{'}) >= \exp(-|s-s^{'}|/l_p)$$

with $\vec{t}(s)$ being the unit tangent vector to the chain at contour length separation s along the chain: it is defined as: $\vec{t}(s) \equiv \frac{\partial \vec{r}(s)}{\partial s}$. As a direct consequence of the tangent-tangent correlations, the mean square end-to-end distance $< R^2(l) >$ of a WLC approaches the following asymptotic limiting cases: When the contour length is much shorter than the persistence length, it is essentially a rod and the radius of gyration is proportional to polymer length. When it is much longer than the persistence length, the chain behaves like a random coil, with $l_K = 2l_p$.

1.2.1.3 Excluded Volume of Polymer Chains

In the previous sections, we were only discussing ideal chain models which do not account for any excluded volume interactions. It was assumed that the monomers are point particles and the interaction between the particles are ignored. In reality, however, real polymers occupy non-zero volume and therefore steric repulsion will be present among the monomers. In many cases these interactions can not be neglected. Flory treated the question of equilibrium conformations of real chains using a mean field approach. The equilibrium size is set by a balance between excluded volume which tends to expand the chain size, and a restoring force due to loss of conformational entropy due to Swelling. I briefly describe his method here, for more details see [18, 12]. Consider a polymer of N_K Kuhn segments in good solvent conditions (meaning that the solvent interacts favorably with the polymer) which are uniformly distributed within volume R^d (d is the dimensionality) with no correlation between them. Note that the argument holds for an arbitrary dimensionality d. The probability of a second monomer being within the excluded volume v of a given monomer is the product of the excluded volume v and the number density of the monomers in the pervaded volume of the chain N/R^d. The energetic cost of being excluded from this volume is kT per exclusion of $kTvN/R^d$ per monomer. For all monomers in the chain, this energy is N_K times larger.

$$F_{int} \approx kTv\frac{N_K^2}{R^d} \tag{1.5}$$

The Flory estimate of the entropic contribution to the free energy of a real chain is based on the fact that the entropic elasticity obeys the Hooke's law, and thus it is equal to the energy required to stretch an ideal chain to end-to-end distance R:

$$F_{ent} \approx kTv\frac{R^2}{N_K l_K^2} \tag{1.6}$$

The total free energy of a real chain in the Flory approximation is the sum of the energetic interaction and the entropic contributions:

$$F = F_{int} + F_{ent} \approx kT(v\frac{N_K^2}{R^d} + \frac{R_F}{N_K l_K^2}) \tag{1.7}$$

The minimum free energy of the chain (obtained by setting $\partial F/\partial R = 0$) gives the optimum size of the real chain in the Flory theory, $R = R_F$:

$$\frac{\partial F}{\partial R} = kT(-dv\frac{N_K^2}{R_F^{d+1}} + 2\frac{R_F}{N_K l_K^2}) \tag{1.8}$$

which yields,

$$R_F^{d+2} \approx \frac{d}{2}vl_K^2 N_K^3 \tag{1.9}$$

The Flory theory yields to a universal power law dependence of polymer size R_F on the number of Kuhn segments N_K:

$$R_F \sim N_K^{\nu} \quad with \quad \nu = \frac{3}{d+2} \tag{1.10}$$

where ν is the scaling exponent characterizing the polymer conformation. It is interesting to note that ν is independent of v in different solvents, for more details see [12]. The predictions of the Flory theory are in good agreement with both experiments and simulations. However, its success is due to a factitious cancellation of errors, because both the entropic and energetic terms in Eq.1.7 are overestimated. Nevertheless, Flory theory is useful because it is simple and provides reasonably accurate results.

To further understand scaling concepts, consider a chain of N_K Kuhn segments of size l_K under tension. The stretching is done by applying a force of magnitude f at both ends of the chain. In this problem the only characteristic lengths involved are (a) the Flory radius R_F and (b) the length $\xi = kT/f$, which defines a tension blob of size ξ containing g monomers each, such that on length scales smaller than ξ the chain statistics are unperturbed, while on larger length scales the chain is a string of independent blobs, see Fig. 1.4. The number of monomers per blob, g, is related to ξ by the Flory law $\xi \approx l_K g^{\nu}$.

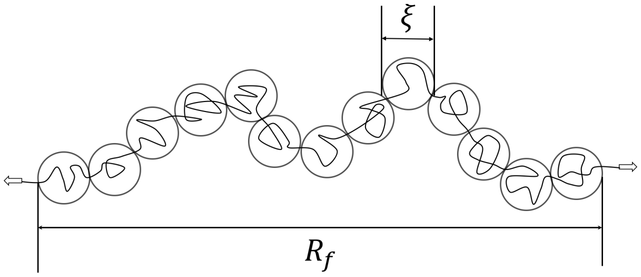

Figure 1.4: The so-called "Flory representation" of a polymer chain.

The end-to-end distance R_F is the product of the tension blob size ξ and the number of these blobs N_K/g

$$R_f \approx \xi \frac{N_K}{g} \approx N_K l_K (\frac{f l_K}{kT})^{1/\nu-1} \tag{1.11}$$

This shows that a chain in good solvent ($\nu = 3/5$) has an elastic response which is nonlinear, than in the case of an ideal chain ($\nu = 1/2$).

This concept of scaling, that is to divide a chain of Kuhn segments into blobs that each contribute of order kT to the free energy, further simplifies the problem at hand.

1.2.1.4 Crumpled (or Fractal) Globule Model

In concentrated conditions, i.e., when many different chains are overlapping, it is well known [2, 18] that the steric interaction between different coils screens the coils self-avoidance. This means that in a melt of linear chains, they return to assume $\nu = 1/2$ (See Sec.1.2.1.1), but what happens to ring polymers? Interestingly, a ring polymer in concentrated solutions does not have the size of an ideal ring polymer (See Chapter. 2 for details).

Ring polymers are appealing macromolecules with significant implications to our understanding of polymer structure [20]. The effect of topological constraints is nontrivial on physical quantities of a ring polymer such as its size. Once a ring polymer is formed, its topological state is fixed. These interactions have important consequences for unknotted and unlinked rings. As two such rings approach, they will increasingly tend to repel each other. The number of attainable conformations of the system decreases. This leads to an entropic repulsion between the rings. For a system consisting of unknotted and unlinked rings in solution this repulsion leads to an increased osmotic pressure.

Recent simulations of topologically constrained unconcatenated ring polymers in concentrated solutions and melts [23, 21, 24] have demonstrated the effect of compression into space-filling configurations but the role of topological constraints in the equilibrium state of a single compact and unknotted ring polymer remains debated.

Although ring polymers compression causes having a subchain of length s with a $s^{1/3}$ scaling relation, reminiscent of a collapsed globule [25, 24], ring polymers, at the same time, display some deviations from a fully crumpled conformation [21]. The collapsed conformation assumed by rings in the melt is broadly accepted, but on the other hand, it is still way not clear what their internal arrangement is. Indeed, although $s^{1/3}$ resembles a collapsed globule, such as the one that could be observed in poor solvent, there are many types of internal arrangements consistent with $s^{1/3}$. Perhaps the most important candidates in this case are (i) the equilibrium globule: a disordered dense packing of coil ; and (ii) the fractal globule: a recursive coiling of mass which appears like a collapsed globule at any length scale (larger than the entanglement length N_e) within the globule [26]. One of the key differences between these two conformations is the contact probability $P_c(s)$ of two segments separated at distance s along the contour of the chains.

$$P_c(s) = s^{-\gamma} = \begin{cases} s^{-3/2} & \text{equilibrium globule} \\ s^{-1} & \text{fractal globule} \end{cases} \tag{1.12}$$

where γ is called the contact exponent. Numerical [21, 27] and experimental [28, 16] observations in fact report a contact exponent close to unity.

Moreover, in the fractal globule the number of contacts between two crumples of lengths $s1$ and $s2$ with $(s_{1,2}) \ll N$ that are separated by a distance l along the chain scales as [16],

$$M_{1,2}(l) \sim \frac{s_1 s_2}{l} \sim \frac{V_1 V_2}{l} \tag{1.13}$$

As follows, the number of interactions is proportional to the product of the crumples' volumes. Such penetration means a great deal of possible cross-talk between individual regions of all sizes. Thus, the fractal globule simultaneously provides two seemingly contradictory features: spatial segregation of local regions on all scales and their extensive cross-talk.

While providing a number of advantages, the fractal globule is a long-lived intermediate on the way to becoming an equilibrium globule. The original theory of the fractal globule [29] suggested that (i) the lifetime of the fractal globule is determined by a time ($\sim N^3$) required to thread the ends of the polymer through the whole globule, allowing the formation of knots; (ii) a chain with attached ends (e.g. a loop or a ring) remains in the fractal globule state forever.

1.2.2 Many Chain Systems: Polymer Solutios

We now introduce the notion of a solution containing many polymer chains (polymer solution). The single conformations of isolated polymers are only limited by the chain generic properties such as connectivity constrains, bond angles and the interactions between the monomers. When the polymer's concentration in the solution is increased, the polymers start to overlap and interpenetrate. The monomer concentration at which polymers begin to overlap is called the overlap concentration (ρ^*). The excluded volume

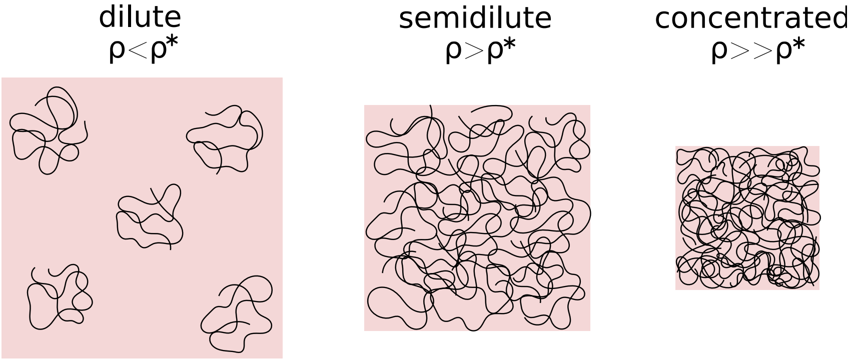

Figure 1.5: The three concentration regimes for polymer solutions: dilute, where the average separation between the coils is much larger than the typical size R_g of the coil; semidilute, above the overlap concentration ρ^*; concentrated solution, much above the concentration ρ^*.

interactions between monomers belonging to different polymers cause entanglements and as a result a change in structure. At first sight, each polymer can be regarded as a sphere with a radius of R_g located at different places in the solution. The overlap concentration (ρ^*) can be estimated as follows: if the "spheres" do not interact with one another, but take up all the available space in the solution, then the concentration is the number of spheres (polymers in the solution) multiplied by the number of monomers in a polymer divided by the volume of the solution. Since the spheres occupy all the space in the solution, then the total volume equals the number of spheres multiplied by their volume.

$$\rho^* \cong \frac{3N}{4\pi R_g^3}$$

For an ideal polymer the $R_g = \frac{R_{ee}}{\sqrt{6}} = \frac{\sqrt{N}b}{\sqrt{6}}$, therefore $\rho^* \propto N^{-1/2}$.

In dealing with polymer solutions, one usually categorizes three concentration regimes, shown in Fig. 1.5. Polymers conformations in the dilute regime are not influenced significantly by other polymer chains present in the solution but are strongly dependent on polymer-solvent interactions. In the semi-dilute regime, both solvent conditions and other surrounding polymer chains influence the polymer chain conformation. In the polymer melt, the solvent can be neglected; only very small quantities of solvent are present. The behavior is therefore dominated by intra-chain and inter-chain monomer interactions. A detailed mathematical treatment of these three regimes can be found in [12].

1.3 Dynamics

1.3.1 Rouse Model For Non-Entangled Chains

The dynamics of non-entangled polymer chains can be described by the Rouse model [12]. It characterizes the internal modes of motion of short polymer chains $N < N_e$ or polymer monomers at short time scales.

A Rouse chain is comparable to a flexible connected string of Brownian particles that interact with a background viscous medium. In case of polymers, individual particles are comparable with the chain segments following a Gaussian distribution. Further, such repeated segments are connected with springs of length b; the only interaction is through the springs (See Fig. 1.6).

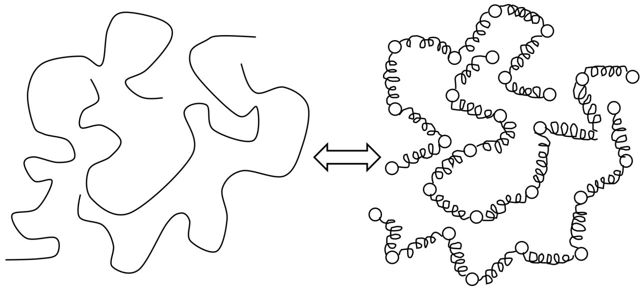

Figure 1.6: Rouse model, a chain of N monomers is mapped onto a bead-spring chain of N beads connected by springs.

In a Rouse chain, each monomer (segment) is dragged in the medium (solution) with a friction coefficient ζ, so the total friction coefficient for a chain of size N is equal to, $\zeta_N = N\zeta$. The relaxation time for a chain with the size of R is then

$$\tau_R \approx \frac{R^2}{D_R} = \frac{\zeta}{kT} N R^2 \tag{1.14}$$

Here, $D_R = \frac{kT}{\zeta_N}$ is the diffusivity of the center of mass depending on the friction coefficient ζ_N via Einstein relation. This relaxation time is known as the Rouse relaxation time. It means at times $t > \tau_R$, polymer diffuses freely, whereas, on shorter times $t < \tau_R$, more complex behavior of sub-diffusive motion appear.

The Rouse model can be used to determine the stress relaxation in a system made of Rouse chains and it can be shown that the shear stress relaxation modulus has the following time dependence [12]

$$G(t) \sim t^{-1/2} \tag{1.15}$$

and the viscosity of the system is equal to $\eta \sim N$. This behavior has been confirmed in experiments on short polymer chains [103]

1.3.2 Reptation Model

To predict chain dynamics in entangled polymer solutions, Doi and Edwards refined reptation theory [2], introduced by de Gennes [18], by making it applicable to highly entangled polymer liquids. For a polymer melt, chains cannot pass through each other due to the topological constraints. According to this model, each chain is confined inside a tube-like region resulting from the excluded-volume interactions with the neighboring chains (See Fig. 1.7). These constraints can be represented by a tube within which the polymer performs a snake-like motion.

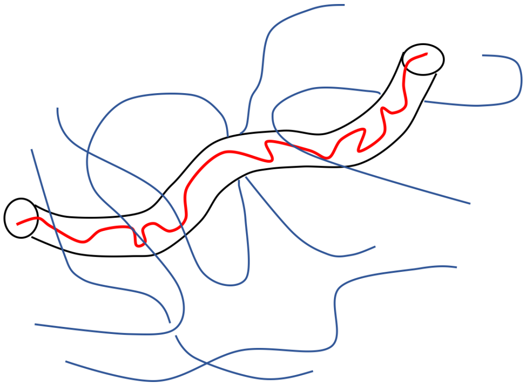

Figure 1.7: Schematic illustration of an entanglement (reptation) tube. The red chain is undergoing reptation inside the tube while entangled with its neighboring blue chains.

The shortest path that lies within the tube and links the two chain ends is called the "primitive path", and characterizes the length of the tube. Another important length scale in this model, which will be used often in this Thesis, is the tube diameter d_T, which determines the transverse dimension of the tube. Based on the random-walk statistics for chain conformations, d_T scales as $N_e^{1/2} l_K$.

For a single reptating chain, the theory predicts that the viscosity and longest relaxation time follow the scaling law of N^3, while the diffusion constant scales as $D \approx N^{-2}$ where N is the polymer length.

1.3.3 How Ring Polymers Relax Their Stress

"The tube model can describe how mutually entangled polymer chains move and interact with the surrounding neighbors, but it heavily relies on the presence of loose ends for the disentanglement process. Ring polymers have no ends, so how do they relax?". Within the framework of the tube model, that makes it hard to think about what strategy they might exploit to explore their mutual space of configurations. The main difficulty of the problem branches from the breakdown of a theory where topological constraints are concerned.

The first theories describing how ring polymers diffuse through each other have been progressed in the 80s [30, 31, 32]. They consider the dynamics of the ring polymer in a melt similar in the array of obstacles happening through random fluctuations which causes a shape evolution like that of amoeba [20]. Within those models, the diffusion constant of the center of mass of such a ring polymer can be estimated if we adopt de Gennes' picture of *kink gas* (or excess of mass along the chain), i.e. the non-interacting length defects, to the ring polymer [33]. The self-diffusion of the ring polymer essentially proceeded by the transport of length defects along the chain contour. These length defects are supposed to diffuse in the same way as those on a linear chain. By assuming that the kinks perform a 1D random walk along the contour, the time required to span a distance R_g scales as $\tau \propto N^3$ and the diffusion coefficient $D \propto N^{-2}$.

Later on, Obukhov et al. [34] argued that, considering a ring polymer in a gel, the diffusion of length defects along the polymer contour differs from that on a linear chain. The ring polymer was constructed as a lattice tree, and the motion is governed firstly by the diffusion of length defects within the branches and then along the trunk. They suggested that these previous works [30, 31, 32] have overlooked some modes of motion available to a ring polymer, thus amount of the change of polymer configuration is underestiamted. They obtained the same result of diffusion coefficient $D \propto N^{-2}$ but a different scaling for the relaxation time, $\tau \propto N^{5/2}$.

More recently, Milner, Iyer, and then Grosberg [35, 36] advanced several other theories for the diffusion of a ring polymer among other chains. Milner and Newhall [37] came up with an approach based on the "centrality" of a node in the lattice animal representation. In that picture, every node is dividing the animal into left and right subtrees, of mass m and $N - m$, where N is the total number of nodes in the animal. The centrality c of a node in this representation is defined as

$$c = min(m, N - m) \tag{1.16}$$

where m is the size of one of the two subtrees generated by cutting the $m - th$ bond of the tree representation.

Their result for the total time required for the centrality to diffuse a "distance" was roughly compatible with the recent experiment [1], however, it predicts a stress relaxation faster than that allowed by the rearrangement of the loops. On the other hand, their theory neglects the motion of other chains and, in particular, inter-chain interactions which are reported in even more recent findings [38, 15].

Smrek and Grosberg [36] proposed analytical methods based on the annealed tree model. This model considers blobs having g monomers each and the ring is defined as an annealed tree composed of crumpled branches designing a self-avoiding path on a Cayley tree. By assuming the existence of an "entanglement length", named M_e, below which the chain is Gaussian(ideal), which is taken as the "blob" size, they have estimates for the diffusion coefficient and the relaxation time which were roughly consistent with the predicted exponents of experimental evidence [1]. Although they could predict well the static and dynamic exponents, it could not be explained why the sub-diffusion of the rings can be observed on length scales many times the ring's gyration radius [4, 22]. This may be due to chains moving and interacting non-trivially with one-another. An essential reason is that mean-field theories analyse the behavior of chains among other "nonmoving" chains. This is not the case in the concentrated solutions of ring polymers where inter-chain interactions are assumed to play an important role [21].

As I mentioned in sec.1.2.1.4, it has been conjectured that ring polymers assume crumpled and segregated [21, 1] conformations suggesting that rings exhibit strong intercoil correlations. In this direction, Michieletto et al [39, 40, 3]and Lee et al, [41] pursued a distinctly different approach and argued that mutual ring interpenetrations can not be ignored. They are responsible for substantial topological slowing down of rings and the possible eventual formation of a glass (See Chapter. 3).

1.4 Molecular Dynamics Simulations

1.4.1 Basics

The molecular dynamics (MD) simulation method was first used in the late 50's [42]. Some of the first MD simulation work was done to examine properties of systems of hard spheres [43] and simple liquids [44]. The majority of molecular dynamics simulations benefit from classical interactions; indeed, classes of problems where classical physics is dominant are where the MD method is among the most effectively used techniques. It is based on the classical Newton's law

$$m\frac{\partial^2 r}{\partial t^2} = -\nabla U(r) \tag{1.17}$$

where m is particle mass, r is particle position, t is time, and U is a potential function that is defined in 1.4.2 to represent the system. The point of using the simulation approach is that one can investigate the behavior of large groups of particles. The particles, often also referred to as ”monomers”, are placed together in a simulation box to perform a MD simulation. Considering that the simulation box size and the number of monomers will be always finite, periodic boundary conditions are used to approximate the behavior of an ‘infinite’ medium.

MD usually consists of four kinds of simulations:

1. Microcanonical ensemble (NVE ensemble) -In the NVE ensemble, the system does not undergo any changes in number of moles (N), volume (V) and energy (E). It is an adiabatic process where there is no heat exchange. A microcanonical molecular dynamics trajectory has its total energy conserved in this ensemble with continuous exchange going on between potential and kinetic energies.
2. Canonical ensemble (NVT ensemble) - In the NVT ensemble, number of moles (N), temperature (T) and volume (V) are conserved and is known as constant temperature molecular dynamics. In this ensemble, the energies of exothermic and endothermic processes are exchanged with a thermostat. Different types of thermostat methods are available to add and remove energy from the MD system.
3. Isothermal-Isobaric (NPT ensemble) - In the isothermal-isobaric ensemble, number of moles (N), pressure (P), and temperature (T) are conserved. Both thermostats and a barostat are needed. The volume is allowed to change freely as a result of the fluctuations occurring due to sudden changes in temperature and pressure.
4. Isoenthalpic-Isobaric (NPH ensemble) - In this ensemble, number of moles (N),

pressure (P), and enthalpy (H) are conserved. One more degree of freedom is added into the system in the form of variable volume (V) to which the coordinates of all particles are relative. Volume (V) becomes a dynamic variable with kinetic energy given by PV. The enthalpy $H = E + PV$ is kept constant while the internal energy E and the kinetic energy PV are allowed to change.

The static and kinetic properties of systems are studied using fixed-volume and constant-temperature molecular dynamics simulations (NVT ensemble) with implicit solvent. MD simulations are performed using the LAMMPS package [45]. The equations of motion are integrated using a velocity Verlet algorithm, in which all monomers are weakly coupled to a Langevin heat bath with a local damping constant $\Gamma = 0.5\tau_{\mathrm{MD}}^{-1}$ where $\tau_{\mathrm{MD}} = \sigma(m/\epsilon)^{1/2}$ is the Lennard-Jones time and $m = 1$ is the conventional mass unit for all considered particles. The integration time step is set to $\Delta t = 0.012\tau_{\mathrm{MD}}$.

1.4.2 Kremer-Grest Polymer Model

To model polymers in solution, we used the bead-spring polymer model introduced by Kremer and Grest [11]. It captures the most essential elements of a many-chain polymer system. Chains consist of many monomers joined together, and become entangled in a melt since chain-chain crossing is prohibited. All beads interact via a Lennard-Jones (LJ) 12-6 potential,

$$U_{LJ}(r) = \begin{cases} 4\epsilon\left[\left(\frac{\sigma}{r}\right)^{12} - \left(\frac{\sigma}{r}\right)^{6} + \frac{1}{4}\right] & r \le r_c \\ 0 & r > r_c \end{cases}, \tag{1.18}$$

where r denotes the separation between the bead centers. The cutoff distance $r_c = 2^{1/6}\sigma$ is chosen so that only repulsive Lennard-Jones interactions are included, and the force between two particles separated by a distance of r_c is zero. The energy scale is set by $\epsilon = k_BT$ and the length scale by σ, both of which are set to unity in our simulations. All other dimensional quantities are expressed in terms of reduced units defined through ϵ, σ, and the monomer unit mass m (See Table. 1.1). Time is measured in the MD time units $\tau_{MD} = \sigma(\frac{m}{\epsilon})^{\frac{1}{2}}$. All bonds along a chain are connected using the finite extensible nonlinear elastic (FENE) potential,

$$U_{FENE}(r) = \begin{cases} -0.5kR_0^2 \ln\left(1 - (r/R_0)^2\right) & r \le R_0 \\ \infty & r > R_0 \end{cases}, \tag{1.19}$$

where $k = 30\epsilon/\sigma^2$ is the spring constant and $R_0 = 1.5\sigma$ is the maximum extension of the elastic FENE bond.

The polymers are given an intrinsic stiffness by including a bond angle potential,

$$U_{bend}(\theta) = k_\theta \Big(1 - \cos\theta\Big) \ . \tag{1.20}$$

Here, θ is the angle formed between adjacent bonds and $k_\theta = 5\,k_BT$ is the bending constant. With this choice, the polymer is equivalent to a worm-like chain with Kuhn length l_K equal to 10σ [46].

Parameter	Description	Value(LJ units)
σ	LJ length scale	1
ϵ	LJ energy scale	1
r_c	LJ cutoff distance	$2^{1/6}$
k	FENE elastic constant	30
R_0	FENE maximum bond elongation	1.5
γ	Damping factor for Langevin dynamics	0.5
m	Mass of particles	1

Table 1.1: Parameters used in the simulation of polymers

1.5 Thesis Overview

This chapter has thus far presented a brief introduction to what polymer physicists have done so far and what has made ring polymers to be one of the last big mysteries in polymer physics. As can be concluded from the above discussions, many aspects of the relaxational and mechanical properties of ring polymers are still poorly understood. This is essentially a result of the absence of a well accepted theory for the relaxation of ring polymers.

This Thesis is focused upon the simulations of concentrated solutions of polymers in the linear and ring shapes with the polymer entities subject to varying the density of the solutions. We aim to study the properties of these solutions to help towards understanding the various behaviors of polymers with differing typologies and to know how differently assorted typologies get affected by altering the density. The following is a brief summary of the content of each following chapter.

2. Density effects in entangled solutions of ring polymers

We have employed extensive Molecular Dynamics computer simulations in order to provide a detailed theoretical description of the equilibrium and dynamical properties of linear and ring polymers. We take into account chains of different sizes, an aspect which has been already considered in many studies. More importantly, we consider solutions of different densities, an aspect which has received considerably less attention in the past. The results provide a vivid quantitative picture concerning the influence of single-chain topology in solutions of entangled polymers of different densities.

3. Ring polymers as topological glasses

We continue to investigate how topological constraints affect the dynamics of ring polymers. These polymers fold as crumpled and space-filling objects, and, yet, they display a large number of inter-penetrations. To understand their role, here we systematically probe the response of solutions of rings at various densities to ”random pinning” perturbations. We show that these perturbations trigger non-Gaussian and heterogeneous dynamics, eventually leading to non-ergodic and glassy behaviors. Our results suggest that deviations from the typical behaviors observed in systems of linear polymers may originate from architecture-specific (threading) topological constraints.

3. Diffusion of colloidal nanoparticles in entangled solutions of linear and ring polymers

We discuss dynamical properties of nanoparticles transport in entangled solutions of linear and ring polymers. Nanoparticles diffusion exhibit seemingly anomalous trends as a function of different length scales of their polymer matrix. we generalize the previous works on nanocomposites by exploring wider ranges of probe sizes and solution densities.

4. Conclusions

The main results and conclusions from this Thesis are presented.

Chapter 2

Density Effects in Entangled Solutions of Ring Polymers

The content of this chapter is published in J. Phys. Cond. Matt, 28, 065101 (2016).

2.1 Introduction

Since the pioneering works of Flory [47], De Gennes [18] and Edwards [2], excluded volume effects and topological constraints have been known to play a crucial role in the comprehension of the structural and dynamical properties of polymers in semi-dilute solutions and melts. Topological constraints (or, *entanglements*) hinder the thermal motion of polymers in a way akin to the process of threading a rope out of a pool: polymer chains can not pass through each other, while they are allowed to slide past each other. This fundamental mechanism is recognised to be responsible for the unique properties of polymer solutions and melts [47, 18, 2, 12].

As I mentioned in 1.2.1, according to current theoretical understanding, linear polymers in entangled solutions follow (quasi) ideal statistics because of screening of excluded volume [2] at large scales, while ring polymers do not display such an analogous "compensation" mechanism and tend to crumple into compact configurations [48, 49, 23, 50, 21, 51, 24]. At odds with their linear counterparts then, topological constraints affect not only the dynamical properties of rings in solution but they do also have consequences on their properties at equilibrium.

If we look at individual rings in the melt of unconcatenated (unlinked) and unknotted rings, their conformation is much different from that of Gaussian statistics expected for linear polymer counterparts. Its clarification has been a subject of intense research for the last several decades [30, 34, 48, 23]. Such a non-trivial conformation would affect the various macroscopic physical properties of the system. The rheology of concentrated solutions of rings would be one of primal examples in the list [1, 37, 52]. Even if considerable theoretical and experimental work have been already dedicated to the subject, there are still several features concerning the equilibrium properties of rings polymers in solutions, either as a function of ring size or solution density which remain mysterious. The latter aspect, in particular, has received less attention in the past and this chapter aims primarily to start filling this gap. For the sake of comparison, we also discuss the same properties for corresponding entangled solutions of linear chains.

2.2 System Description

2.2.1 Simulation Details

We consider polymer solutions of (ring and linear) polymer chains: each chain is constituted by $N = 250, 500, 1000$ monomers for a total number of chains $M = 160, 80, 40$ respectively. The total number of monomers is then fixed to $40'000$ units. The volume of the simulation box accessible to chain monomers has been chosen in order to fix the monomer density ρ to the values $\rho\sigma^3 = 0.1, 0.2, 0.3$ and 0.4. The chosen values of ρ span from the overlap density (explained in Sec. 1.2.2) to one which the inter-chain entanglement is significant.

We first need to provide a justification for why our polymers can effectively be considered as "entangled". In semidilute solutions, linear chains with a contour length exceeding a characteristic value, $L \gg L_e$, become mutually entangled. In particular, L_e depends on chain stiffness as well as on the contour length density of the polymer melt or solution. In solutions where the individual polymers exhibit worm-like chain statistics, a reasonable approximation is given by [53],

$$L_e/l_K = (0.06(\rho\sigma l_K^2))^{-2/5} + (0.06(\rho\sigma l_K^2))^{-2}. \tag{2.1}$$

With solution densities $\rho\sigma^3 = 0.1, 0.2, 0.3, 0.4$ and chain Kuhn length $l_K/\sigma = 10$, corresponding entanglement lengths are given by $L_e/l_K \approx 4.00, 1.62, 1.10, 0.89$. At the highest density then, our longest chains have a contour length $L/L_e \approx 100$.

The equilibrium and kinetic properties of these polymer systems are studied using fixed-volume and constant-temperature (NVT ensemble) Molecular Dynamics (MD) simulations (See Sec. 1.4 for details). The equations of motion are integrated using a velocity Verlet algorithm, in which the polymer-solvent interactions are effectively accounted for through the Langevin thermostat with $T = 1$ and and the damping constant $\Gamma = 0.5\tau_{MD}^{-1}$. LAMMPS is used for all simulations [45].

2.2.2 Sample Preparation

Linear polymers- The initial configurations of linear polymers are first obtained by placing the chains at random in the simulation box at $\rho\sigma^3 = 0.1$. The simulation as presented above will very likely not run smoothly, since the particles are placed randomly and therefore might overlap. Overlapping monomers are pushed off each other using a soft potential,

$$E = A[1 + cos(\pi r/r_c)]. \tag{2.2}$$

when $r < r_c$. A is linearly increased from 0 to 50 within a short MD run (of the order of a few τ_{MD}s) to remove any overlaps of monomers. Then, this soft potential is replaced by a short (about $500\tau_{MD}$ MD steps) NPT simulation to increase the density of the system to the target values. NPT does not "fix" the pressure, instead it adjusts the volume of the simulation box according to the sign and magnitude of the pressure.
Ring polymers- For rings solutions the situation is more complex, as rings need to satisfy the supplementary (and highly non-trivial) constraint of avoiding mutual concatenation. Hence, the density of the system was initially set to a few percent with the rings widely spaced to avoid any linking. In order to reach the correct monomer density of $\rho\sigma^3 = 0.1$ we then performed a short (about $400\tau_{MD}$ MD steps) simulation by imposing an external pressure on the system, which shrinks the simulation box until it reaches the desired value. To reach our highest density $\rho\sigma^3 = 0.4$, we have applied an external pressure of about $P = 5.0\epsilon/\sigma^3$. For all systems, desired densities are obtained within $5 \times 10^3\tau_{MD}$.

Once any given system was prepared at the correct density, we switched to the NVT ensemble. Then, each system was equilibrated by performing single MD runs up to $1 \cdot 10^9 \Delta\tau = 12 \cdot 10^6 \tau_{\mathrm{MD}}$ (for $N = 250$) and $2 \cdot 10^9 \Delta\tau = 24 \cdot 10^6 \tau_{\mathrm{MD}}$ (for $N = 500$ and $N = 1000$). Nearly for all polymer solutions, the simulation times are long enough to reach the diffusive regime, see Fig. 2.1. Of course, during this preparatory phase the complete set of interaction terms described in Sec. 2.2.1 was employed.

2.3 Results and Discussions

2.3.1 Average Square Internal Distances

In order to characterize the effects of density on single chain conformations, we have first analyzed the mean-square spatial distance $\langle R^2(l)\rangle$ between monomers located at contour length separations $l = |i - j|$ where $i < j \in [1, N]$ are the monomer indices. The ensemble average $\langle ...\rangle$ is performed over all the chains and the last portion (10%) of the simulations where polymer chains have surely reached equilibrium.

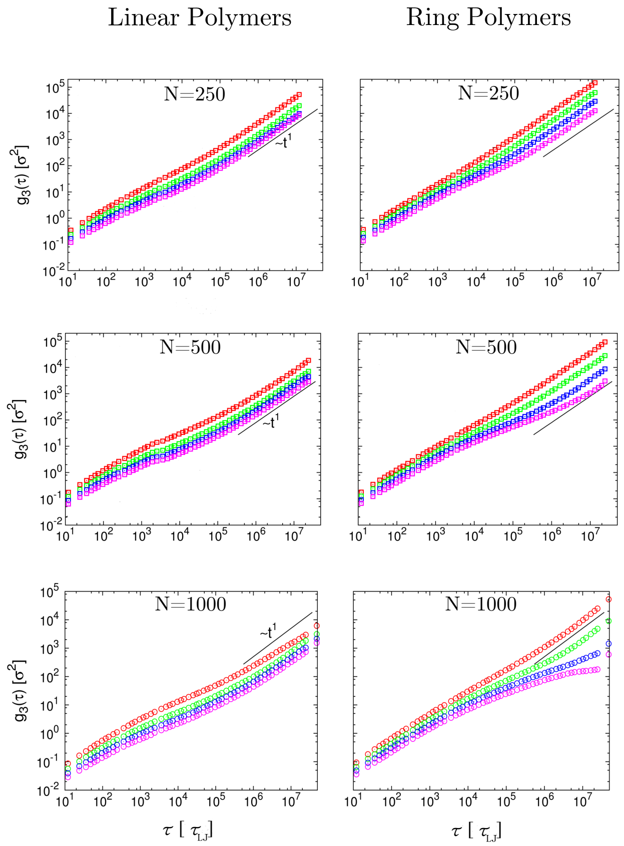

Figure 2.1: The mean square displacement of the chains center of mass ($g3(\tau)$). The reported power-laws correspond to the expected [2] long time behavior after complete chain relaxation. At long times, all the systems except rings with $N = 1000$ and the highest density reach diffusive regime. This emerging slow down will be discussed in details in Chapter. 3.

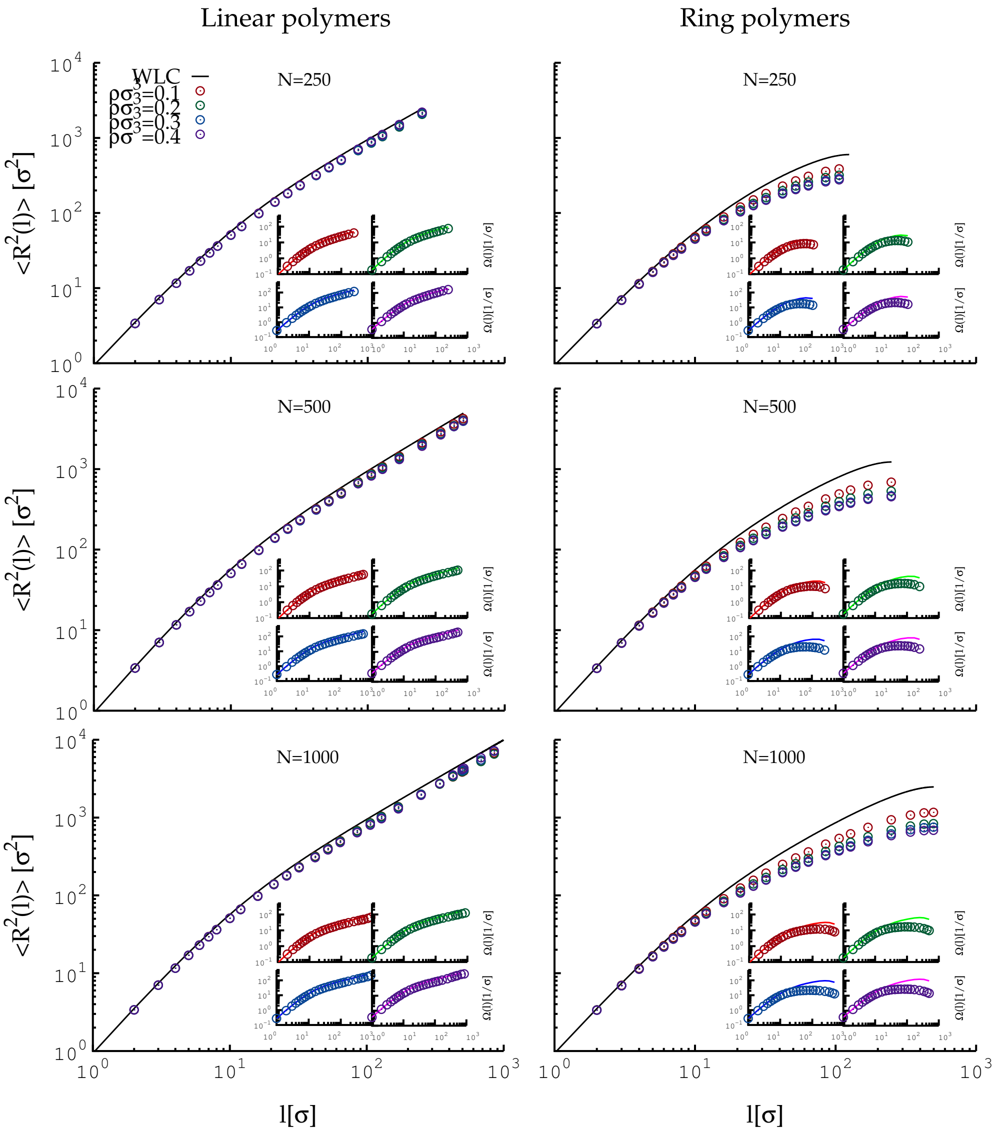

Figure 2.2: Average-square internal distances $\langle R^2(l) \rangle$ between chain monomers at contour length separation l (symbols), and corresponding theoretical predictions for worm-like chains and rings (black lines, Eqs. 2.3 and 2.4 respectively) with Kuhn length $l_K = 10\sigma$. Insets: corresponding overlap parameters $\Omega(l) = \rho \frac{\langle R^2(l) \rangle^{3/2}}{l}$.

We find that numerical results (symbols in Fig. 2.2) for linear and ring polymers are well described by, respectively, the exact worm-like chain (WLC) expression [12] for semi-flexible linear polymers with Kuhn length l_K:

$$\langle R^2(l)\rangle^{WLC} = \frac{l_K^2}{2}\left(\frac{2\,l}{l_K} + e^{-2\,l/l_K} - 1\right) \,, \tag{2.3}$$

and the approximate formula for ideal semi-flexible rings:

$$\langle R^2(l)\rangle^{WLR} = \left(\frac{1}{\langle R^2(l)\rangle^{WLC}} + \frac{1}{\langle R^2(L-l)\rangle^{WLC}}\right)^{-1} \tag{2.4}$$

which gives an accurate description provided $L \gg l_K$. Analytical results are represented as black solid lines in Fig. 2.2. We remark the striking difference between linear chains and rings: as expected based on the theoretical scenario (see Sec. 1.2.1.1) predicting the screening of excluded volume interactions, numerical results for $\langle R^2(l)\rangle$ of linear chains (Fig. 2.2, left panels) show little or no dependence on density and agree well with the WLC prediction, Eq. 2.3. Conversely, in solutions of ring polymers where screening is absent [48, 49, 23, 50, 21, 24] numerical predictions for $\langle R^2(l)\rangle$ markedly deviate from Eq. 2.4 (right panels of Fig. 2.2). In particular, rings show the tendency of becoming more and more compact as density increases. Alternatively [24], the same data can be recast in terms of the so-called overlap parameter $\Omega(l) \equiv \rho\frac{\langle R^2(l)\rangle^{3/2}}{l}$ which gives the total number of sub-chains of contour length l contained inside the corresponding occupied volume. Results are shown as insets in Fig. 2.2, highlighting the important difference between chains and rings: in fact, for the latter $\Omega(l)$ tends to plateau at increasing chain size (*i.e.* $\langle R^2(l)\rangle \sim l^{2\nu}$ with critical exponent [12] $\nu = 1/3$), the value of the plateau slightly increasing from ≈ 12 for $\rho = 0.1$ to ≈ 28 for $\rho = 0.4$.

2.3.2 Distribution Functions of End-to-End Distances

To complete the statistical characterization of end-to-end distances, we now look at the distribution functions $p(R|l)$ of end-to-end distances $R = R(l)$ as a function of $l = 15, 30, 60, 120$ and density ρ, see Fig. 2.3. Both linear and ring polymers show the expected shift from the non-universal short chain behaviour ($l = 15$) where fiber stiffness plays the dominant role to the universal, entropy-governed long chain behaviour. There are noticeable differences between linear and ring polymers: For linear chains, the progressive screening of excluded volume effects [2] at increasing ρ is well exemplified by the fact that $p(R|l)$ super-imposes on the semi-empirical formula

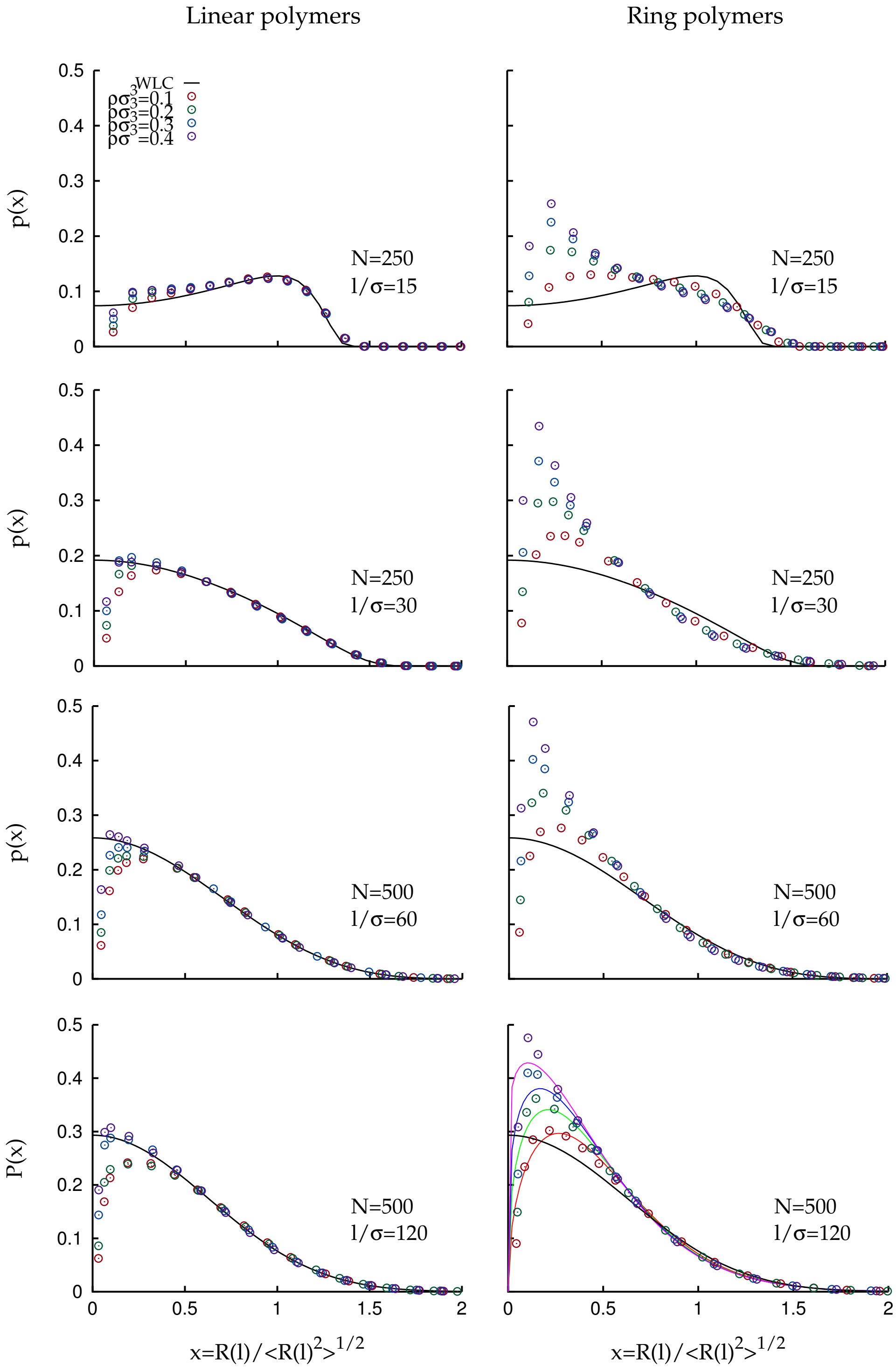

Figure 2.3: Distribution functions of end-to-end distances, $R(l)$ at fixed contour length separations, $l = 15, 30, 60, 120$. Black lines correspond to the semi-empirical WLC formula, Eq. 2.5. Solid coloured lines in the bottom right panel correspond to the RdC function, Eq. 2.7, with fit parameters given in Eq. 2.8.

of ideal worm-like chains given in [54] (left panels in Fig. 2.3, black lines):

$$p(R|l)^{\mathrm{WLC}} = J(l)\left(\frac{1-cR^2}{1-R^2}\right)^{5/2} e^{\frac{\sum_{i=-1}^{0}\sum_{j=1}^{3} c_{ij}\left(\frac{l_K}{2l}\right)^i R^{2j}}{1-R^2}} \times e^{-\frac{d\,\frac{l_K}{l}\,ab(1+b)R^2}{1-b^2R^2}}\, I_0\left(-\frac{d\,\frac{l_K}{l}\,a(1+b)R}{1-b^2R^2}\right) \tag{2.5}$$

with numerical constants $a = 7.027$, $b = 0.473$, and $c_{ij} = \begin{pmatrix} -3/4 & 23/64 & -7/64 \\ -1/2 & 17/16 & -9/16 \end{pmatrix}$, I_0 the modified Bessel function of the first kind and

$$1-c = \left(1+\left(0.734\left(\frac{l_K}{l}\right)^{-0.95}\right)^{-5}\right)^{-1/5}$$

$$1-d = \begin{cases} 0, & \frac{l_K}{l} < \frac{1}{4} \\ \frac{1}{\frac{0.354}{l_K/l-0.222}+3.719\left(\frac{l_K}{l}-0.222\right)^{0.783}}, & \text{otherwise} \end{cases}$$

$$J(l) = \begin{cases} 28.01\left(\frac{l_K}{l}\right)^2 e^{0.492\frac{l}{l_K}-a\frac{l_K}{l}}, & \frac{l_K}{l} > \frac{1}{4} \\ \left(\frac{3\,l}{2\pi\,l_K}\right)^{3/2}\left(1-\frac{5\,l_K}{8l}\right), & \frac{l_K}{l} \le \frac{1}{4} \end{cases} \tag{2.6}$$

In particular, for large l's $p(R|l)$ becomes *nearly* Gaussian (Fig. 2.3, last panel on the left). In striking contrast, the large-l behaviour of $p(R|l)$ for ring polymers is markedly non-Gaussian. In particular, $p(R|l = 120)$ for well equilibrated rings with $N = 500$ are well described (solid lines, last panel on the right of Fig. 2.3) by the classical Redner-des Cloizeaux (RdC) function [55, 56, 57, 58]:

$$\begin{aligned} p(R|l)^{\mathrm{RdC}} &= \frac{1}{\langle R^2(l)\rangle^{3/2}}\, q\left(\frac{R(l)}{\sqrt{\langle R^2(l)\rangle}}\right) \\ q(\vec{x}) &= C\,x^{\theta}\,\exp\left(-Kx^t\right), \end{aligned} \tag{2.7}$$

x being the rescaled length. In this Redner-des Cloizeaux (RdC) ansatz, the two constants C and K are determined by the conditions (1) that the distribution is normalized ($\int q(x)\, 4\pi x^2\, dx \equiv 1$) and (2) that the second moment was chosen as the scaling length ($\int x^2 q(x)\, 4\pi x^2\, dx \equiv 1$): $C = t\, \frac{\Gamma(\frac{5}{2})\Gamma^{\frac{3+\theta}{2}}(\frac{5+\theta}{t})}{3\,\pi^{3/2}\,\Gamma^{\frac{5+\theta}{2}}(\frac{3+\theta}{t})}$ and $K^2 = \frac{\Gamma(\frac{5+\theta}{t})}{\Gamma(\frac{3+\theta}{t})}$. Fit of data with $l = 120$ to the two-parameter RdC function gives the following estimates for θ and t:

$$\begin{aligned} \rho\sigma^3 = 0.1: &\quad \theta = 0.5 \pm 0.1, \quad t = 1.6 \pm 0.1 \\ \rho\sigma^3 = 0.2: &\quad \theta = 0.4 \pm 0.2, \quad t = 1.5 \pm 0.2 \\ \rho\sigma^3 = 0.3: &\quad \theta = 0.3 \pm 0.2, \quad t = 1.5 \pm 0.2 \\ \rho\sigma^3 = 0.4: &\quad \theta = 0.1 \pm 0.2, \quad t = 1.5 \pm 0.2 \end{aligned} \tag{2.8}$$

Interestingly, t appears compatible with 3/2, a result which is consistent with the Fisher-Pincus [59, 60] relationship $t = 1/(1-\nu)$ with $\nu = 1/3$. On the other hand, the excluded-volume exponent [56] θ tends to become small as density increases, suggesting for the asymptotic high-density limit the simple and elegant stretched-exponential form $q(\vec{x}) \sim \exp(-Kx^{3/2})$ with $K = \sqrt{\frac{\Gamma(10/3)}{\Gamma(2)}} \approx 1.667$.

2.3.3 Distribution of Segments About the Center of Mass

We now proceed to examine (Fig. 2.4) the distribution $p(\vec{\delta r})$ of segments about the center of mass of polymers $\vec{\delta r} \equiv \vec{r} - \vec{r}_{\mathrm{cm}}$, whose second moment corresponds to the mean-square gyration radius $\langle R_g^2(L)\rangle$. The results of this study provide another important measure of the average molecular dimensions related to the properties of concentrated solutions.

Let us consider the distribution function $p_l(\vec{\delta r}_l)$ of the distance $\vec{\delta r}_l$ from the center of mass to segment l. All the segments of a linear chain in concentrated solutions are distributed according to a Gaussian distribution function from the center of mass [61],

$$p_j(\vec{\delta r}_j) = \left(\frac{3}{2\pi\langle\vec{\delta r}_j^{\,2}\rangle}\right)^{3/2} exp\left(-\frac{3\vec{\delta r}_j^{\,2}}{2\langle\vec{\delta r}_j^{\,2}\rangle}\right) \tag{2.9}$$

$\langle\vec{\delta r}_l^{\,2}\rangle$ can be evaluated to be:

$$\langle(\vec{\delta r}_l)^2\rangle = 2\langle R_g^2(L)\rangle \left(1 - 3\frac{l}{L}\left(1 - \frac{l}{L}\right)\right) \tag{2.10}$$

with $\langle R_g^2(L)\rangle = l_K L/6$. Equation 2.9 with 2.10 is the formula obtained by Isihara [62] and by Debye and Bueche [63]. It is seen from Eq. 2.10 that $\langle(\vec{\delta r}_l)^2\rangle$ takes the maximum value at $l = 0$ or $l = L$, and the minimum value at $l = L/2$. In other

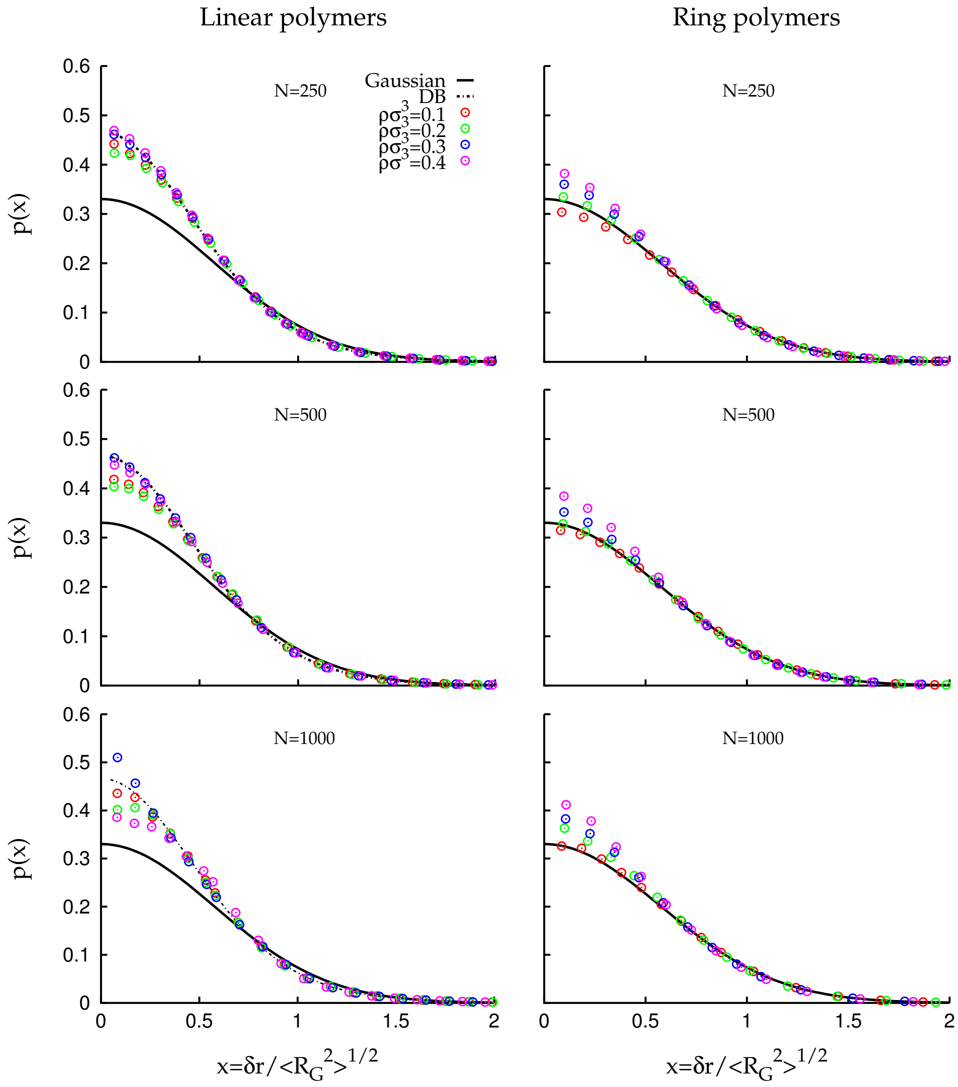

Figure 2.4: Probability distribution function of monomer spatial distances from the chain center of mass, δr (symbols), in comparison to the Gaussian distribution function (black solid lines), Eq. 2.11, and the analytical distribution function by Debye and Bueche (black dashed lines), Eq. 2.12.

words, the end segments are located, on the average, at the positions most remote from the center of mass, while the middle segment is the nearest to the center of mass. Linear chains and rings exhibit different trends. Consistent with the generic result for worm-like chains [63], the Gaussian form underestimates the extension of the molecule in space (black solid lines):

$$p(\vec{\delta r})^G = \left(\frac{3}{2\pi \langle R_g^2(L) \rangle} \right)^{3/2} \exp\left(-\frac{3(\vec{\delta r})^2}{2\langle R_g^2(L) \rangle} \right) , \tag{2.11}$$

and instead $p(\vec{\delta r})$ for linear chains can be well described by the exact analytical prediction by Debye and Bueche [63] (black dashed lines):

$$p(\vec{\delta r})^{\mathrm{DB}} = \frac{1}{L} \int_0^L dl \left(\frac{3}{2\pi \langle (\vec{\delta r_l})^2 \rangle} \right)^{3/2} \exp\left(-\frac{3(\vec{\delta r_l})^2}{2\langle (\vec{\delta r_l})^2 \rangle} \right) , \tag{2.12}$$

Since L is large, the summation in Eq. 2.11 is replaced by integration. Interestingly, distribution functions for ring polymers appear to be much closer to the Gaussian distribution with noticeable deviations in the limit $r \to 0$.

2.3.4 Intrachain Contact Probability

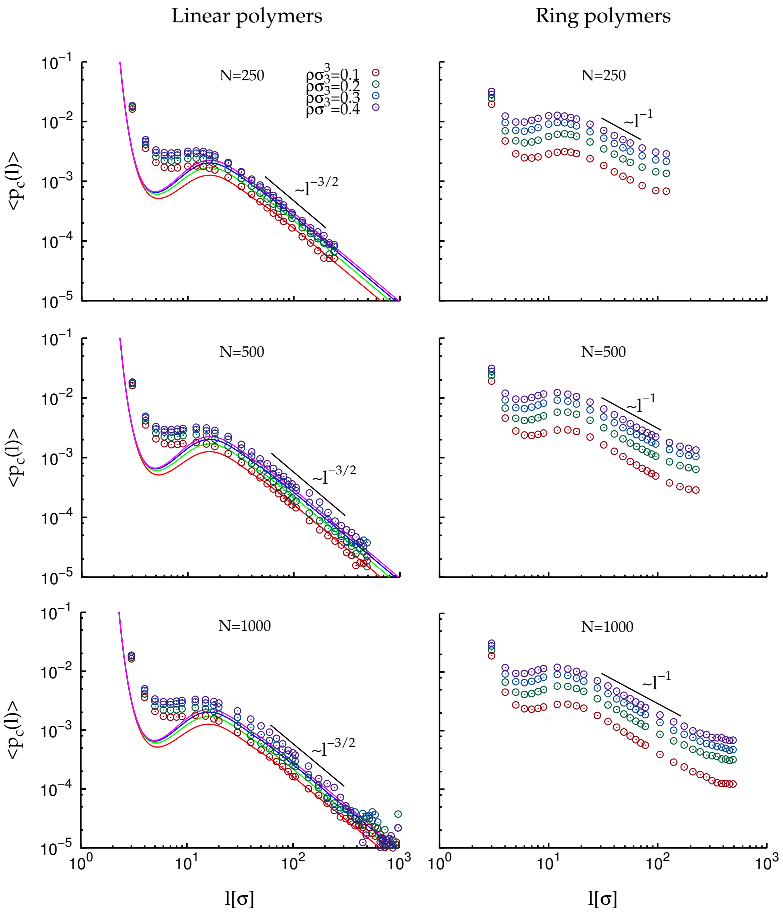

Figure 2.5: Average-square contact frequencies $\langle p_c(l) \rangle$ between monomers at contour length separation, l. Solid lines in left panels correspond to numerical integration of Eq. 2.14 with $p(R|l)$ given by the semi-empirical WLC formula, Eq. 2.5.

It is well known that the loop formation in macromolecules plays an important role in a number of biochemical processes, such as stabilization of globular proteins [64, 65], regularization of genes, and DNA compactification in the nucleus [66, 67]. The loop corresponds to a contact between two monomers i and j, which can be separated by a large distance along the polymer chain. The probability to find a loop of a size $l = |i - j|$ obeys a scaling law,

$$p_c(l) \approx |i - j|^{-\lambda} \tag{2.13}$$

where λ is an exponent that depends on the polymers universality class. For instance in $3d$, Gaussian chains have $\lambda = 1.5$ while for self-avoiding walks we have $\lambda \approx 1.92$ [104, 18]. Hence, polymer complexity has profound influences on the formation of loops between chain loci.

In order to characterize more systematically the interplay between topological constraints and loops, we focus on the contact frequency between chain monomers at contour length separation l, $\langle p_c(l) \rangle$, defined as :

$$\langle p_c(l) \rangle \equiv \frac{\int_{r_{ev}}^{r_c} p(R|l)\, 4\pi R^2 dR}{\int_0^l p(R|l)\, 4\pi R^2 dR}\,, \tag{2.14}$$

where r_{ev} is the distance of closest approach due to intra-monomer excluded volume effects and $r_c = 2\sigma$ is the chosen contact cutoff distance. For both linear and ring polymers $\langle p_c(l) \rangle$ increases as a function of density, Fig. 2.5. For linear chains, this is arguably due to the progressive screening of excluded volume effects. In particular, by using Eq. 2.14 with the WLC expression Eq. 2.3, the long-l behaviour of $\langle p_c(l) \rangle$ can be well reproduced (solid lines in left panels of Fig. 2.5) by the following values for r_{ev}: $r_{ev}/\sigma = 1.6, 1.4, 1.2, 1.0$ for, respectively, $\rho\sigma^3 = 0.1, 0.2, 0.3, 0.4$. At large contour length separations, the contact probability scales as $\langle p_c(l) \rangle \sim l^{-3/2}$ at all densitites, consistent with a random walk conformation. On the contrary, in ring polymers, the observed tendency of $\langle p_c(l) \rangle$ to shift towards higher values is the consequence of rings becoming more and more compact as density increases (Fig. 2.3, right panels). Furthermore, the observed scaling law is different, $\langle p_c(l) \rangle \sim l^{-1}$, compatible with the predictions of crumpled globules [28, 21, 24].

2.3.5 Average Number of Contacts per Chain Monomer

Statics analysis is complemented by considering separately the two contributions to the average number of contacts of each monomer of the chain: the first arising from contacts between monomers along the same chain, $\langle \rho_c \rangle_{\text{intra}}$, and the second arising from contacts between monomers belonging to different chains, $\langle \rho_c \rangle_{\text{inter}}$. The results are shown in Fig. 2.7. As expected, $\langle \rho_c \rangle_{\text{intra}}$ for linear chains, show almost no variation with solution density or chain length, in agreement with the picture that chains remain nearly ideal. On the other hand, $\langle \rho_c \rangle_{\text{intra}}$ for rings increases significantly with density. This effect can not be ascribed to local contacts along the chain (otherwise we should have seen a similar effect for linear chains, too), while it can be easily understood

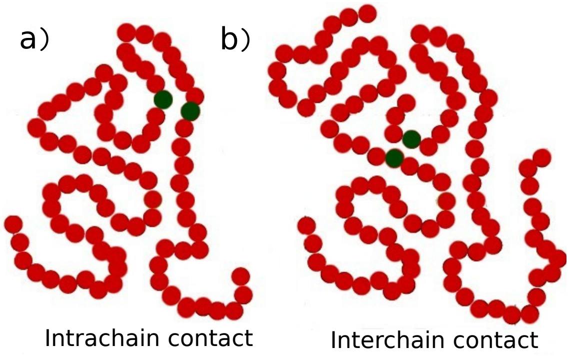

Figure 2.6: Two monomers (in green) of diameter σ along a polymer chain (a) or by another chain (b) are said to be in contact if their center to center distance is smaller than $r_c = 2\sigma$.

in terms of the crumpling of the rings which constrains distal monomers along the chain to move close in space. The second contribution, $\langle \rho_c \rangle_{\text{inter}}$, increases in a similar manner for both linear and ring polymers, demonstrating in particular that crumpling does not prevent a single ring to maintain substantial interactions with its neighbours. As shown in Fig. 2.7, rings are more compact and have (on average) less external contacts.

2.4 Summary and Conclusions

The stochastic Brownian motion of dense solutions of polymer chains is notably conditioned by the property that two chain fragments moving randomly one against the other can not cross each other. These topological constraints (or,entanglements) are expected to dramatically influence chains properties in solutions, compared to the case of single isolated chains. However, while they are assumed to have little or no influence on the structure of linear chains, entanglements affect significantly circular (ring) polymers: due to the non-concatenation constraint. In particular, rings in concentrated solutions are more compact than corresponding configurations of isolated ring polymers.

In this chapter, I have presented the results of Molecular Dynamics computer simulations for the characterization of the statics of semi-flexible linear and ring polymers in semi-dilute solutions. Chains of different sizes and at different solution densities have been considered.

In agreement with the well known picture invoking screening [2] of excluded volume

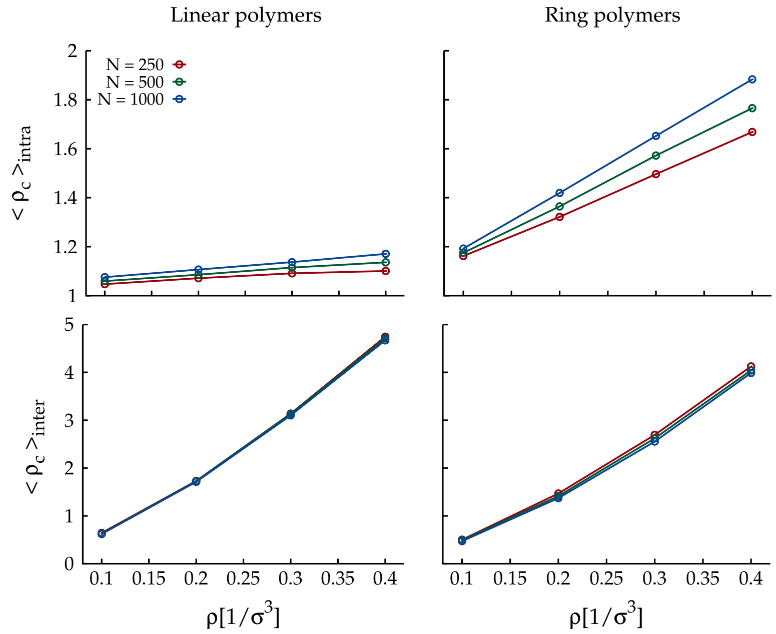

Figure 2.7: Average number of contacts per chain monomer: separate contributions arising from contacts between monomers inside the same chain, $\langle \rho_c \rangle_{\rm intra}$ (top panels), and from contacts between monomers belonging to different chains, $\langle \rho_c \rangle_{\rm inter}$ (bottom panels).

effects, we confirm that linear chains behave as quasi-ideal at all considered densities (Fig. 2.2, left). Conversely (Fig. 2.2, right), ring polymers at same physical conditions tend to become increasingly more compact. These results prompted us to consider the full chain statistics given by the distribution function $p(R|l)$ of spatial distances between the ends of subchain of linear size l (Fig. 2.3): at high densities screening effects in linear chains extend down to small scales and $p(R|l)$ is well described by the worm-like chain statistics. In particular, at large l's chain statistics is almost Gaussian.

On the other hand, chain compaction in rings induces deviations from the ideal statistics at all l's. Interestingly, by describing the large-l behavior of $p(R|l)$ by the classical Redner-des Cloizeaux [55, 56] statistics we suggest that $p(R|l)$ ought to obey the universal stretched exponential form $\sim \exp\left[-1.667 \left(\frac{R(l)}{\langle R^2(l)\rangle^{1/2}}\right)^{3/2}\right]$, which satisfies the Fisher-Pincus relationship [59, 60].

We finalised the description of chain statistics by measuring the frequencies of monomer-monomer interactions inside the same chain (Fig. 2.5) and between different chains

(Fig. 2.7). In particular, we explain the observed increasing of contact frequencies with the solution density (at fixed chain length l) by taking into account the progressive screening of excluded volume effects (for linear polymers) and chain compaction (for ring polymers).

Chapter 3

Ring Polymers as Topological Glasses

The content of this chapter is published on Arxiv, https://arxiv.org/abs/1703.09688

3.1 Background and Motivation

The static properties of rings in solution have been studied for some decades (See Sec. 1.2.1.4). In recent years, accurate computational work [50, 21, 24] reported evidence that in the limit of large N, $\nu \to 1/3$, according with a picture in which rings fold into crumpled-globule-like conformations [26] whose compaction increases with solution density (See also Chapter 2). Later on, Grosberg [69] provided a Flory-like theory in order to depict the scaling of ring polymers in the melt. The theory assumes that the ring forms an effective annealed branched object. He computed its primitive path and it was shown that rings behavior follows self-avoiding statistics and can be characterized by the corresponding Flory exponent of a polymer with excluded volume. In spite of having crumpled conformations, the surface of each ring, *i.e.* the fraction of contour length in contact with other chains, is “rough” [70] and scaling as N^{β} with $\beta \lesssim 1$ [21, 22, 6, 71]. In fact, crumpled rings do not fully segregate or expel neighbouring chains from the occupied space [21], rather, they fold into interpenetrating or “threading” conformations [39, 40] that are akin to interacting “lattice animals” [24] with long-range (loose) loops [72, 73]. Inter-chain penetrations or threadings have always been assumed to play an important role in solutions of rings [32, 4], but in general, it is very challenging to provide a quantitative definition

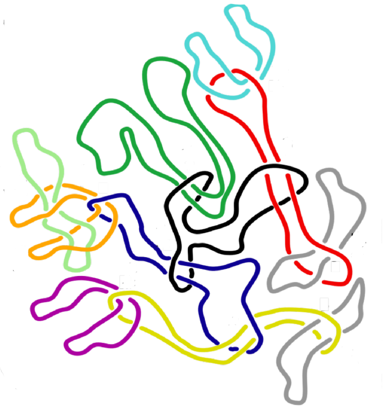

Figure 3.1: Snapshot of a system of rings that are threaded.

of them. As a consequence, the effect of threadings on the dynamics of the rings is even more elusive and for this reason very poorly understood.

It has been suggested that, in the case of dense solutions of ring polymers, the threading of a chain through another, can result in dramatic slowing of the polymer dynamics [41]. Threadings between the rings is suspected to be the main reason of this slowing. While open chains (*e.g.* linear polymers) do not interact in this way (via *threadings*), due to their different topology [3].

In Fig. 3.1, you see a possible configuration where multiple threadings (interpenetrations) are shown. A loop of a ring has passed through another; and when this happens the penetrated loop cannot retract until the first loop has moved back out. This interaction is expected to slow down the dynamics significantly.

Threadings are architecture-specific topological constraints that characterize systems of polymers whose contours display (quenched) closed loops (see Fig. 3.3(A)) [40]. This picture of interpenetrating rings leads to the main topic of this chapter, the topological constraints affect the molecular motion and make the ring polymers resemble a glassy material.

The glass transition of polymers is of great interest in industry. Many commercial products of polymers are indeed used in the glassy state. For example, thermoplastics such as polystyrene and poly(methyl methacrylate) [105]. Despite its great importance in a lot of daily usages, a detailed theoretical description of the glass transition in polymers is missing. Generally speaking, the topological constraints of entangled polymers make them to be excellent glass candidates since the molecular motion can be extremely prohibited, but the mathematics to describe the transition process is inevitably complicated [106].

Recently, theoretical investigations have been put forward that potentially make accessing and testing the behavior of ”glass” states by using concepts borrowed from studies of fluids in porous media. In particular, the physics of a fluid in the presence of a small fraction of randomly pinned particles has been shown numerically [74] and theoretically [75] to share essentially the same glassy physics as bulk supercooled liquids, which justifies more the use of this particular strategy in the context of general studies of glass formation.

Random pinning presents two distinctive features with respect to bulk liquids. Firstly, glassy dynamics and the transition to glassy states occur at temperatures that are higher than in bulk, because pinning a fraction f_p of the particles restricts the available configurational space. Secondly, configurations produced by randomly pinning particles within a thermalized supercooled liquids are, by construction, at thermal equilibrium. Together, these two features suggest that equilibrium configurations created by randomly pinning correspond to a degree of supercooling at finite f_p that can not be reached by conventional means.

Michieletto et al [3], studied a novel glass transition in systems made of ring polymers by exploiting the topological constraints that are conjectured to populate concentrated solutions of rings. They showed that such rings strongly interpenetrate through one another, generating an extensive network of topological constraints that dramatically affects their dynamics. They found out that a kinetically arrested state can be induced by randomly pinning a small fraction of the rings, interestingly linear polymers were substantially insensitive to this perturbations. [3].

This work [3] suggested that in rings, at a constant solution density ρ, a putative glassy state is achieved by randomly pinning a fraction of rings, f_p, above an empirical “critical” value (see Fig.3.2):

$$f_p^{\dagger}(N) = -f_N \log\left(\frac{N}{N_g}\right), \tag{3.1}$$

where N_g is the theoretical length required for spontaneous ($i.e.$, $f_p \to 0$) vitrification and f_N a non-universal parameter.

Here, we shall adopt a strategy similar to this work [3], i.e., by randomly pinning different fraction of the rings. We rather varied the monomer density of the solutions and probed its effect on the dynamics of the unpinned chains. We try to extract the functional form of the dependence of the critical fraction of the pinned rings $f_p^{\dagger}(\rho)$ on

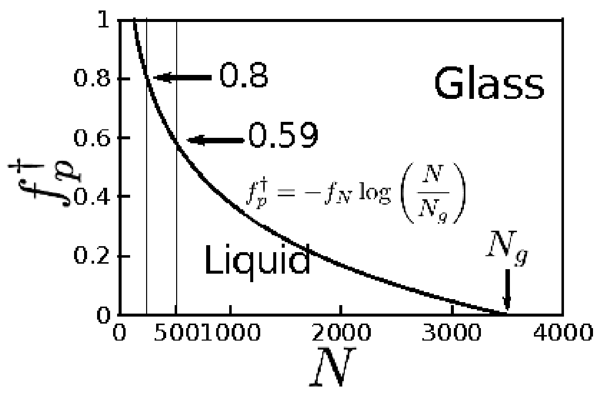

Figure 3.2: Phase diagram for solutions of semi-flexible ring polymers at monomer density $\rho = 0.1\sigma^{-3}$ [3]. The two vertical lines represent the values of N chosen in this chapter and the intersections $f_p^\dagger = -f_N \log(N/N_g)$ are the predicted values of $f_p^\dagger(\rho)$ for the onset of glassiness at $\rho = 0.1\sigma^{-3}$. N_g is the (empirical) value at which the system is expected to display the onset of topological freezing at zero pinning fraction.

the solution density and see if it is sharing any similarities with Eq. 3.1.
Topological freezing is the consequence of the proliferation of inter-ring constraints [40, 3], with the latter depending either on the polymerization index, N, or the density of the solution, ρ. While it has been shown that longer rings generate more topological constraints [3], it remains unclear how they behave if solutions become denser, rings more crumpled [70] and less space is available to threading.

Motivated by these considerations, in this chapter we study the effect of topological constraints by "randomly pinning" solutions of semi-flexible ring polymers, and probe the dynamic response of the rings for different solution densities and chain lengths. We show that the threshold pinning fraction $f_p^\dagger$ obeys an empirical relation akin to Eq. (3.1) and we derive universal scaling relations for the values of N_g and ρ_g at which spontaneous ($f_p \to 0$) glassiness is expected. We further discuss the dynamics of rings in terms of ensemble- and time-average observables and report, for the first time, numerical evidence for ergodicity breaking effects and pronounced heterogeneous non-Gaussian dynamics, even in unperturbed ($f_p = 0$) solutions.

3.2 Our Model System

Similarly to Chapter. 2, equilibrated solutions of ring polymers are prepared by avoiding unwanted linking between close by rings, the chains were initially arranged inside a large simulation box at very dilute conditions. In order to reach the correct monomer density of $\rho\sigma^3 = 0.1$ we performed then a short ($\approx 400\,\tau_{\mathrm{LJ}}$) MD simulation under fixed external pressure which shrinks the simulation box until it reaches the desired value. Similarly, the other densities were reached by compressing the solutions under even higher imposed pressures. Once any given system was prepared at the correct density, we switched to the NVT ensemble (see for more details Section 2.2.1). Each system was equilibrated by performing single MD runs up to $1 \cdot 10^9 \Delta\tau = 12 \cdot 10^6 \tau_{\mathrm{LJ}}$ (for $N = 250$) and $2 \cdot 10^9 \Delta\tau = 24 \cdot 10^6 \tau_{\mathrm{LJ}}$ (for $N = 500$), during which the center of mass of each chain moves on average a distance comparable to $\approx 3 - 4$ times its corresponding gyration radius, R_g. After equilibration, ring dynamics was studied by performing MD simulations up to $1 \cdot 10^9 \Delta\tau = 12 \cdot 10^6 \tau_{\mathrm{LJ}}$ for both $N = 250$ and $N = 500$. We studied systems with different pinning fractions f_p of the total number of rings in the range $f_p = 0.1 - 0.7$. For reference, nonfrozen rings solutions are then considered i.e., at zero pinning fraction $f_p = 0$.

3.3 Results and Discussions

3.3.1 Dynamics of Ring Polymers in Solutions

The dynamics of a single non-frozen ring is captured by the mean-square displacement of its center of mass, $g_3(T, \Delta)$, as a function of the lag-time Δ and measurement time T [3]:

$$g_3(T, \Delta) \equiv \frac{1}{T - \Delta} \int_0^{T-\Delta} \left[\boldsymbol{r}_{CM}(t + \Delta) - \boldsymbol{r}_{CM}(t)\right]^2 dt\,. \tag{3.2}$$

The time-average displacement can be defined as $g_3(\Delta) \equiv \overline{g_3(T, \Delta)}$ while its ensemble average as

$$\langle g_3(T, \Delta)\rangle \equiv \frac{1}{M_f} \sum{}' g_3(T, \Delta)\,, \tag{3.3}$$

with $\sum{}'$ indicating that the average is performed over the set of M_f "free",*i.e.* not explicitly pinned rings. Accordingly, we indicate the time- *and* ensemble-average displacement as $\langle g_3(\Delta)\rangle$. Fig. 3.3(B,C,D) directly compare the behaviour of $\langle g_3(\Delta)\rangle$ in response to the random pinning of different fractions f_p of rings. For unperturbed solutions ($f_p = 0$), the curves show a crossover from sub-diffusive ($\langle g_3(\Delta)\rangle \sim \Delta^{3/4}$) to diffusive ($\langle g_3(\Delta)\rangle \sim \Delta$) behaviour [4, 5, 6]. Perturbed systems, instead, display a reduced average diffusion, the more severe the higher the value of f_p. In particular, for

f_p larger than $f_p^\dagger(\rho, N)$, the average displacement remains well below one ring diameter (marked by the horizontal dashed lines) and does not diverge in time, indicating [3] a solid-like (glassy) behaviour. Furthermore, we observe that $f_p^\dagger(\rho, N)$ decreases as a function of both, ring length N [3] and, unexpectedly, monomer density ρ. Other $\langle g_3(\Delta) \rangle$ measurements are shown in Fig. 3.4.

As demonstrated in Chapter. 2, rings compactify when the system density is increased. In turn, this would imply that less intra-chain space is available for inter-penetrations which could lead the system to a state where fewer rings are affected by the "random pinning" procedure. Ultimately, this argument leads to the conjecture that denser systems of rings would make, if at all, less effective "topological glasses" while what we observe in Fig. 3.3 is that denser solutions make better topological glasses.

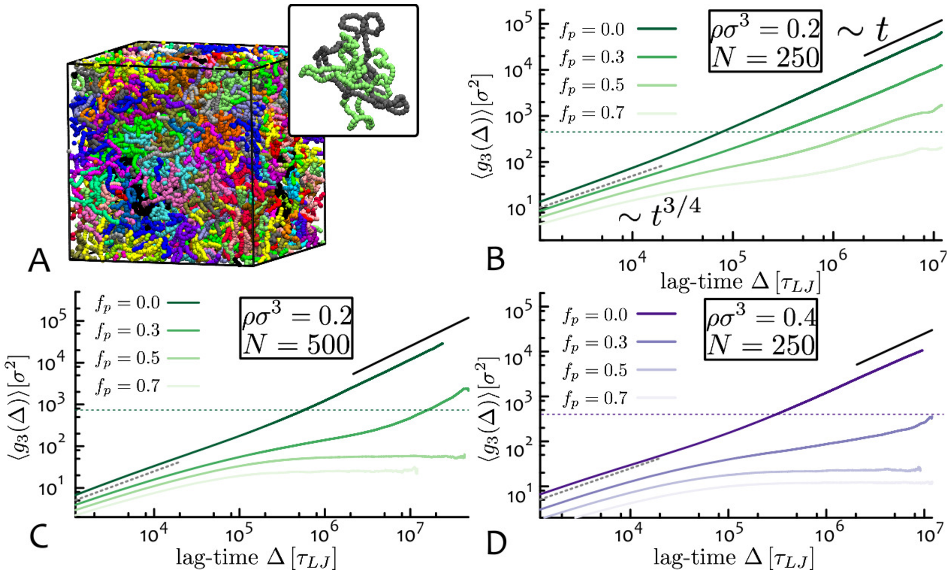

Figure 3.3: **Random Pinning Triggers Slowing Down and Glassiness.** (**A**) Typical melt structure for rings of $N = 250$ monomers with $f_p = 0$ and $\rho = 0.2\sigma^{-3}$. Inset: Two rings isolated from the melt and showing mutual threading. (**B,C,D**) Mean-square displacement of rings centre of mass, $\langle g_3(\Delta) \rangle$ (Eq. (3.3)) as a function of lag-time Δ for ring solutions with selected N and ρ. Rings display glassy behaviour (suppressed diffusion, $\langle g_3(\Delta) \rangle \sim \Delta^0$) for $f_p > f_p^\dagger$ where $f_p^\dagger$ is found to decrease with both, N and ρ. Dashed horizontal lines are for the mean-square ring diameter, $4\langle R_g^2 \rangle$.

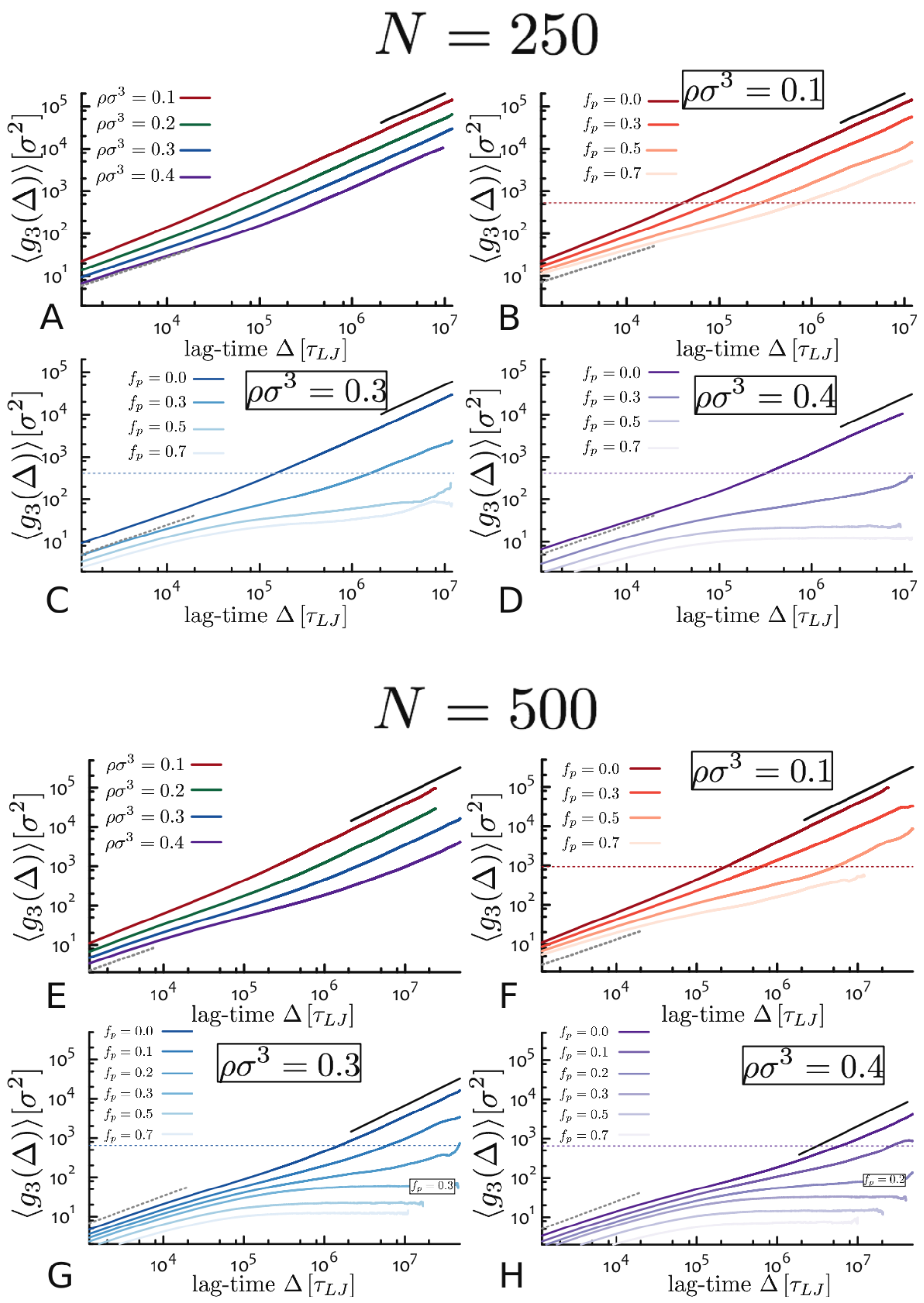

Figure 3.4: **Dynamics of Ring Polymers in Solutions of Density ρ and Ring Pinning Fraction f_p.** The curves correspond to the mean-square displacement of ring center of mass, $\langle g_3(\Delta)\rangle$, at lag-time Δ, and for chain sizes $N = 250$ and $N = 500$. Solid black lines correspond to the long-time diffusive ($\sim \Delta^1$) regime, whereas dashed grey lines represent the short-time sub-diffusive ($\sim \Delta^{3/4}$) regime [4, 5, 6]. Dashed horizontal lines in panels B-D and F-H are for corresponding mean-square ring diameters, $4\langle R_g^2\rangle$.

3.3.2 Exponential Slowing Down: Phase Diagram and Universality

In order to obtain the functional form of $f_p^\dagger(\rho, N)$, firstly, the asymptotic diffusion coefficient $D(\rho, f_p) \equiv \lim_{\Delta\to\infty}\langle g_3(\Delta)\rangle/6\Delta$ at given $(N,\,\rho,\,f_p)$ is computed by best fit of the long-time behaviour of the corresponding $\langle g_3(\Delta)\rangle$ to a linear function. Fig. 3.5 show $D(\rho, f_p)/D_0(\rho)$ – where $D_0(\rho) \equiv D(\rho, f_p = 0)$ – as a function of f_p. Corresponding datasets are well fitted by exponential functions $\exp(-kf_p)$.

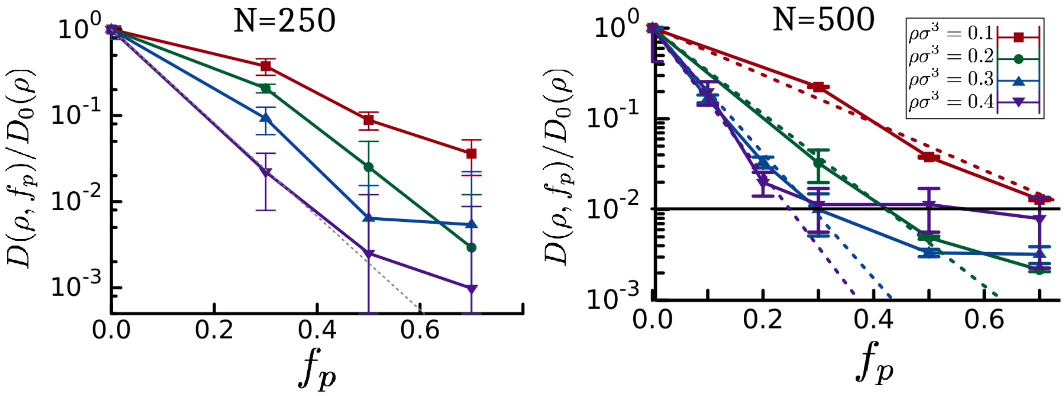

Figure 3.5: **Exponential Slowing Down and Universal Phase Diagram.** $D(\rho, f_p)/D_0(\rho)$ is compatible with exponential decay (dashed line) in f_p. An arbitrarily small (0.01) value is chosen to determine the transition to glassy behaviour [3]. For high densities and large f_p, the reported values are overestimates due the insufficient length of simulation runs.

We now can extract $f_p^\dagger(\rho, N)$ by finding their intersection with a convenient small value of 0.01 (The same value that was chosen in [3]), *i.e.*, the data points are obtained by fitting $D(\rho, f_p)/D_0(\rho)$ with an exponential function $d(f_p) = \exp(-f_p/a)$ and by solving $d(f_p) = 0.01$. The obtained "critical" lines $f_p^\dagger(\rho, N)$ (see Fig. 3.6) separate regions of the parameter space (ρ, f_p) with finite (liquid) and vanishing (glassy) diffusion coefficients. This gives the "critical" $f_p^\dagger$ at fixed ρ and N. The functional dependence appears to follow an empirical scaling relation similar to that found for N, *i.e.*,

$$f_p^\dagger(\rho, N) = -f_\rho \log\left(\frac{\rho}{\rho_g}\right). \tag{3.4}$$

where $\rho_g(N = 250) = 0.84 \pm 0.05$ and $\rho_g(N = 500) = 0.56 \pm 0.05$ are the theoretical threshold densities for the spontaneous onset of glassiness. Both curves have $f_\rho = 0.43$

suggesting that this parameter depends very weakly on N or ρ. It is rather intriguing that the functional form of the dependence of the critical fraction of pinned rings on the chain length (Eq. 3.1), is identical to its functional dependence on the density Eq. 3.4. As a consequence, what we found was that the data points collapse onto a master curve by plotting $f_p^{\dagger}(x = \rho/\rho_g(N))/f_\rho = -\log(x)$ (see Fig. 3.7). Thus, our data for $N = 250$ and $N = 500$ can be collapsed onto a master curve with $f_\rho = 0.44 \pm 0.05$. Given that both, Eqs. 3.1 and 3.4, describe the same quantity, we argue that their right-hand-side must also be equal. By combining them under the assumption that the only dependence on ρ is contained in N_g, the values of ρ_g and N_g for spontaneous *topological* vitrification obey the following universal scaling relations

$$\rho_g(N) \sim N^{-\eta}\,,\;\; N_g(\rho) \sim \rho^{-1/\eta}\,, \tag{3.5}$$

with $\eta = f_N/f_\rho = 0.68 \pm 0.1$ (using $f_N = 0.30 \pm 0.05$ from [3]).

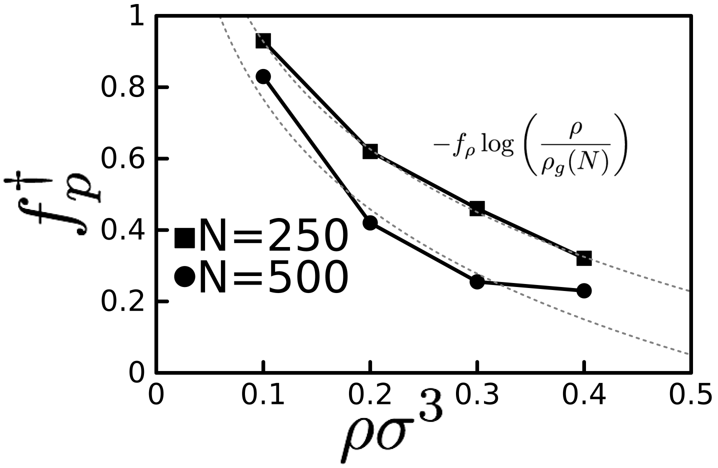

Figure 3.6: Phase diagram in the plane $(f_p, \rho\sigma^3)$ for the ring solutions studied in this chapter.

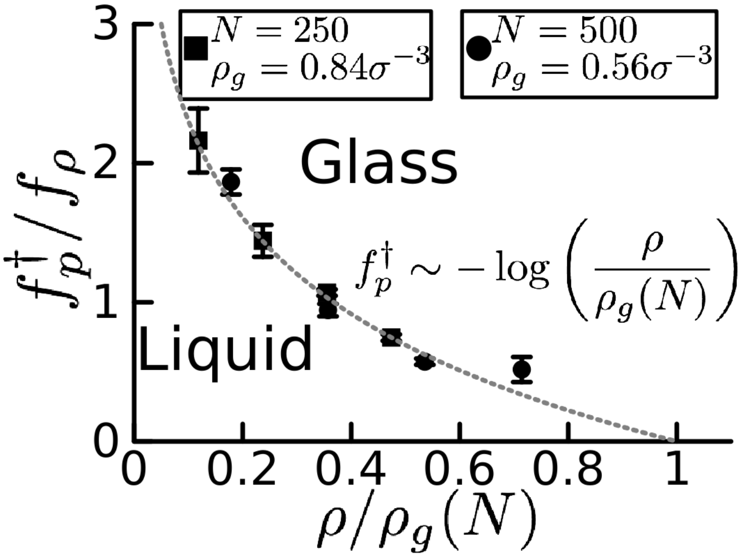

Figure 3.7: Curve for $f_p^\dagger(\rho, N)/f_\rho$ as a function of $\rho/\rho_g(N)$ (see Eq. (3.4)) showing collapse onto the universal curve $-\log(x)$ for $N = 250$ and $N = 500$ data and with $f_\rho = 0.44 \pm 0.05$, $\sigma^3\rho_g(N = 250) = 0.84 \pm 0.05$ and $\sigma^3\rho_g(N = 500) = 0.56 \pm 0.05$.

To validate our argument we can also make use of the results presented in [3] and extract the value of $A = \rho^{1/\eta} N_g$, which is the prefactor of the Eq. 3.5. It should be constant and equal to the one obtained in this work (through the equation $\rho_g(N) = A^\eta N^{-\eta}$) if the scaling relation is universal. Using $N_g(0.1) \simeq 3500$ [3] one obtains a value for A in the range $A = 3500(0.1)^{1/\eta} \simeq 66 - 182$, or $A^\eta \simeq 11 - 57$ (with $\eta = 0.68$ one gets $A \simeq 118$ and $A^\eta \simeq 25$), whereas fitting of the values of $\rho_g(N)$ found in this work ($\rho_g(N = 250) = 0.84 \pm 0.05$ and $\rho_g(N = 500) = 0.56 \pm 0.05$) against N with a power law gives a constant $A^\eta = 22.1$ and a decay with an exponent of $\eta = 0.6$ (no error can be obtained as we have only two points).

These values of η are in agreement with one another, and are obtained (almost) independently (we make use of the value of η obtained here to get the value of A from the results of [3]). By making use of these values of η and A one can then predict a value for the "critical" polymerisation index N_g for high density systems in the range $N_g(\rho = 0.3) = A(0.3)^{-1/\eta} \simeq 520 - 850$ and $N_g(\rho = 0.4) = A(0.4)^{-1/\eta} \simeq 320 - 600$.

In light of these clarifications, I would like to point out that these results are in agreement with the fact that the systems with $\rho\sigma^3 = 0.3 - 0.4$ and $N = 500$ are very close to the predicted N_g and are therefore expected to display spontaneous deviations from the typical behaviours of rings observed at low density or short lengths. In addition to this, a transition to vitrification in these systems is not expected to occur abruptly. In fact, one can speculate that systems close to the topological freezing point may be very sensitive to small (and/or temporary) pinning perturbations and freezing even a very small fraction of rings may tip the system beyond the transition. On the other hand, we do not expect that rings close to the transition line will suddenly stop diffusing spontaneously (at least in simulations). In fact, these systems are initialised from a situation in which there are no threadings at all (rings are ordered and their contours non-overlapping) and are let equilibrate for long time. Since we report that unpinned systems ($f_p = 0$) display large-time diffusion at any density and polymer lengths (Fig. 3.3), we may argue that this long initial equilibration time may still not be enough to allow the system to reach the equilibrium value for the total number of inter-penetrations in the system. Whereas other observables quickly evolve towards their steady state (say, the rings gyration radius), threadings may be more slow to evolve (unfortunately, at present we cannot monitor the number of threadings in these systems as we do not currently have an algorithm to directly detect inter-penetrations in the melt). This argument is supported by the self-consistent observation that the more threadings populate the system, the slower its dynamics (also towards steady state), as it was previously shown [39, 76, 71]. In turn, this implies that our pinning perturbation may be applied to systems in which threadings are *en route* to equilibrium, and is therefore expected to be less effective than in systems with equilibrated threadings.

3.3.3 Non-Gaussian Response of Pinned Ring Systems

We now turn our attention on the role of topological constraints in the dynamics of single rings. To this end, we consider the distribution of $1d$ displacements, $P(\Delta x) = \langle \delta(\Delta x - |x(t+\Delta) - x(t)|)\rangle$, which corresponds to the self-part of the van-Hove function [77, 78]. Because the system is isotropic, we can average the above function along all three space directions. From this function one should be able to extract information about different populations, i.e., if there exist different "typical" travel distances in the system. It provides a direct measure of the dynamical behavior of the system. For definitiveness, we focus exclusively on the "special" and physically relevant *crossover* lag-time $\Delta = \Delta_c$, in which rings in unpinned systems ($f_p = 0$) have moved a distance equal to their average size: $\langle g_3(\Delta_c)\rangle \equiv 4\langle R_g^2\rangle$ (see dashed lines in

Fig. 3.3).

For purely diffusing particles, the distributions of rescaled displacements $X \equiv \Delta x/\sqrt{\langle \Delta x^2 \rangle}$ are expected to be described by the universal Gaussian function with zero mean and unit variance [77]. Here, instead, two additional features emerge: First, a prominence of rings with short "cage-like" displacements, identified by the region centred around $X = 0$ where $P(X)$ remains above the Gaussian. Second, the appearance of a sub-population of rings traveling faster than the average ring, giving rise to "fat" exponential tails. Intriguingly, both are akin to features observed in generic systems of particles close to glass and jamming transitions [78]: accordingly, here they appear either in perturbed solutions of short rings (Fig. 3.8(B,C)) or in unperturbed systems close to the critical length $N_g(\rho)$ (see Eq. (3.5), Fig. 3.8(D)). Thus, we claim that the non-Gaussian behaviour reported here is manifestly triggered by pinning perturbations, arguably via threading TCs. Further, we conjecture that threading configurations may also account for the spontaneous caging observed in

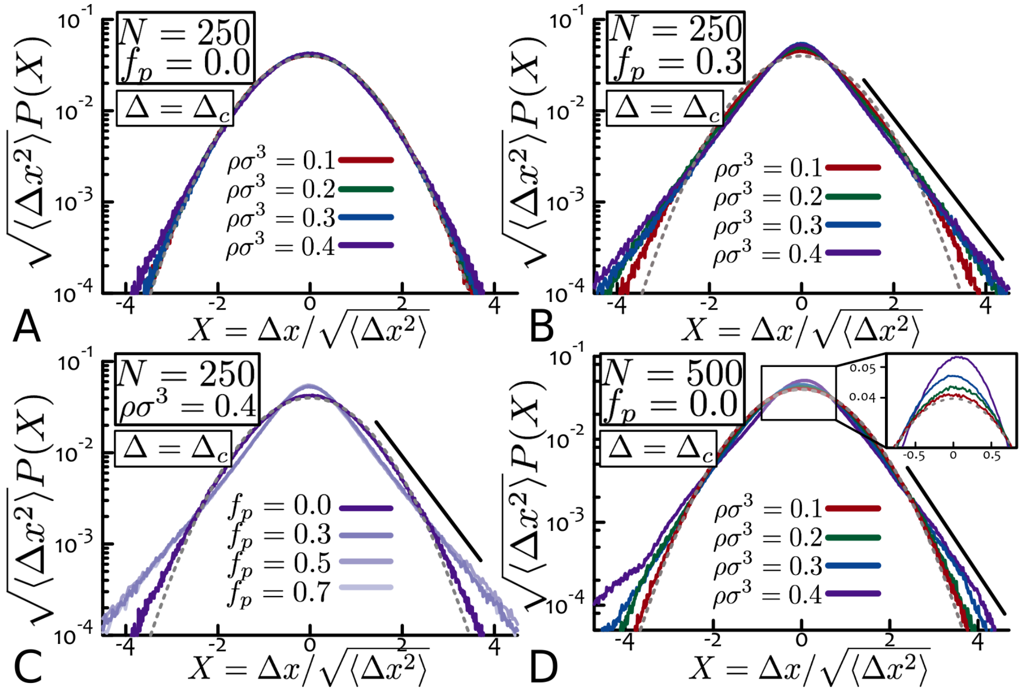

Figure 3.8: **Distributions of Displacements are non-Gaussian.** Distribution functions, $P(X)$, of $1d$ scaled displacements of the centers of mass of non-pinned rings, $X \equiv \Delta x/\sqrt{\langle \Delta x^2 \rangle}$, at lag-times Δ. $P(X)$ is described by a Gaussian function with zero mean and unit variance (dashed lines) in non-pinned systems (**A**), while it displays caging and fat, exponential tails (solid lines) in pinned solutions (**B**,**C**). (**D**) Deviations from Gaussian behaviour (exponential tails) are also observed in unperturbed solutions with $N = 500$ and $\rho\sigma^3 \geq 0.3$.

unperturbed solutions at large ρ's and $N = 500$ (Fig. 3.8(D)). We then argue that threadings may in general be responsible for the cage-like, non-Gaussian, motion of synthetic ring polymers seen in experiments [5]. Transient threadings between rings may act as temporary cages [39], which are the more long-lived the denser the solutions and the longer the rings [3, 41, 76].

The non-Gaussian behaviour reported here is manifestly triggered by pinning perturbations (Fig. 3.8(C)), arguably via threading topological constraints. Similarly, threading configurations may also account for the (weaker) non-Gaussian behaviour observed in unperturbed ($f_p = 0$) solutions at large ρ's and $N = 500$ (Fig. 3.8(D)). Threadings may in general be responsible for the cage-like, non-Gaussian, motion of large PEO ring polymers seen in experiments [5]. In that work, they synthesized highly pure hydrogeneous (h) and deuterated (d) poly- ethylene oxide (PEO) rings of different molecular weights. They observed a pronounced non-Gaussian behavior for the *c.m.* motion of the rings.

Transient threadings between rings may in fact act as temporary cages [73], and our findings suggest that they are the more long-lived the denser the solutions and the longer the rings. To our knowledge, it is the first time that threadings and non-Gaussian behaviour are explicitly connected and present even in the zero-pinning limit (Fig. 3.8(D)).

3.3.4 Heterogeneity in Entangled Solutions of Ring Polymers

In order to better understand deviations from Gaussian behaviour, we now examine time-average quantities of single ring trajectories. In Fig. 3.10(A,B) we report $g_3(T, \Delta_c)$, *i.e.* the centre of mass displacement of single rings at fixed lag-time $\Delta = \Delta_c$ and increasing measurement time T(see also Fig.3.11). Importantly, we show that unperturbed solutions of short rings display $\lim_{T\to\infty} g_3(T, \Delta_c) = \langle g_3(\Delta_c)\rangle$, *i.e.* every ring tends to travel at the same average speed (Fig. 3.10(A), $f_p = 0$). Conversely, pinning triggers heterogeneity in the trajectories which thus cluster into distinct sub-populations of fast- and slow-moving rings (Fig. 3.10(A) and Fig. 3.11) with well defined diffusivities. While slow rings reflect the presence of cages, there are also examples of rings displaying temporally-heterogeneous dynamics alternating from slow to fast diffusion (Fig. 3.10(A), gray line). Taken together, these observations agree with the concept of permanent or transient caging due to threading TCs.

Another distinct feature of weakly non-ergodic processes and heterogeneous diffusion type is the fact that time averaged observables become random quantities even in the long time limit and thus display a distinct distribution of amplitudes between individual realisations for a given lag time. This irreproducibility due to the scatter of individual traces around their mean is described by the ergodicity breaking parameter [110] which is defined as:

$$EB(T) \equiv \frac{[\langle g_3(T,\Delta_c)^2\rangle - \langle g_3(T,\Delta_c)\rangle^2]}{\langle g_3(T,\Delta_c)\rangle^2}\,, \tag{3.6}$$

which captures how fast the single-ring trajectories $g_3(T,\Delta_c)$ narrow around the mean $\langle g_3(\Delta_c)\rangle$. For standard diffusive solutions, $EB(T) \sim T^{-1}$ [7] whereas non-ergodic systems display $EB(T) \sim T^0$ [79]. As shown in Fig. 3.10(C) (see also Fig. 3.12) ergodicity breaking can indeed be triggered by random pinning.

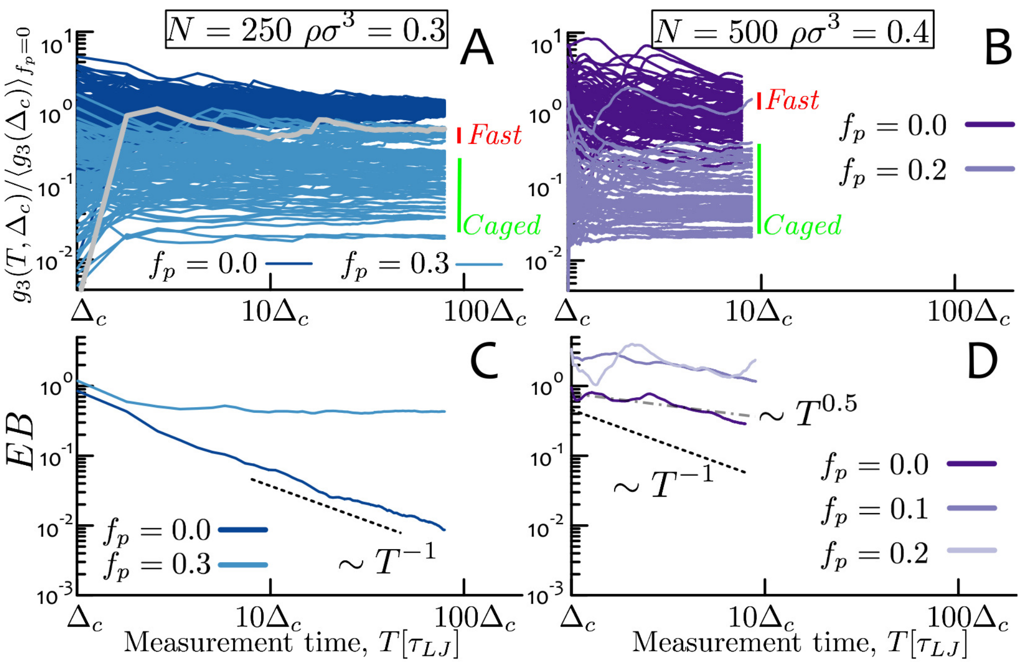

Figure 3.10: **Heterogeneity and Ergodicity Breaking.** (**A,B**) Representative curves for $g_3(T,\Delta_c)/\langle g_3(\Delta_c)\rangle_{f_p=0}$ at fixed lag-time $\Delta = \Delta_c$ as a function of measurement time T displaying spatial and temporal (grey trace) heterogeneity. (**C,D**) Corresponding ergodicity-breaking (EB) parameters (Eq. (3.6)). "T^{-1}"-decay marks standard diffusive processes, whereas "T^0" is a signature of ergodicity-breaking. The system with $N = 500$ at the highest density $\rho\sigma^3 = 0.4$ shows weaker convergence $\sim T^{-0.5}$ even at $f_p = 0$.

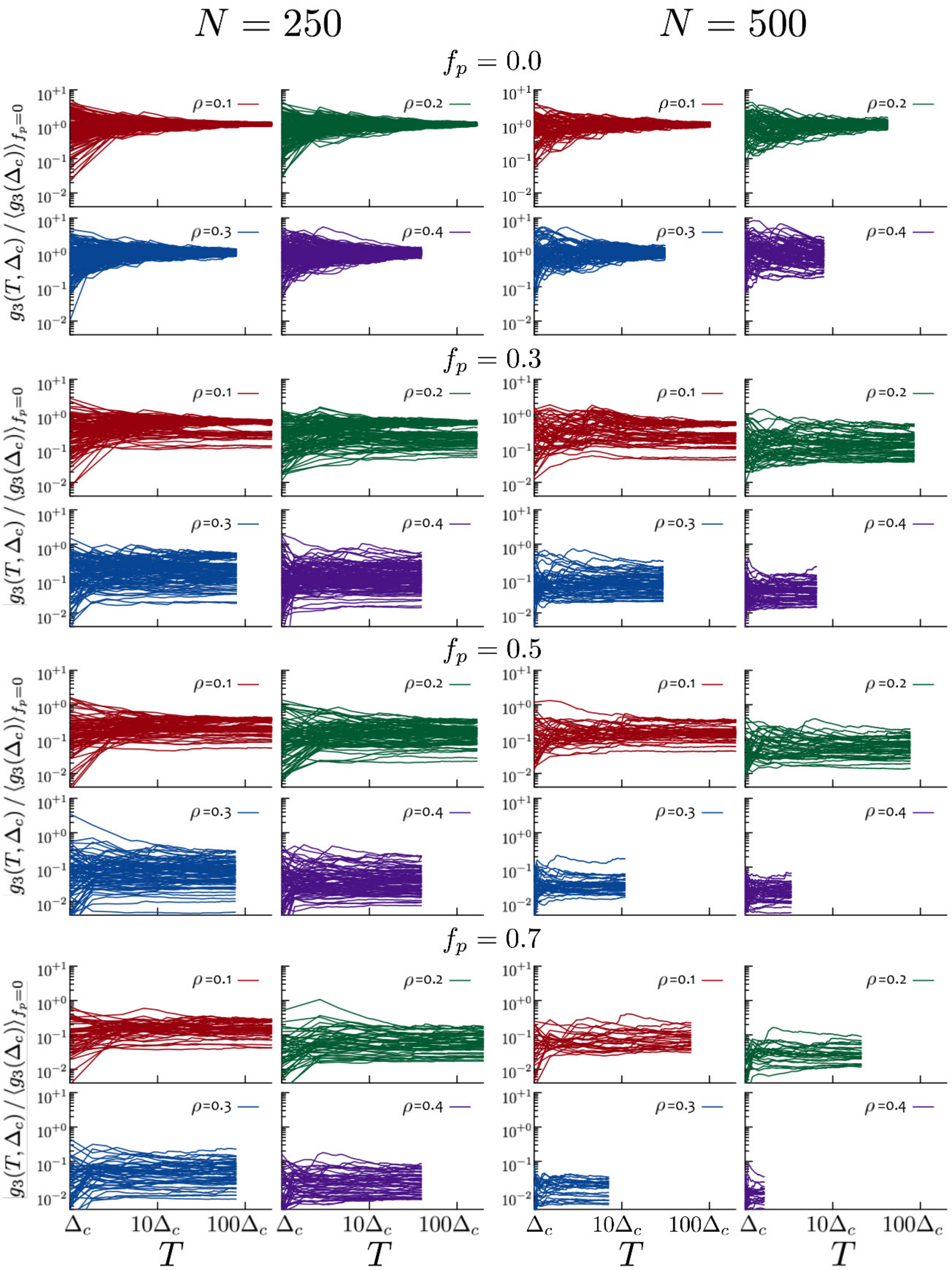

Figure 3.11: **Ageing Properties of Single-Ring Motion (A).** $g_3(T, \Delta = \Delta_c)/\langle g_3(\Delta = \Delta_c)\rangle_{f_p=0}$ *vs.* measurement time T at *fixed* lag-time Δ_c. Δ_c is defined as $\langle g_3(\Delta_c)\rangle_{f_p=0} = 4\langle R_g^2\rangle$, namely it corresponds to the (crossover) lag-time for unperturbed rings to move by a distance equal to the corresponding mean ring diameter.

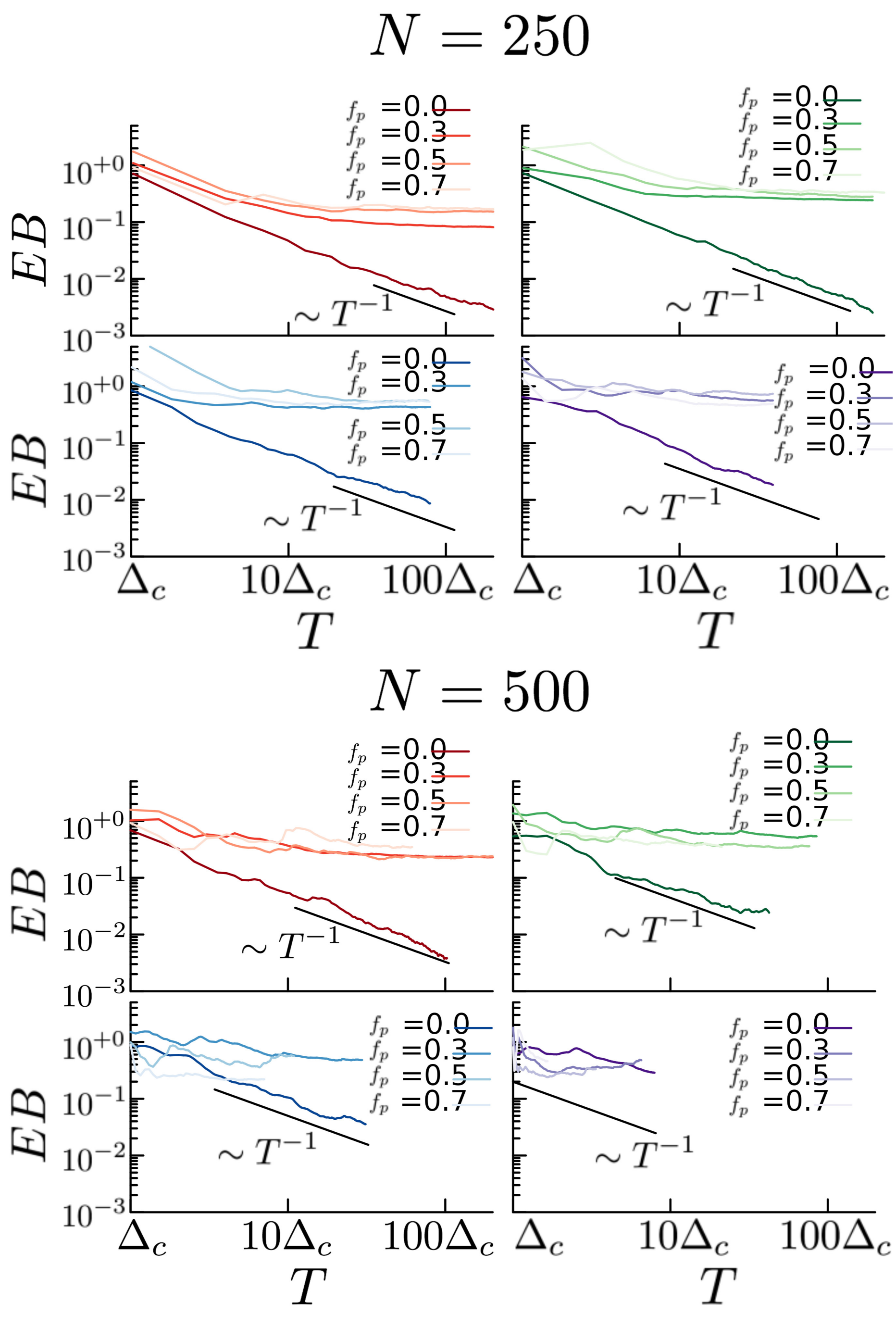

Figure 3.12: **Ergodicity-Breaking of Single-Ring Motion.** Ergodicity-breaking (EB) parameter defined as [7, 110]: $EB = EB(T) \equiv [\langle g_3(T, \Delta = \Delta_c)^2 \rangle - \langle g_3(T, \Delta = \Delta_c) \rangle^2] / \langle g_3(T, \Delta = \Delta_c) \rangle^2$. In general, the heterogeneity in g_3 decreases with measurement time as T^{-1} for unperturbed systems, as expected for standard diffusion. On the other hand, for perturbed ($f_p > 0$ systems), EB flattens and the system displays heterogeneous dynamics and ergodicity breaking. Δ_c corresponds to the (crossover) lag-time defined in Fig. 3.11.

Remarkably and again in agreement with the predictions of Eq. (3.5), unperturbed ($f_p = 0$) solutions of rings with $N = 500$ and monomer density $\rho = 0.4\sigma^{-3}$ show little if no decay (Fig. 3.10(D)), thereby suggesting non-standard statistics in the waiting times of diffusing rings [79, 7].

To our knowledge, this is the first instance that spontaneous caging (Fig. 3.8D) and deviations from Gaussian ergodic convergence (Fig. 3.10D) are directly observed in unperturbed solutions of polymers (of any topology).

3.3.5 Cluster Analysis in Ring Polymer solutions

In order to detect populations of rings with different dynamics, we apply the clustering algorithm `FindClusters` embedded in Mathematica [80] with Euclidean metric to the values of $g_3(T_{max}, \Delta_c)$ for the largest measurement time $T = T_{max}$. `FindClusters` treats pairs of elements as being less similar when their distances are larger and by default uses a squared Euclidian distance. In general, the algorithm detects the presence of a few clusters (4, at most) in most of the cases. In other cases ($N = 500$, $\rho\sigma^3 = 0.4$ and $f_p = 0.0$ for instance) different clusters have markedly different diffusivities.

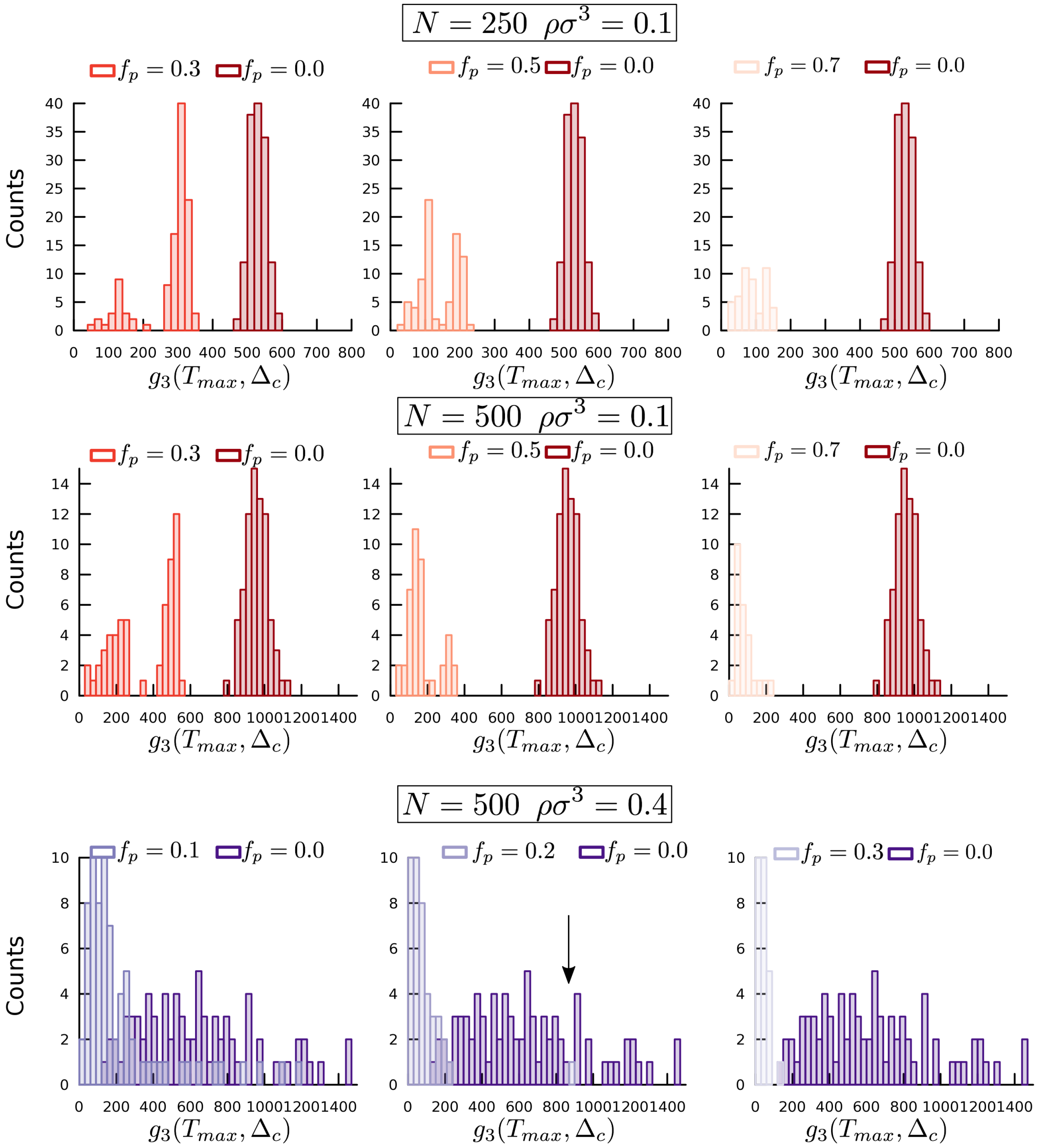

Figure 3.13: **Distributions of Displacements, $g_3(T_{max}, \Delta_c)$, at the Largest Measurement Time $T = T_{max}$ and Lag-Time $\Delta = \Delta_c$.** In general, pinning splits the distributions into a small number of sub-populations which may be aptly identified by cluster analysis (see Sec. 3.3.5). Here, the arrow points to the only fast ring in the system for $N = 500$, $\rho\sigma^3 = 0.4$ and $f_p = 0.2$.

Overall, these observations agree with numerical distributions of $g_3(T_{max}, \Delta_c)$ (Fig. 3.13) and the reported decays of corresponding EB parameters (Fig. 3.12). This analysis has been further complemented by calculating the average diffusivity of each cluster and the associated standard deviation. Then, the physical significance of detected clusters has been checked by measuring the average value and standard deviation of $g_3(T_{max}, \Delta_c)$ in each cluster. A summary of the cluster analysis is presented in Table 3.1.

$N = 250$		
$\rho\sigma^3$	f_p	#rings/cluster ($\overline{g_3(T_{max}, \Delta_c)} \pm$ SD)
0.1	0.0	160 (530.2 ± 22.5)
	0.3	90 (308.1 ± 17.9), 22 (125.3 ± 40.0)
	0.5	44 (93.7 ± 25.5), 36 (196.2 ± 12.1)
	0.7	30 (65.9 ± 21.2), 18 (132.5 ± 12.3)
0.2	0.0	160 (412.1 ± 20.8)
	0.3	60 (219.7 ± 15.3), 52 (75.0 ± 26.5)
	0.5	40 (69.4 ± 12.4), 26 (31.6 ± 10.5), 14 (133.9 ± 10.8)
	0.7	32 (19.3 ± 7.3), 16 (51.9 ± 12.4)
0.3	0.0	160 (411.4 ± 38.4)
	0.3	45 (90.1 ± 11.9), 44 (37.5 ± 15.5), 23 (193.5 ± 24.0)
	0.5	80 (37.5 ± 28.1)
	0.7	48 (24.3 ± 18.0)
0.4	0.0	52 (411.9 ± 12.0), 47 (371.9 ± 11.0), 33 (321.9 ± 21.2), 28 (476.5 ± 29.6)
	0.3	75 (33.2 ± 14.5), 37 (107.8 ± 40.0)
	0.5	59 (12.3 ± 5.7), 21 (44.8 ± 19.3)
	0.7	21 (4.7 ± 1.5), 17 (12.0 ± 2.5), 10 (24.8 ± 4.8)

$N = 500$		
$\rho\sigma^3$	f_p	#rings/cluster ($\overline{g_3(T_{max}, \Delta_c)} \pm$ SD)
0.1	0.0	50 (920.1 ± 39.7), 30 (1015.2 ± 33.8)
	0.3	30 (498.2 ± 27.8), 26 (176.0 ± 63.1)
	0.5	32 (130.9 ± 37.8), 8 (317.0 ± 21.0)
	0.7	12 (45.5 ± 10.8), 9 (94.2 ± 18.2), 3 (185.5 ± 30.8)
0.2	0.0	34 (629.5 ± 42.9), 33 (752.2 ± 38.8), 13 (922.1 ± 80.0)
	0.3	56 (113.7 ± 84.1)
	0.5	17 (24.9 ± 7.8), 14 (51.5 ± 6.9), 9 (98.5 ± 21.0)
	0.7	17 (16.2 ± 5.3), 7(42.6 ± 12.0)
0.3	0.0	43 (555.2 ± 62.2), 37 (761.8 ± 73.3)
	0.3	39 (35.4 ± 12.8), 17 (104.8 ± 37.5)
	0.5	18 (13.6 ± 2.8), 15 (21.0 ± 3.0), 7 (47.8 ± 29.0)
	0.7	11 (13.5 ± 1.9), 8 (5.3 ± 1.5), 5 (20.2 ± 1.8)
0.4	0.0	24 (555.2 ± 68.0), 24 (297.3 ± 81.5), 19 (819.7 ± 91.8), 13 (1295.2 ± 198.8)
	0.3	21 (31.5 ± 4.6), 21 (15.0 ± 4.0), 14 (63.6 ± 26.2)
	0.5	26 (9.7 ± 3.3), 14 (23.2 ± 8.1)
	0.7	24 (7.3 ± 5.0)

Table 3.1: Cluster analysis of ring diffusivities, $g_3(T_{max}, \Delta_c)$, taken at the largest

3.3.6 Overlapping Conformations of Ring Polymers in Dense Solutions

Having investigated the heterogeneous dynamics of single rings, we now aim to connect the observed non-Gaussian dynamics to the spatial organisation of the chains. A ring molecule in concentrated solution must be collapsed and hence (See chapter. 2) large entropic penalty may be required. To prevent from the entropic penalty, the surrounding rings are compelled to invade and the target ring is threaded and overlapped with a number of neighbors. To a first approximation, one may argue [30] that a ring of size R_g experiences an entropic penalty proportional to the average number of overlapping neighbours $\langle m_{\rm ov} \rangle$

$$\frac{S}{k_B T} \sim \langle m_{\rm ov} \rangle \sim \frac{\rho}{N} R_g^3 \sim \rho^{\alpha} \,, \tag{3.7}$$

where we assume that [50, 21, 24], in the large-N limit, the number of chains in a volume R_g^3 converges to a (density dependent) constant characterized by an exponent $\alpha < 1$ (See section. 2.3.1), *i.e.* $R_g^3/N \sim \rho^{-(1-\alpha)}$. In Eq. (3.7), $\langle m_{\rm ov} \rangle$ is defined as the average number of chains whose centres of mass are within $2R_g$ [41] from any other ring.

We assign a probability $p_o(\mathcal{S}_1, \mathcal{S}_2)$ for any ring in a given set $\mathcal{S}_1$ to be overlapping with any other ring in another set $\mathcal{S}_2$ as

$$p_o(\mathcal{S}_1, \mathcal{S}_2) = \frac{1}{|\mathcal{S}_1||\mathcal{S}_2|} \sum_{i \in \mathcal{S}_1} \sum_{j \in \mathcal{S}_2} \Theta(2R_g - |\boldsymbol{r}_i - \boldsymbol{r}_j|) \tag{3.8}$$

where $|\mathcal{S}_i|$ is the number of elements in the set $\mathcal{S}_i$. A ring in the set k has then an average number of overlaps that can be computed as

$$m_{ov}(\mathcal{S}_k) = \sum_{i = \{\text{free,pinned}\}} |\mathcal{S}_i| p_o(\mathcal{S}_k, \mathcal{S}_i) \tag{3.9}$$

and it can be compared with the value of $\langle m_{ov} \rangle$ reported in Fig. 3.14 of the main text. We expect that in equilibrium p_o should be independent on the choice of the sets considered (especially given the fact that we select the pinned fraction at random). We therefore compute p_o for $\mathcal{S} = \{\text{free}, \text{pinned}\}$ and report here typical values found. We find that $\lim_{N\to\infty} \langle m_{\rm ov} \rangle$ is indeed independent on N and $\alpha \simeq 0.60 - 0.74$ (see Fig. 3.14(A)). Importantly, Eq. (3.7) implies that *higher* monomer densities lead to a larger number of overlapping neighbours [70] and, in turn, larger entropic penalties [30], which consequently drive more compact conformations. On the other hand, results from Figs. 3.3 suggest that denser systems are more susceptible to random pinning, and display glassy behaviour at *lower* values of f_p.

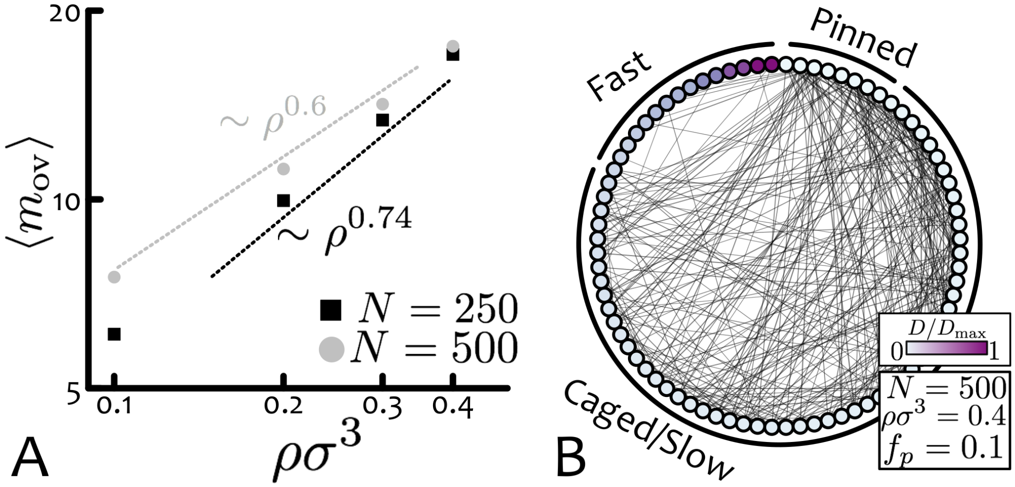

Figure 3.14: **Slowing Down of Overlapping Rings.** (**A**) Average number of overlapping chains per ring, $\langle m_{\rm ov}(\rho) \rangle$. Dashed lines correspond to power-law behaviors determined from best fits to the data. Plotted values are listed in Table 3.2. (**B**) Abstract network representation for rings solutions: nodes (which represent rings) are colour coded according to corresponding diffusion coefficients, $D \equiv \lim_{\Delta\to\infty} g_3(\Delta)/6\Delta$. Edges between nodes are drawn if their weight is larger than 0.5, for clarity. Slow-moving rings overlap with frozen ones, whereas fast rings show little or no persistent overlap.

We consider rings as nodes of an abstract network, where a link between two nodes indicates that the corresponding rings overlap for a total time longer than half of the overall simulation runtime. An example of such a network is given in Fig. 3.14(B), where nodes have been ordered and coloured according to the corresponding single-ring diffusion coefficients, $D \equiv \lim_{\Delta\to\infty} g_3(\Delta)/6\Delta$. This representation intuitively shows that slow rings are connected (overlapping) either with other slow rings or with frozen ones, whereas rings with large diffusion coefficients have virtually zero degree. The network thus connects the static and dynamic properties of rings, by showing that overlapping rings slow down reciprocally owing to topological constraints.

3.3.7 Ring Solutions as Percolating "Bethe Lattices"

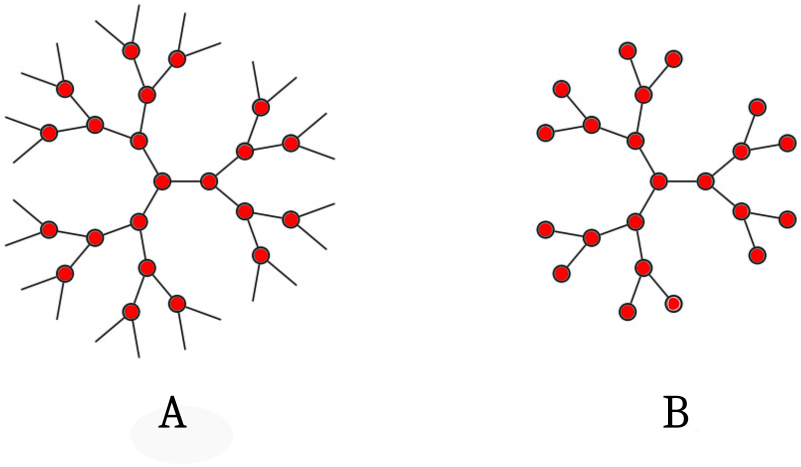

Figure 3.15: (A) Bethe lattice and (B) Cayley tree with coordination number (degree of nodes) $k = 3$. The Cayley tree has boundaries (nodes of degree 1, called leaves). The Bethe lattice is infinite and does not contain boundaries: all nodes are of the same degree.

The Bethe lattice is an infinite graph, where any two points are connected by a single path and each vertex has the same number of branches k, as shown in Fig. 3.15 for $k = 3$. A finite portion of the Bethe lattice is called Cayley tree. It plays an important role in statistical and condensed-matter physics because some problems involving disorder and/or interactions can be solved exactly when defined on a Bethe lattice, e.g., Ising models, [81] percolation, [82] and etc. Percolation on a Bethe lattice is the simplest branching medium which can be solved exactly.

To obtain then a quantitative estimation of how topological constraints affect the dynamics of rings, we approximate the network as a Bethe lattice [12] of coordination $\langle m_{\mathrm{ov}} \rangle$. Due to the hierarchical nature of the network, the number of rings in generation g (the last generation) of the network is $\langle m_{\mathrm{ov}} \rangle (\langle m_{\mathrm{ov}} \rangle - 1)^{g-1}$, while the total number of rings in the solution or network (from the core to generation g) is

$$\begin{aligned} M &= 1 + \langle m_{\mathrm{ov}} \rangle + \langle m_{\mathrm{ov}} \rangle (\langle m_{\mathrm{ov}} \rangle - 1) + \langle m_{\mathrm{ov}} \rangle (\langle m_{\mathrm{ov}} \rangle - 1)^2 + ... \\ &= 1 + \langle m_{\mathrm{ov}} \rangle \left[\frac{(\langle m_{\mathrm{ov}} \rangle - 1)^{\bar{g}} - 1}{\langle m_{\mathrm{ov}} \rangle - 2} \right] \end{aligned} \tag{3.10}$$

where the last step in the derivation used the sum of a geometric series. Thus, the maximum number of shells, $\bar{g}$, is given by

$$\bar{g} = \frac{\log\left(\frac{\langle m_{\rm ov}\rangle-2}{\langle m_{\rm ov}\rangle}(M-1)+1\right)}{\log(\langle m_{\rm ov}\rangle-1)}\,, \tag{3.11}$$

where M is the total number of nodes (rings) of the network. We now assume that the effect of pinning a single ring results in the caging of its first neighbours with an *unknown* probability p_c, of its second neighbours with probability p_c^2, and so on. The whole process therefore results in a "caging cascade" producing a fraction of trapped rings equal to f_c'. Assuming that for small f_p, all pinned rings act independently on their neighbours, we obtain the total fraction of caged rings, f_c, as

$$f_c = f_p\, f_c' = f_p\, p_c \langle m_{\rm ov}\rangle \frac{(p_c\,(\langle m_{\rm ov}\rangle-1))^{\bar{g}}-1}{p_c\,(\langle m_{\rm ov}\rangle-1)-1}\,. \tag{3.12}$$

Interestingly, Eqs. (3.11)-(3.12) link a measurable quantity (fraction of caged rings, f_c) to an imposed quantity (fraction of pinned rings, f_p) and, by inversion, allows to determine the caging (or threading) probability between close-by rings, p_c [39, 3]. In particular, Eq. (3.12) implies that the system becomes "critical" when $p_c = p_c^\dagger \equiv 1/(\langle m_{\rm ov}\rangle - 1)$, for there exists a finite fraction f_c of caged rings even in the limit $f_p \to 0$.

By combining the Eqs. (3.11)-(3.12) and evaluating f_c at $f_p = 0.3$ as the rings displaying a single-ring diffusion coefficient $D/D_{\rm max} \simeq 0$, we can numerically extract values for p_c at any given ρ (see Table 3.2). Interestingly, p_c increases with ρ up to where p_c is approximately given by the predicted $p_c^\dagger$. Although through this crude approximation, we find that, curiously, the only two cases for which $p_c > p_c^\dagger$ are the ones displaying spontaneous ($f_p = 0$) deviations from Gaussian behaviour (Fig. 3.8(D), $N = 500$ and $\rho\sigma^3 \geq 0.3$).

	$N = 250$					$N = 500$				
$\rho\sigma^3$	$\langle m_{\rm ov} \rangle$	$\bar{g}$	f_c	$p_c^\dagger$	p_c	$\langle m_{\rm ov} \rangle$	$\bar{g}$	f_c	$p_c^\dagger$	p_c
0.1	6.098	2.874	0.129	0.196	0.053	7.520	2.175	0.283	0.153	0.080
0.2	9.958	2.213	0.312	0.112	0.063	11.184	1.804	0.556	0.098	0.094
0.3	13.383	1.953	0.515	0.081	0.070	14.186	1.641	0.623	0.076	0.086
0.4	17.032	1.785	0.606	0.062	0.065	17.549	1.519	0.649	0.060	0.076

Table 3.2: Measured values for: (1) the average number of overlapping chains per ring, $\langle m_{\rm ov} \rangle$; (2) the maximum number of shells in the Bethe-lattice representation of rings solutions, $\bar{g}$, Eq. 3.11 ; (3) fraction of caged rings, f_c, at pinning fraction $f_p = 0.3$ (value chosen for corresponding to the smallest pinning fraction used in this work); (4) "critical" caging probability, $p_c^\dagger \equiv 1/(\langle m_{\rm ov} \rangle - 1)$, corresponding to a finite fraction f_c of caged rings in the limit $f_p \to 0$; (5) caging probability, p_c, obtained from Eqs. 3.12.

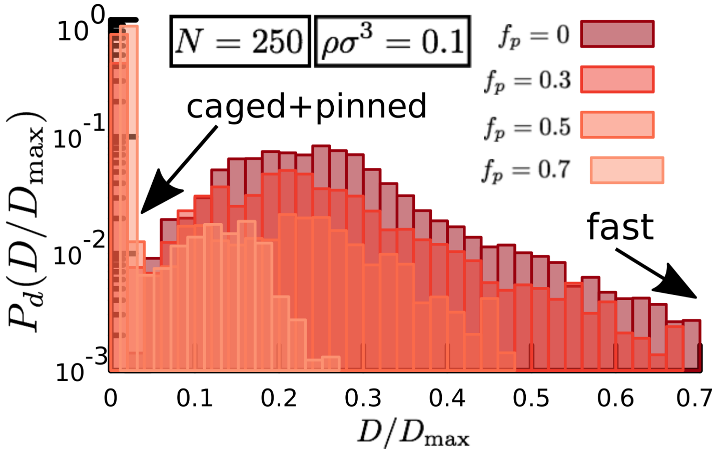

Figure 3.16: **Distribution of Diffusion Coefficients.** Example of distribution function, $P_d(D/D_{\rm max})$, of the scaled rings diffusion coefficients $D/D_{\rm max}$ for $N = 250$, $\rho\sigma^3 = 0.1$ and different values of f_p. The first bin contains both, pinned and caged rings; from this, we can readily extract the fraction of caged rings as $f_c = P_d(0) - f_p$. Specific values for f_c are reported in Table 3.2.

Intriguingly, the onset of criticality is marked by a qualitative change in the shape of the distribution function of diffusion coefficients, $P_d(D/D_{\rm max})$ (Fig. 3.16). When the system is subject to no perturbation, the corresponding $P_d(D/D_{\rm max})'s$ are broad and single peaked, while at any $f_p > 0$, they show a bimodal shape, where the emergence of the first peak reflects the presence of a slow (caged) subset of rings.

3.4 Conclusions

In this chapter, I discussed the use of MD simulations to investigate the dynamics of semiflexible ring polymers in solutions at various polymer concentrations. The main strategy we adopted was pinning a certain fraction of the polymers and tracking the motions of the unpinned ones.

Earlier work [3] had suggested that, at a constant solution density, the critical fraction of pinned chains necessary for vitrification decreases with an increase in the chain length. Extrapolating this result, it was found that spontaneous vitrification can occur at a certain, large chain length even at a constant solution density. This result which suggests a progressively greater effect due to topological constraints upon increasing the chain length, obtains even though the increase in the chain length leads to a more compact chain conformation.

As I mentioned in Chapter.2, It is known that ring polymers adopt a more compact chain conformation if the solution density is increased. Here, we varied the monomer density of the solution and probed its effect on the dynamics of the unpinned chains. We observe that denser solutions are counter-intuitively more susceptible to the random pinning procedure, and that the critical pinning fraction $f_p^\dagger$ significantly decreases with increasing ρ. It strongly suggests that denser solutions of rings possess abundant inter-ring threadings.

We have reported the first evidence of (i) ergodicity breaking in perturbed solutions of rings and (ii) non-trivial convergence towards ergodicity together with spontaneous caging (Fig. 3.8- 3.10) in unperturbed systems at $N \simeq N_g(\rho)$. Further, we reported that upon random pinning, rings appear to cluster into components with slow/fast diffusivities corresponding to more/less persistent overlaps with other slow or pinned rings (Fig. 3.14. These results can be rationalized by arguing that threadings may act as transient cages which are then quenched by the random pinning protocol).

An intriguing finding of this work was that, even in the limit $f_p \to 0$, solutions of rings may deviate from standard Gaussian behavior (Fig. 3.8(D) and 3.10(D)) and display features at the onset of "topological glasses" provided $\rho \simeq \rho_g(N)$ or $N \simeq N_g(\rho)$ (see Eq. 3.5 and Fig. 3.5).

We conclude that a topological glass may form when the probability p_c of any pinned ring to cage any of its neighbors is $\geq p_c^\dagger$, with $p_c^\dagger$ given by a simple analytical expression for networks in the Bethe lattice approximation. We argue that the experimentally observed [5] non-gaussian, cage-like behavior of ring polymer melts may be well reconciled with this intuitive picture.

Chapter 4

Nanoparticle Motion in Polymer Solutions: The Influence of Chain Architecture

The present chapter is based on the preliminary results of an ongoing research.

4.1 Introduction

4.1.1 Physical Motivation

The diffusion of nanoparticles (NP's) in complex fluids is a problem of broad importance in materials science and cellular biophysics. For instance, the micro-mechanical and visco-elastic properties of complex polymer fluids can be characterized by monitoring the motion of freely diffusing particles in solutions (a technique known as microrhelology [83, 84, 85, 86, 87]). In particular, based on the post-processing of the motion of the probes, some important rheological properties of the material like its elastic and viscous moduli can be efficiently and rapidly obtained [83, 84]. At the same time, selected amounts of these probes dispersed in polymer solutions may significantly alter the elastic properties of these host matrices [88], and help designing materials with novel properties. For all these reasons, understanding the dynamic behavior of small probes in polymer solutions is a problem of theoretical as well as of practical interest.

Prototypical examples of complex polymer fluids are semi-dilute solutions and melts of polymer chains [47, 18, 2, 12]. As it was recognized long ago [47, 18, 2] and also discussed many times in this Thesis, a key feature of these systems is represented by their typically long relaxation times [47, 18, 2, 12], stemming from the fact that individual chains subjected to thermal motion can not cross each other owing to the presence of long-lived topological constraints (TCs). Not surprisingly, TCs influence also the dynamics of the colloidal probes dispersed in the solution: in particular, colloidal probes diffusion is strongly coupled to the relaxation dynamics of the surrounding chains and displays a rather complex and non-trivial scaling behavior [89, 8]. Very recently, it has been suggested that the diffusive response of nanoparticles might depend on the specific architecture of the surrounding polymers. In particular, left unchanged the microscopic details of the solution (like its density, chain stiffness, etc.), nanoparticles diffusion in the two cases of entangled solutions of linear chains vs. entangled solutions of ring polymers should behave differently [90, 89]. This suggests indeed the existence of a surprising link between colloidal probes motion and chain architecture that deserves to be explored in deeper detail.

In this Chapter, we present preliminary computational results concerning the thermal motion of probe nanoparticles of size d in solutions of polymer chains with linear and circular architectures. We assume here no adsorption of polymers onto probe nanoparticles and no interaction between probe particles. We stress that, in relation to recent literature [70, 90] we consider wider ranges of probe sizes and solution densities.

4.1.2 Nanoparticle Diffusion in Polymer Solutions: A Brief Account of Theoretical Considerations

Although numerical tools still represent the most feasible way to study nanoparticle motion in polymer solutions, there has been at the same time considerable theoretical progress in this field.

For completeness, in this Section we summarize the key points of the recent work by Rubinstein and coworkers [90], which represents, in our opinion, the most complete theoretical scheme to understand nanoparticle diffusion in polymer matrices to date.

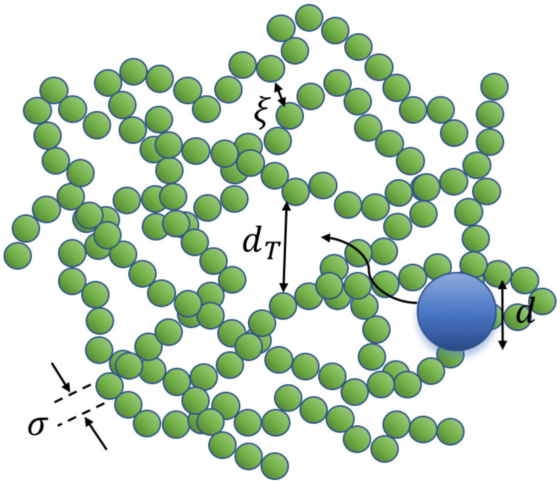

Figure 4.1: A cartoon for a single nanoparticle dissolved in an entangled polymer melt. Each arrow represents a distinct length scale present in this system.

Mobility of nanoparticles in polymer solutions depends on the relative particle size with respect to two important length scales (schematically shown in Fig. 4.1):
a) The correlation length ξ, defined as the average distance from a monomer on one chain to the nearest monomer on another chain [12].
b) The tube diameter d_T (transverse polymer localization length) which was introduced in Section. 1.3.2.
According to the scaling theory by Rubinsten and Cai, there are different scenarios for nanoparticle motion in the linear polymer matrix depending on the relative size of the probe particle with respect to the main length scales:
a) The dynamics of small particles ($d < \xi$) does not depend on the polymer medium, while for intermediate particle sizes ($\xi < d < d_T$) the diffusion process begins to be affected by the chains dynamics yet not controlled by the entanglements.
b) Diffusion of relatively large particles ($d > d_T$) is controlled to a large extent by the relaxation dynamics of the entanglement mesh of the solutions (See Figure. 4.2). Cai et al [8] recently advanced a hopping diffusion mechanism for nanoparticles fairly larger than d_T to overcome the confinement by the entanglement network.

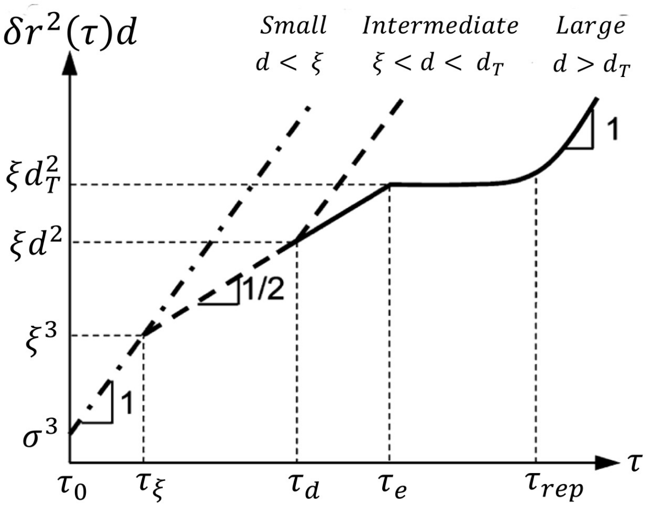

Figure 4.2: Time dependence of the product of mean-square displacement $\delta r^2(\tau)$ and the particle size d for small particles ($\sigma < d < \xi$, dash-dotted line), intermediate size particles ($\xi < d < d_T$, dashed line), and large particles ($d > d_T$, solid line) in polymer solutions. Here τ_0 is the relaxation time of a monomer, τ_ξ is the relaxation time of a correlation blob, τ_d is the relaxation time of a polymer segment with size comparable to particle size d, τ_e is the relaxation time of an entanglement strand, and τ_{rep} is the relaxation (reptation) time of a whole polymer chain. See Reference [8] for more details.

The theory predicts that NP diffusion will be controlled by a constraint release mechanism, which opens up the network locally (hopping), enabling NP motion. They introduced a crossover particle size d_c at which the hopping time scale $\tau_{hopping}$ is comparable to the reptation time scale $\tau_{reptation}$. When the particle size d is moderately larger than the tube diameter d_T and less than the crossover size d_c, NPs trapped in entanglement cells relax mainly by hopping from one cell (entanglement cage) to a neighboring one, whenever an entanglement strand in the original cell slips around the particle. This hopping relaxation mechanism act in conjunction with reptation of the host polymer chains. Particles with intermediate size $d_T < d < d_c$ diffuse primarily by hopping between neighboring entanglement cages, while larger particles ($d > d_c > d_T$) have to wait for the polymer liquids to relax as the entropic energy barrier for hopping between neighboring entanglement cages becomes prohibitively high.

4.2 Model Overview and Simulated Systems

4.2.1 Modelling Colloidal Nanoparticles

Colloid-monomer and colloid-colloid interactions are described by the model potentials introduced by Everaers and Ejtehadi [97]. The total interaction energy between colloidal particles at center-to-center distance r can be represented as the sum of two functions:

$$U_{\mathrm{cc}}(r) = \begin{cases} U^{A}_{\mathrm{cc}}(r) + U^{R}_{\mathrm{cc}}(r) & r \leq r_{cc} \\ 0 & r > r_{\mathrm{cc}} \end{cases} . \tag{4.1}$$

$U^{A}_{\mathrm{cc}}(r)$ is the attractive component and it is given by:

$$U^{A}_{\mathrm{cc}}(r) = -\frac{A_{\mathrm{cc}}}{6}\left[\frac{2a^2}{r^2-4a^2} + \frac{2a^2}{r^2} + \ln\left(\frac{r^2-4a^2}{r^2}\right)\right] . \tag{4.2}$$

The repulsive component of the interaction, $U^{R}_{\mathrm{pp}}(r)$, is:

$$U^{R}_{\mathrm{cc}}(r) \quad = \quad \frac{A_{\mathrm{cc}}}{37800}\frac{\sigma^6}{r}\left[\frac{r^2-14ar+54a^2}{(r-2a)^7} + \frac{r^2+14ar+54a^2}{(r+2a)^7} - 2\frac{r^2-30a^2}{r^7}\right] . \tag{4.3}$$

where $A_{\mathrm{cc}} = 39.478\, k_B T$ [97]. In order to study the relevant crossover of nanoparticle sizes smaller/larger than the tube diameter, we have considered non-sticky, athermal colloid particles with diameters $d = \sigma = 2.5, 5.0, 7.5$, in which the NP diameter d then ranges from being slightly smaller than the tube diameter of the solutions at $\rho\sigma^3 = 0.4$ to being a little larger than d_T in solutions with $\rho\sigma^3 = 0.1$. These values of NP sizes correspond to truncating the interaction $U_{\mathrm{cc}}(r)$ to $r_{\mathrm{cc}}/\sigma = 3.08, 5.60, 8.08$.
Finally, the interaction energy, U_{mc}, between a single monomer and a colloidal particle with center-to-center distance r is given by:

$$U_{\mathrm{mc}}(r) = \begin{cases} \frac{2a^3\sigma^3 A_{\mathrm{mc}}}{9(a^2-r^2)^3}\left[1 - \frac{(5a^6+45a^4r^2+63a^2r^4+15r^6)\sigma^6}{15(a-r)^6(a+r)^6}\right] & r \leq r_{\mathrm{mc}} \\ 0 & r \geq r_{\mathrm{mc}} \end{cases} \tag{4.4}$$

where $A_{\mathrm{mc}} = 75.358\, k_B T$ [97]. According to our choices for colloid diameters, the interaction $U_{\mathrm{mc}}(r)$ is truncated to $r_{\mathrm{mc}}/\sigma = 2.11, 3.36, 4.61$.

4.2.2 Preparation of Initial Samples

Linear polymers – Solutions of *linear* chains and nanoparticles were prepared first at $\rho\sigma^3 = 0.1$ and the smallest particle size $d = 2.5\sigma$. Linear chains were arranged as random walks in space and placed at random positions inside the simulation box. Random positions were also chosen for colloidal particles. In order to remove possible overlaps a short (of the order of a few τ_{MD}'s) MD run with capped, soft (*i.e.* non-diverging) repulsive interactions was used. The workflow is akin to the steps explained in Sec. 2.2.1.

Ring polymers – This first setup is not applicable for ring polymers which needs to satisfy the accompanying constraint of avoiding mutual concatenation. Hence, ring polymers were initially arranged in a very large simulation box, *i.e.* at very dilute conditions. In order to reach the correct monomer density of $\rho\sigma^3 = 0.1$ we performed then a short (about $400\tau_{\text{MD}}$ MD steps) simulation by imposing an external pressure on the system which shrinks the simulation box until it reaches the desired value. Configurations with larger nanoparticles sizes were obtained with the same scheme described for *Linear polymers.*

For both systems of linear and circular chains, higher densities were obtained by compressing the solutions by means of higher external pressures. During this preparatory phase the complete set of interaction terms described in Sec. 4.2.1 was employed.

4.2.3 Evaluation of Mean-Square Internal Distances During Equilibration

At any given ρ, we started from the *equilibrated* solutions of polymers and probes with $N = 250, 500$ and probe diameter $d/\sigma = 2.5$. For simulations with larger probes diameter, $d/\sigma = 5.0, 7.5$, we have proceeded to inflate simultaneously the probes and the simulation box. We have accomplished this task by performing short (of the order of a few tens of τ_{MD}'s) MD runs with a soft (*i.e.* non-diverging), capped repulsive interactions between chain monomers and probes. At the end of these preparatory runs, we have checked the perturbation of chains conformations after the deflation/inflation steps by measuring [46] the mean-square internal distances, $\langle R^2(\ell) \rangle$, between pairs of monomers at contour length separation ℓ, see Fig. 4.3. The perfect agreement between different curves at each density demonstrates that the probes have perturbed in no sensible manner the overall chains conformations.

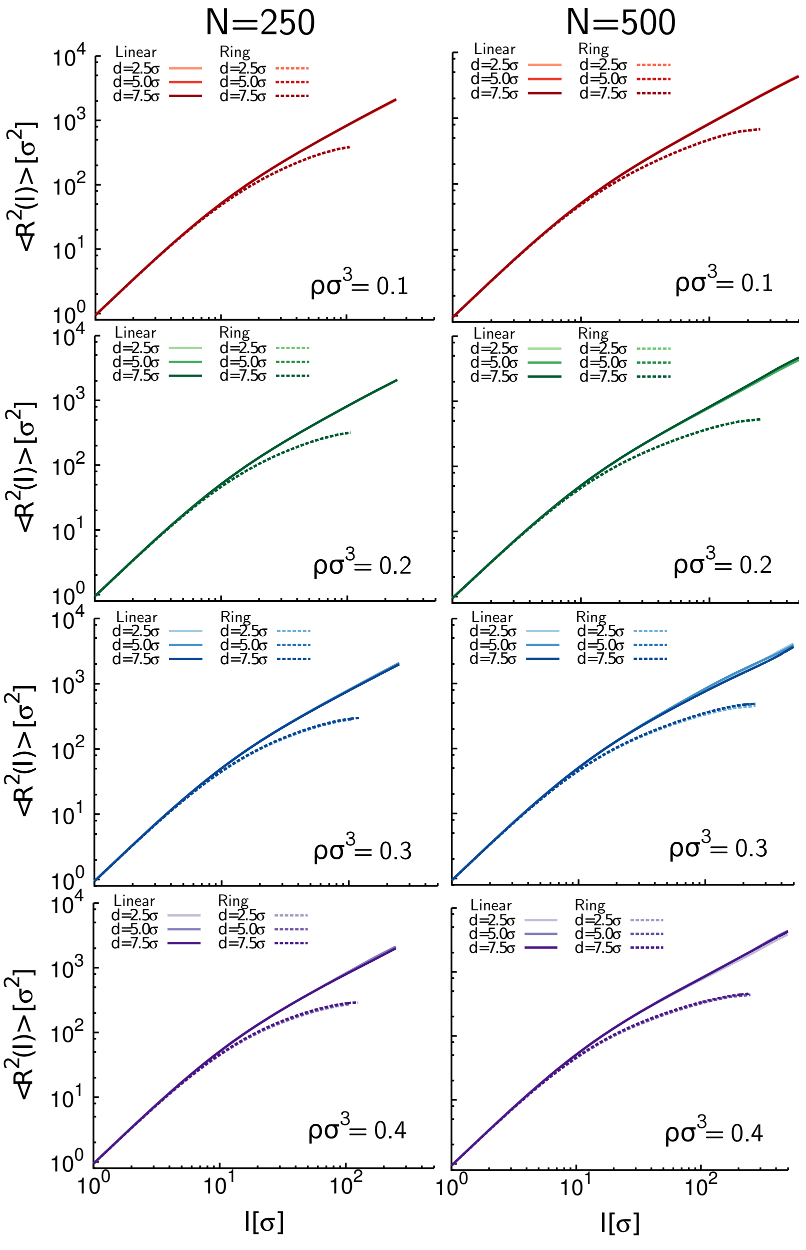

Figure 4.3: Mean-square internal distances, $\langle R^2(\ell)\rangle$, between pair of monomers at contour length separation ℓ: results for linear chains (solid lines) and ring polymers (dashed lines). Averages correspond to the first parts of the corresponding MD trajectories, immediately after the introduction of the colloidal particles.

4.3 Results

4.3.1 Mean-Square Displacement of Nanoparticles Depends on Chain Topology

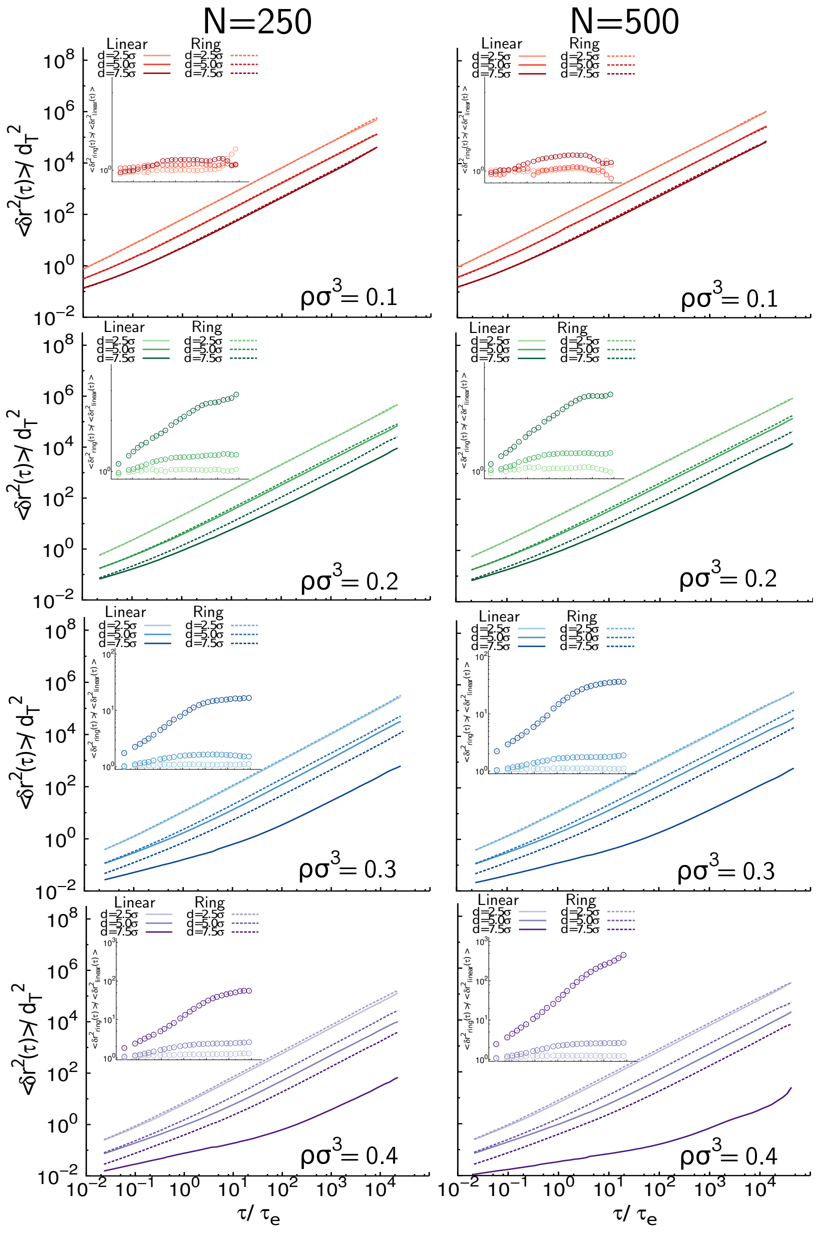

Figure 4.4: Mean-square displacement $\delta r^2(\tau)$ as a function of lag-time τ for colloids of diameter $d/\sigma = 2.5, 5.0, 7.5$ in entangled solutions of linear polymers (solid lines) and non-concatenated ring polymers (dashed lines). Insets: corresponding ratios $\delta r^2_{ring}(\tau)/\delta r^2_{lin}(\tau)$. Colloids of diameter d larger than the tube diameter d_T of the corresponding polymer solution diffuse markedly faster in rings systems.

In order to study the influence of chain architecture on the diffusion of dispersed probes embedded in the polymer solutions, we consider the probe mean-square displacement $\delta r^2(\tau)$ at lag-time τ defined as:

$$\delta r^2(\tau) \equiv \frac{1}{n_{\text{coll}}} \sum_{i=1}^{n_{\text{coll}}} \langle (\vec{r}_i(t+\tau) - \vec{r}_i(t))^2 \rangle \,, \tag{4.5}$$

where $\vec{r}_i(t)$ is the spatial position of the i-th colloidal probe ($i = 1, ..., n_{\text{coll}}$) at time t and brackets mean time average over the molecular dynamics (MD) trajectory. We employ the notation $\delta r^2_{\text{lin}}(\tau)$ (respectively, $\delta r^2_{\text{ring}}(\tau)$) for solutions of linear (resp., ring) polymers. Results are shown in Fig. 4.4, with the x- and y- axes shown in units of the corresponding entanglement time τ_e and tube diameter d_T, respectively. The tube diameter of the solutions is taken as the average size of an entanglement strand $\sim \sqrt{\langle R_g^2(L_e) \rangle} = \sqrt{\langle l_K L_e / 6 \rangle}$ (l_K and L_e values are reported in Chapter. 2). The entanglement time τ_e can be obtained from $g_1(\tau_e) = 2R_g^2(L_e, l_K)$ [**?**]. Insets display the ratio of the mean-square displacements of probes in nonconcatenated rings to the corresponding mean-square displacements in linear chains $\delta r^2_{\text{ring}}(\tau) / \delta r^2_{\text{lin}}(\tau)$.

By comparing the results for different densities ρ and probe diameters d, two regimes emerge:

(1) For $d < d_T$, entanglements have no effect and probes diffusion does not depend on chain topology. In this regime, subdiffusion ($\langle \delta r^2(\tau) \rangle \sim \tau^\alpha$, with $\alpha \approx 1/2$) is expected at short time-scales resulting from the coupling of the probes with the short-time Rouse modes of the chains [89]. However, α in the subdiffusive regime is affected by the crossover to the Fickian regime and its measured values are larger than 1/2.

(2) Conversely, for $d > d_T$, entanglements do affect colloids diffusion. In particular, $\langle \delta r^2(\tau) \rangle \sim \tau^\alpha$ with $\alpha < 1$ (subdiffusion) for $\tau \ll \tau_e$ and $\sqrt{\langle \delta r^2(\tau) \rangle} \, / \, d_T < 1$, and $\alpha = 1$ (Fickian diffusion) and $\sqrt{\langle \delta r^2(\tau) \rangle} \, / \, d_T > 1$ for $\tau \gg \tau_e$. This phenomenon is particular evident in the last row panels of Fig. 4.4. In particular, in high-density solutions of linear chains (dark violet solid line) probes have, on average, moved very little from their original position inside the polymer solution: as a matter of fact, they can be considered then as effectively "caged". Even more remarkably, there is now a striking difference between linear chains and rings: probes appear more mobile when dispersed in rings solutions, with the corresponding terminal diffusion coefficient $D \equiv \lim_{\tau \to \infty} \frac{\langle \delta r^2(\tau) \rangle}{6\tau}$ growing up to about two orders of magnitude (see Table 4.1 for

specific results) than in analogous solutions of linear chains.

We report the measurements of the diffusion coefficients in Fig. 4.5. The emerging entanglement constraints reduce the diffusion coefficients of NPs. The larger the size of the NP is, the more extent the diffusion coefficient will be reduced. Once the size of the NP, d becomes comparable to the size of the mesh formed by entanglements ($d = 5\sigma, \rho\sigma^3 = 0.3$ in Fig. 4.5) NPs start to distinguish in which topology the are immersed in due to the "caging" effect.

Interestingly, at the highest density ($\rho\sigma^3 = 0.4$) and the largest NP size ($d = 7.5\sigma$), the diffusion coefficient is actually larger in solution of linear chains with length $N = 500$ than that with $N = 250$. Following [8], the reason for that may be ascribed to the fact that the probability for hopping to occur decreases exponentially with increasing particle size d: in this regime, NPs have to wait for the surrounding polymers to relax and flow around them in order to diffuse [8]. Conversely, in solutions of ring polymers at the same condition, we observe very little difference in diffusivities of NPs.

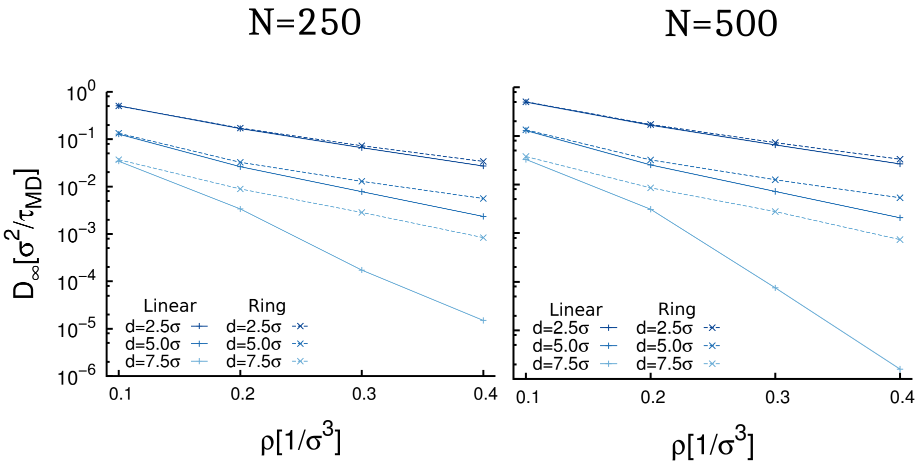

Figure 4.5: Concentration dependence on the diffusion coefficient for entangled solutions of linear and ring polymers. The results for $N = 250$ are shown in the left panel and those for $N = 500$ in the right panel.

					$N = 250$		$N = 500$	
					Linear polymers	Ring polymers	Linear polymers	Ring polymers
$\rho\sigma^3$	L_e/σ	d_T/σ	τ_e/τ_{MD}	d/σ	$D\,[\sigma^2/\tau_{\text{MD}}]$	$D\,[\sigma^2/\tau_{\text{MD}}]$	$D\,[\sigma^2/\tau_{\text{MD}}]$	$D\,[\sigma^2/\tau_{\text{MD}}]$
0.1	40.0	8.2	1625.5	2.5	$(5.05 \pm 0.02) \times 10^{-1}$	$(5.04 \pm 0.01) \times 10^{-1}$	$(4.96 \pm 0.04) \times 10^{-1}$	$(5.02 \pm 0.01) \times 10^{-1}$
				5.0	$(1.277 \pm 0.001) \times 10^{-1}$	$(1.337 \pm 0.002) \times 10^{-1}$	$(1.288 \pm 0.004) \times 10^{-1}$	$(1.332 \pm 0.001) \times 10^{-1}$
				7.5	$(3.42 \pm 0.01) \times 10^{-2}$	$(3.70 \pm 0.01) \times 10^{-2}$	$(3.28 \pm 0.01) \times 10^{-2}$	$(3.76 \pm 0.01) \times 10^{-2}$
0.2	16.2	5.2	571.6	2.5	$(1.676 \pm 0.002) \times 10^{-1}$	$(1.718 \pm 0.002) \times 10^{-1}$	$(1.658 \pm 0.002) \times 10^{-1}$	$(1.715 \pm 0.001) \times 10^{-1}$
				5.0	$(2.62 \pm 0.01) \times 10^{-2}$	$(3.25 \pm 0.01) \times 10^{-2}$	$(2.529 \pm 0.003) \times 10^{-2}$	$(3.211 \pm 0.002) \times 10^{-2}$
				7.5	$(3.38 \pm 0.03) \times 10^{-3}$	$(8.91 \pm 0.03) \times 10^{-3}$	$(3.10 \pm 0.04) \times 10^{-3}$	$(8.53 \pm 0.02) \times 10^{-3}$
0.3	11.0	4.3	490.6	2.5	$(6.61 \pm 0.01) \times 10^{-2}$	$(7.27 \pm 0.04) \times 10^{-2}$	$(6.513 \pm 0.003) \times 10^{-2}$	$(7.286 \pm 0.004) \times 10^{-2}$
				5.0	$(7.79 \pm 0.02) \times 10^{-3}$	$(1.29 \pm 0.01) \times 10^{-2}$	$(7.19 \pm 0.02) \times 10^{-3}$	$(1.256 \pm 0.001) \times 10^{-2}$
				7.5	$(1.73 \pm 0.3) \times 10^{-4}$	$(2.85 \pm 0.03) \times 10^{-3}$	$(7.5 \pm 0.2) \times 10^{-5}$	$(2.78 \pm 0.01) \times 10^{-3}$
0.4	8.9	3.9	546.0	2.5	$(2.72 \pm 0.01) \times 10^{-2}$	$(3.386 \pm 0.002) \times 10^{-2}$	$(2.653 \pm 0.003) \times 10^{-2}$	$(3.310 \pm 0.004) \times 10^{-2}$
				5.0	$(2.34 \pm 0.02) \times 10^{-3}$	$(5.60 \pm 0.01) \times 10^{-3}$	$(2.07 \pm 0.01) \times 10^{-3}$	$(5.33 \pm 0.01) \times 10^{-3}$
				7.5	$(1.5 \pm 0.1) \times 10^{-5}$	$(8.36 \pm 0.02) \times 10^{-4}$	$(1.6 \pm 0.3) \times 10^{-6}$	$(7.36 \pm 0.03) \times 10^{-4}$

Table 4.1: Terminal diffusion coefficients D for colloidal particles of diameter d, immersed in entangled solutions of semiflexible polymer chains at monomer density ρ. D is estimated by taking the average slope of the last $10\%, 15\%, 20\%$ of the colloids mean-square displacements curve data points into consideration. L_e, d_T and τ_e correspond, respectively, to the entanglement length, the tube diameter, and the entanglement time of the chains in solution (see Sec. 1.3 for definitions).

4.3.2 Local Scaling Exponent of Mean-square Displacement

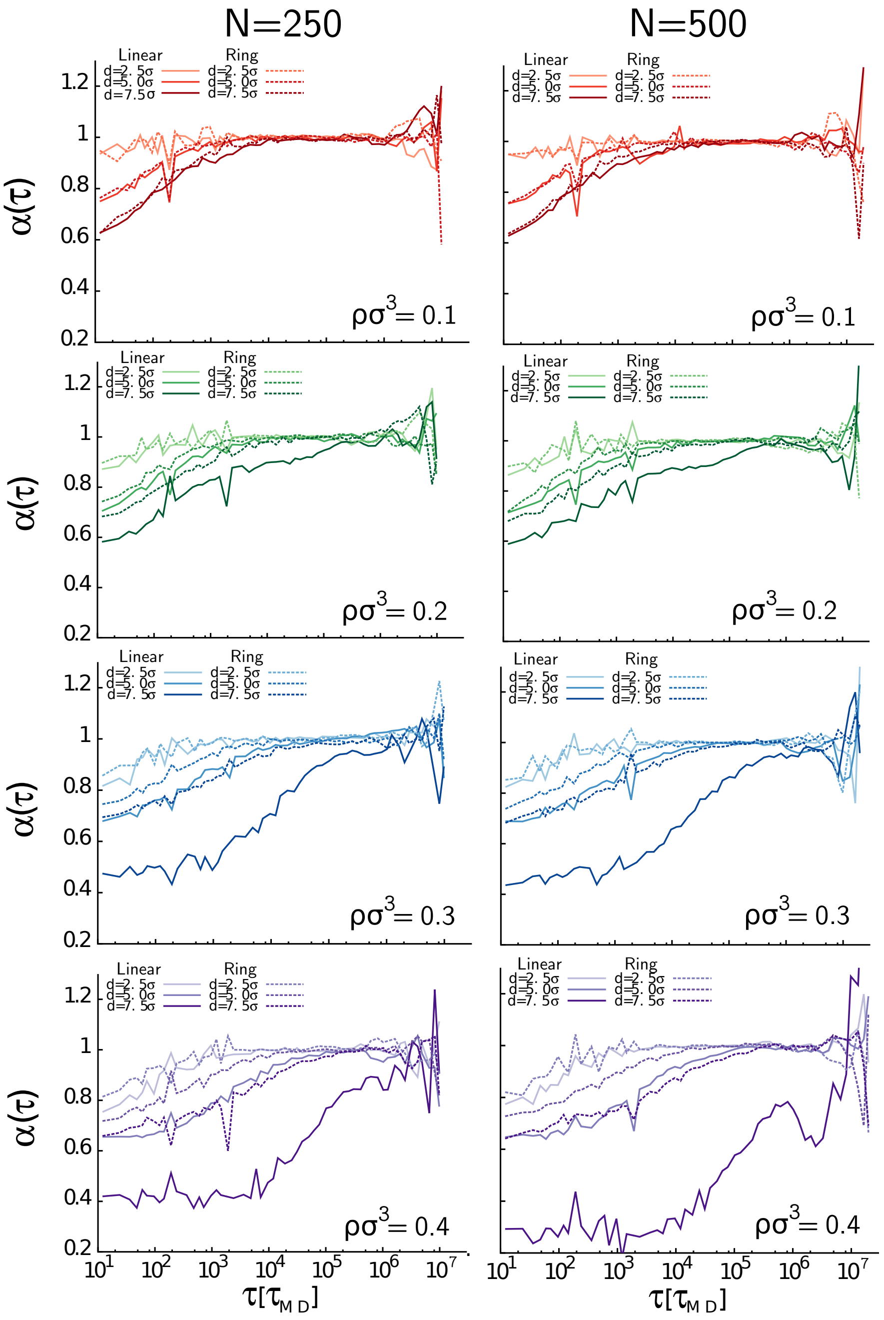

Figure 4.6: Effective local exponent of probes mean square displacement, $\alpha(\tau) = \dfrac{d\log < \langle \delta r^2(\tau) \rangle >}{d\log\tau}$

Local scaling exponent of nanoprobe mean-square displacement is a direct and intuitive quantity to highlight possible deviations from normal Brownian diffusion. It is defined as the slope of $log(\delta r^2(\tau))$ versus $log(\tau)$. It is linked to the degree of coupling of probe particles to the dynamics of entangled solutions at $\tau > \tau_e$.

The value of α is of biological interest as well. It has been suggested that transport by subdiffusive mechanisms may provide advantages to the cell as a means to increase the encounter probability between intracellular species and various targets [98]. A subdiffusive particle becomes somewhat localized in its position during the subdiffusive time period resulting in an increased likelihood of contact with a binding partner albeit at a slower association rate.

This subdiffusive behavior is well known in the physics of random systems. It arises when a particle interacts with the random medium in which it is moving. Whereas a particle moving in a uniform medium, whatever the viscosity, regularly makes small jumps due to thermal energy, some types of random media can trap the particle in one location for varying and widely distributed periods, allowing only infrequent "jumps" between locations and leading to the observed subdiffusion on the relevant time-scale interaction [108, 109].

Let us now focus on how α behaves in time, see Fig. 4.6. Again, we may appreciate the profound interplay between the density of the solution and the size of the nanoprobe. At the lowest densities, the time dependence of α for all probe diameters in both topologies is almost identical suggesting that probes diffusion is not much coupled to the motion of polymers. As the density increases and the diameter of the NP becomes larger than the mesh size of the solution, curves describing probes motion in ring and linear polymer solution start to separate from each other already at early times .

4.3.3 Distribution of Mean-Square Displacement

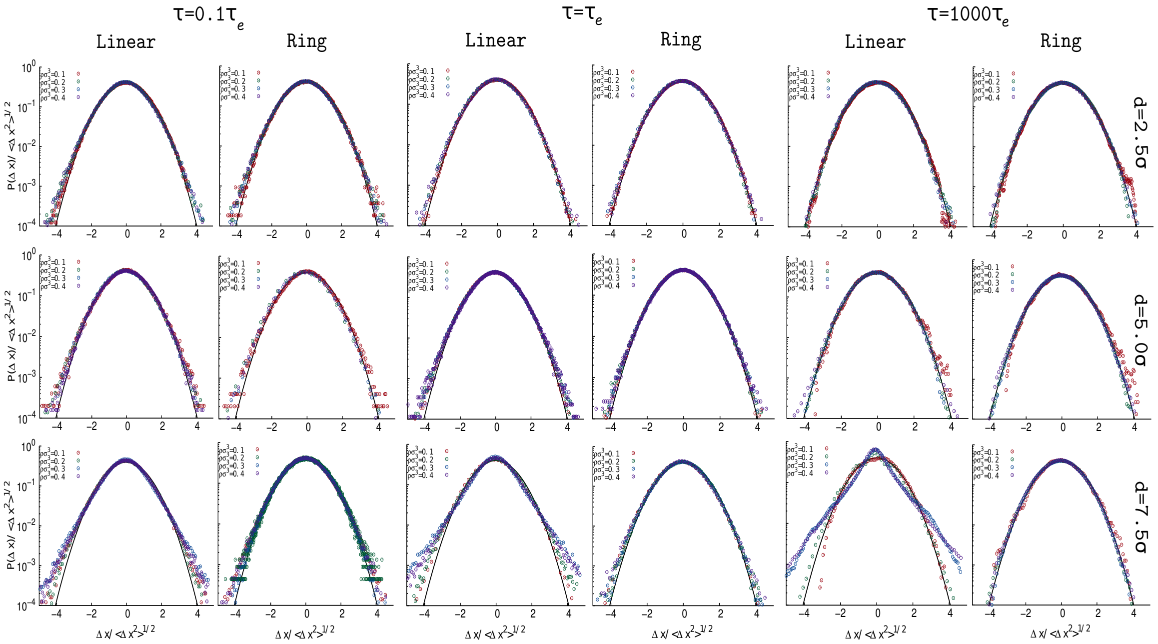

Figure 4.7: Log-linear plots of probability distribution functions of 1d displacements of probes at selected lag-times τ for $N = 250$. The black solid line corresponds to the Gaussian distribution.

In order to explore and characterize further the phenomenology of probes diffusion, we examine the complete distribution functions $P(\tau; \Delta x) \equiv \langle \delta(\Delta x - |x(t+\tau) - x(t)|) \rangle$ of *one-dimensional* displacements Δx at a given lag-time τ. It measures the probability that a probe reaches the spatial position $x(t+\tau)$ from $x(t)$ after time τ. While $\delta r^2(\tau)$ corresponds simply to the second moment of $P(\tau; \Delta x)$ along the three spatial directions, the full knowledge of $P(\tau; \Delta x)$ provides a deeper understanding of the whole diffusion process.

Results for the three representative lag-times $\tau/\tau_e = 10^{-1}, 10^0, 10^3$ are illustrated in Fig. 4.7 and Fig. 4.8. To facilitate comparisons with the Gaussian distribution, we scaled both vertical and horizontal axes by the average square-root of the corresponding second moment $\sqrt{\langle \Delta x^2(\tau) \rangle}$. By calculating the distribution of displacements of particles over various lag times τ, we obtained both the spatial and temporal characterization of probes thermal fluctuations.

For $d = 2.5\sigma$ and $d = 5.0\sigma$, the different $P(\tau; \Delta x)$ collapse onto the universal Gaussian curve. Also, the mean-square displacement(MSD) for all trajectories of this NP size was scaling linearly with time down to the smallest measured lag-time (See Fig. 4.4). For $d = 7.5\sigma$ at $\tau = 0.1\tau_e$, NPs in solutions of linear chains display little but clear deviations from the Gaussian curve . Instead, ring polymers at $\tau = 0.1\tau_e$ are Gaussian. For $d = 7.5\sigma$ at $\tau = \tau_e$, distinctive differences between solutions of polymers with the two architectures start to emerge (See Fig. 4.7 and Fig. 4.8, middle panels). For these large NPs, the greater heterogeneity suggested by the broader distribution displacements could reflect local obstacle constraints of the solutions of linear polymers. Finally, for largest NP size and the longest considered lag-time, $\tau = 1000\tau_e$, all curves are Gaussian except the two highest densities for linear chains. The distribution show that a nontrivial fraction of particles do move small distances.

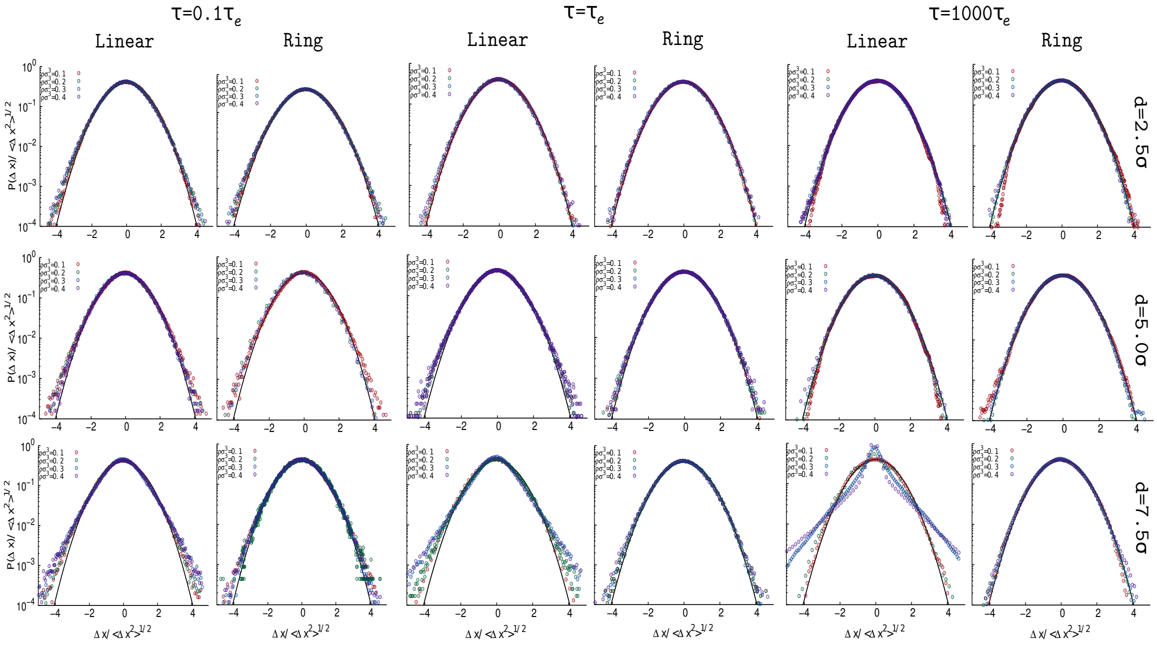

Figure 4.8: Log-linear plots of probability distribution functions of $1d$ displacements of probes at selected lag-times τ for $N = 500$. The black solid line corresponds to the Gaussian distribution.

4.4 Conclusions

In this chapter, the motion of nanoparticles (NPs) in entangled solutions of linear polymers and nonconcatenated ring polymers at different solution densities are compared by large-scale molecular dynamics simulations. The comparison provides a criterion for the effects of polymer architecture on the dynamical coupling between NPs and polymers in nanocomposites.

Our simulations show that the motion of NPs can be strongly suppressed prior to Fickian diffusion in entangled linear polymers. Such a strong suppression occurs progressively as the NP diameter d becomes increasingly larger than the entanglement spacing or the tube diameter of the solutions d_T. The motion of NPs with $d > d_T$ in entangled nonconcatenated ring polymers is not strongly suppressed as in entangled linear polymers. The decrease of diffusion coefficient D with increasing d in entangled rings is more gradual compared to the steep reduction of D in entangled linear chains as d exceeds d_T as it shown in Fig. 4.5.

The remarkable difference between probes diffusion in solutions of linear chains and rings has been ascribed to the fact that large probes in solutions of linear polymers remain temporarily caged (as we have qualitatively observed in Fig. 4.7 and Fig. 4.8) and tend to make “jumps” between cages, while in solutions of ring polymers their motion is not caged but instead coupled to the space-filling, fractal nature of ring polymers conformations.

Chapter 5

Summary

This Thesis is primarily focused on characterizing the local structure and dynamics of ring polymers through molecular dynamics computer simulations using a coarse-grained bead-spring model. Depending on the architecture, polymers (linear and circular chains) are observed to show different rheological and dynamical properties. The aim here was to acquire a better understanding of how architecture affects polymer behaviors in concentrated solutions. We consider linear and ring polymers at different solution densities. The number of monomers per polymer ranges from 250 to 1000 or $5L_e$ to $100L_e$.

Bearing in mind the results of this work, one could say that linking the two open ends of a linear chain has extremely significant effects on both polymers statics and dynamics.

In the next paragraphs, a short description will be given of the problems addressed together with the most important conclusions of the work.

A diverse set of approaches are used to study different properties of ring polymers.

1. Starting from Chapter. 2, we present our major remarks relevant to the structural properties of linear and circular (ring) polymer chains in entangled solutions. In linear polymers, the screening of excluded volume effects leads them to be quasi-ideal at all the considered densities, whereas ring polymers turn into more compact objects as the density of the solutions increases. These differences provoked us to compare the full chain statistics obtained from the distribution function $p(R|l)$ of spatial distances along the chains: For linear chains at high densities and large l's, the chain statistics is almost Gaussian. On the other side, chain compression in ring polymers causes non-ideal behavior.

We next tracked the probability of contacts between monomers at separation length l along the polymers. Its estimation is a key step to elucidate the spatial organization of polymers in concentrated solutions. For both the linear and ring polymers, contacts in the polymers (pairs of monomers located adjacent to each other) increases as a function of density ρ but governing different scaling laws.

2. After investigating the effect of density on ring polymers conformations, we discussed the notion of a topologically driven glass in ring polymers in Chapter. 3.

To better understand the role of topological constraints for melts of rings, in Chapter. 3, we systematically probed the response of solutions of rings at various densities to "random pinning" perturbations.

One of the most important and remarkable results of this Chapter was that the number of "threadings" or inter-chain interactions extensively grow with the density of the solutions. Correspondingly, these threadings cause dramatic slowing down in rings diffusivities.

We observed that denser solutions are counter-intuitively more susceptible to the perturbation, and that the critical pinning fraction $f_p^{\dagger}$ (for which every single unfrozen ring polymer is permanently trapped.) significantly decrease with increasing ρ.

Deducing this result, it was found that spontaneous vitrification can arise at a certain, large chain length even at a constant solution density. This result, which advocates a progressively larger effect due to the topological constraints (threadings) upon increasing the chain length, attains even though the increase in the chain length leads to a more compact chain conformation.

Next, we claimed that the non-Gaussian behavior reported in the distribution of displacements is clearly triggered by pinning perturbations, arguably via threading topological constraints. Furthermore, we conjecture that threading configurations, may also account for the spontaneous caging observed in unperturbed solutions at large ρ's.

Lastly, we reported the first evidence of ergodicity breaking in perturbed ($f_p > 0$) solutions of rings and non-trivial convergence towards ergodicity together with spontaneous caging. Further, we addressed that consequent to random pinning, rings go to cluster into components with slow/fast diffusivities corresponding to more/less persistent overlaps, with other slow or pinned rings. These results can be rationalized by arguing that threadings may act as transient cages which are then quenched by the random pinning protocol.

3. Chapter 4 focused on the dynamics of colloidal nanoparticles in a matrix of concentrated solutions of linear and ring polymers.

Our simulations show that the motion of nanoparticles can be vigorously slowed down prior to Fickian diffusion in entangled solutions of linear polymers.

The significant difference between NPs motion in solutions of linear chains and ring polymers can be attributed to the fact that large NPs ($d > d_T$) in solutions of linear polymers become temporarily caged and make “jumps” between cages, whereas in solutions of ring polymers their diffusion is not caged but rather coupled to the space-filling conformations of ring polymers.

Appendix A

Additional Information

List of Symbols

a	Monomeric link length
d_T	Tube diameter
ϵ	Energy scale
η	Viscosity
f_p	Pinning fraction
g	Number of correlations per blob
γ	Contact exponent
Γ	Damping constant
k	Boltzmann constant
k_θ	Bending constant
L	Contour length
L_e	Entanglement length
l_K	Kuhn length
l_p	Persistence length
m	Mass
N	Degree of polymerization
N_g	Contour length at spontaneous glassiness
N_K	Number of Kuhn segments of a polymer
r_c	Cutoff distance
ρ	Monomer density
ρ_g	Monomer density at spontaneous glassiness
ρ^*	Overlap monomer density
R_{ee}	End-to-end distance of a polymer
R_F	Flory radius
R_g	Gyration radius
s	Subchain length
σ	Length scale
T	Temperature
τ_{LJ}	Lennard-Jones time
v	Excluded volume
ν	Flory exponent
ξ	Correlation length

Bibliography

[1] M. Kapnistos, M. Lang, D. Vlassopoulos, W. Pyckhout-Hintzen, D. Richter, D. Cho, T. Chang, and M. Rubinstein. Unexpected power-law stress relaxation of entangled ring polymers. *Nature Materials*, 7:997, 2008.

[2] M. Doi and S. F. Edwards. *The Theory of Polymer Dynamics*. Oxford University Press, New York, 1986.

[3] D. Michieletto and M. S.Turner. A topologically driven glass in ring polymers. *Proc. Natl. Acad. Sci. USA*, 113:5195–5200, 2016.

[4] J. D.Halverson, W. B.Lee, G. S.Grest, A. Y.Grosberg, and K. Kremer. Molecular dynamics simulation study of nonconcatenated ring polymers in a melt: II. Dynamics. *J. Chem. Phys.*, 134:204905, 2011.

[5] A R.Brás et al. Compact structure and non-Gaussian dynamics of ring polymer melts. *Soft Matter*, 10:3649–3655, 2014.

[6] A. Y.Grosberg. Annealed lattice animal model and flory theory for the melt of non-concatenated rings: towards the physics of crumpling. 10:560–565, 2014.

[7] R. Metzler et al. Protein Anomalous diffusion models and their properties: non-stationarity, non-ergodicity, and ageing at the centenary of single particle tracking. *Phys. Chem. Chem. Phys.*, 16:24128–24164, 2014.

[8] Li. H.Cai, S. Panyukov and M. Rubinstein. Hopping diffusion of nanoparticles in polymer matrices. *Macromolecules*, 48(3):847–862, 2015.

[9] R. D.Kamien. The geometry of soft materials: a primer. 74:953–971, September 2002.

[10] V. Vitelli and W. Irvine. The geometry and topology of soft materials. *Soft Matter*, 9:8086–8087, 2013.

[11] K. Kremer and G. S. Grest. Dynamics of entangled linear polymer melts: A molecular-dynamics simulation. *J. Chem. Phys.*, 92:5057–5086, 1990.

[12] M. Rubinstein and R. H. Colby. *Polymer Physics*. Oxford University Press, New York, 2003.

[13] R. Pasquino, T. C. Vasilakopoulos, Y. C.Jeong, H. Lee, S. Rogers, G. Sakellariou, J. Allgaier, A. Takano, A. R. Brás, T. Chang, S. Gooßen, W. Pyckhout-Hintzen, A. Wischnewski, N. Hadjichristidis, D. Richter, M. Rubinstein and D. Vlassopoulos. Viscosity of ring polymer melts. *ACS Macro Letters*, 2(10):874–878, 2013.

[14] D. Kawaguchi, Y. Ohta, A. Takano and Y. Matsushita. Temperature and molecular weight dependence of mutual diffusion coefficient of cyclic polystyrene/cyclic deuterated polystyrene bilayer films. *Macromolecules*, 45(16):6748–6752, 2012.

[15] S. Gooßen, A. R. Brás, M. Krutyeva, M. Sharp, P. Falus, A. Feoktystov, U. Gasser, W. Pyckhout-Hintzen, A. Wischnewski, and D. Richter. Molecular scale dynamics of large ring polymers. *Phys. Rev. Lett.*, 113:168302, Oct 2014.

[16] L. A.Mirny. The Fractal Globule As a Model of Chromatin Architecture in The Cell. 19:37–51, 2011.

[17] A. Yu.Grosberg. How two meters of DNA fit into a cell nucleus: Polymer models with topological constraints and experimental data. *Polym. Sci. Ser. C*, 54:1–10, 2012.

[18] P.-G. De Gennes. *Scaling Concepts in Polymer Physics*. Cornell University Press, Ithaca, 1979.

[19] D. Boal. *Mechanics of the Cell*. Cambridge University Press, 2002.

[20] T. McLeish. Polymers without beginning or end. *Science*, 297(5589):2005–2006, 2002.

[21] J. D.Halverson, W. B.Lee, G. S.Grest, A. Y.Grosberg, and K. Kremer. Molecular dynamics simulation study of nonconcatenated ring polymers in a melt: I. Statics. *J. Chem. Phys.*, 134:204904, 2011.

[22] J. D.Halverson, J. Smrek, K. Kremer and A. Y.Grosberg. From a melt of rings to chromosome territories: the role of topological constraints in genome folding. *Reports on Progress in Physics*, 77(2):022601, 2014.

[23] T. Vettorel, A. Y.Grosberg, and K. Kremer. Statistics of polymer rings in the melt: a numerical simulation study. *Phys. Biol.*, 6:025013, 2009.

[24] A. Rosa and R. Everaers. Ring polymers in the melt state: the physics of crumpling. *Phys. Rev. Lett.*, 112:118302, 2014.

[25] A.M. Gutin and A. Y.Grosberg. Polymers with Annealed and Quenched Branchings Belong to Different Universality Classes. 26:1293–1295, 1993.

[26] S. Havlin A. Y.Grosberg, Y. Rabin and A. Neer. Crumpled Globule Model of the Three-Dimensional Structure of DNA. 23:373–378, 1993.

[27] A. Y.Grosberg J. D.Halverson, K. Kremer. Comparing The Results of Lattice and Off-Lattice Simulations For The Melt of Nonconcatenated Rings. 46:065002, 2013.

[28] E. Lieberman-Aiden et al. Comprehensive mapping of long-range interactions reveals folding principles of the human genome. *Science*, 326:289–293, 2009.

[29] E. I.Shakhnovich A. Y.Grosberg, S. K.Nechaev. The Role of Topological Constraints in the Kinetics of Collapse of Macromolecules. 49:2095–2100, 1988.

[30] M. E.Cates and J. M.Deutsch. Conjectures on the statistics of ring polymers. *J. Physique*, 47(12):2121–2128, 1986.

[31] M. Rubinstein. Dynamics of ring polymers in the presence of fixed obstacles. 57:3023–3026, 1986.

[32] J. Klein. Dynamics of entangled linear, branched, and cyclic polmyers. *Macromolecules*, 118:105–118, 1986.

[33] P.-G. De Gennes. Reptation of a polymer chain in the presence of fixed obstacles. *J. Chem. Phys.*, 55:572–579, 1971.

[34] S. P.Obukhov, M. Rubinstein, and T. Duke. Dynamics of a ring polymer in a gel. *Phys. Rev. Lett.*, 73:1263–1266, 1994.

[35] V. S.Iyer and A. Gaurav. Lattice animal model of chromosome organization. *Phys. Rev. E*, 86:011911, Jul 2012.

[36] J. Smrek and A. Y.Grosberg. Understanding the dynamics of rings in the melt in terms of annealed tree model. 27:064117, 2015.

[37] S. T.Milner and J. D.Newhall. Stress relaxation in entangled melts of unlinked ring polymers. 105:208302, 2010.

[38] R. Pasquino, T. C.Vasilakopoulos, Y. C.Jeong, H. Lee, S. Rogers, G. Sakellariou, J. Allgaier, A. Takano, A R. Brás, T. Chang, S. Gooßen, W. Pyckhout-Hintzen, A. Wischnewski, N. Hadjichristidis, D. Richter, M. Rubinstein, and D. Vlassopoulos. Viscosity of ring polymer melts. *ACS Macro Letters*, 2(10):874–878, 2013.

[39] D. Michieletto, D. Marenduzzo, E. Orlandini, G. P.Alexander and M. S.Turner. Threading dynamics of ring polymers in a gel. *ACS Macro Letters*, 3(3):255–259, 2014.

[40] D. Michieletto, D. Marenduzzo, E. Orlandini, G. P.Alexander and Matthew S. Turner. Dynamics of self-threading ring polymers in a gel. *Soft Matter*, 10:5936–5944, 2014.

[41] E. Lee, S. Kim and Y. Jung. Slowing down of ring polymer diffusion caused by inter-ring threading. *Macromolecular Rapid Communications*, 36(11):1115–1121, 2015.

[42] B. J.Alder and T. E.Wainwright. Studies in Molecular Dynamics I: General Method. *Journal of Chemical Physics*, 31:459–466, 1959.

[43] B. J.Alder and T. E.Wainwright. Phase Transition for a Hard Sphere System. *J. Chem. Phys.*, 27:1208–1209, 1957.

[44] A. Rahman. Correlations in The Motions of Atoms in Liquid Argon. 136A:405–411, 1959.

[45] S. Plimpton. Fast parallel algorithms for short range molecular dynamics. *J. Comp. Phys.*, 117:1–19, 1995.

[46] R. Auhl, R. Everaers, G. S. Grest, K. Kremer and S. J.Plimpton. Equilibration of long chain polymer melts in computer simulations. *J. Chem. Phys.*, 119:12718–12728, 2003.

[47] P. J.Flory. *Statistical Mechanics of Chain Molecules.* Interscience, New York, 1969.

[48] M. Müller, J. P. Wittmer, and M. E. Cates. Topological effects in ring polymers: A computer simulation study. *Phys. Rev. E*, 53:5063–5074, 1996.

[49] M. Müller, J. P. Wittmer, and M. E. Cates. Topological effects in ring polymers. II. influence of persistence length. *Phys. Rev. E*, 61:4078–4089, 2000.

[50] J. Suzuki, A. Takano, T. Deguchi, and Y. Matsushita. Dimension of ring polymers in bulk studied by Monte-Carlo simulation and self-consistent theory. *J. Chem. Phys.*, 131:144902, 2009.

[51] J. D.Halverson, G. S.Grest, A. Y.Grosberg and K. Kremer. Rheology of ring polymer melts: From linear contaminants to ring-linear blends. *Phys. Rev. Lett.*, 108:038301, 2012.

[52] T. Ge, S. Panyukov and M. Rubinstein. Self-similar conformations and dynamics in entangled melts and solutions of nonconcatenated ring polymers. *Macromolecules*, 49(2):708–722, 2016.

[53] N. Uchida, G. S.Grest, and R. Everaers. Viscoelasticity and primitive-path analysis of entangled polymer liquids: from f-actin to polyethilene. *J. Chem. Phys.*, 128:044902, 2008.

[54] N. B., A. Rosa, and R. Everaers. The radial distribution function of worm-like chains. *Eur. Phys. J. E*, 32:53–69, 2010.

[55] S. Redner. Distribution functions in the interior of polymer chains. *J. Phys. A: Math. Gen.*, 13:3525–3541, 1980.

[56] J. des.Cloizeaux and G. Jannink. *Polymers in Solution.* Oxford University Press, Oxford, 1989.

[57] R. Everaers, I. S.Graham, and M. J.Zuckermann. -to-end distance distributions and asymptotic-behavior of self-avoiding walks in 2 and 3 dimensions. *J. Phys. A: Math. Gen.*, 28:1271–1288, 1995.

[58] A. Rosa et al. Conformations of randomly branching polymers with volume interactions. *In preparation*, 2015.

[59] M. E.Fisher. Shape of a self-avoiding walk or polymer chain. *J. Chem. Phys.*, 44:616–622, 1966.

[60] P. Pincus. Excluded volume effects and stretched polymer chains. *Macromolecules*, 9:386–388, 1976.

[61] H. Yamakawa. *Modern theory of polymer solutions*. Harper's chemistry series. Harper & Row, 1971.

[62] F. T.Wall and J. J.Erpenbeck. New method for the statistical computation of polymer dimensions. *J. Chem. Phys.*, 30:634–637, 1959.

[63] P. Debye and F. Bueche. Distribution of segments in a coiling polymer molecule. *J. Chem. Phys.*, 20(8):1337–1338, 1952.

[64] J. A. Thomson C. N. Pace, G. R. Grimsley and B. J. Barnett. Conformational stability and activity of ribonuclease ti with zero, one, and two intact disulfide bonds. *J. Biol. chem.*, 263:11820, 1988.

[65] A. D.Nagi and L. Regan. An inverse correlation between loop length and stability in a four-helix-bundle protein. *Folding and Design*, 2(1):67 – 75, 1997.

[66] R Schleif. Dna looping. *Science*, 240(4849):127–128, 1988.

[67] K. B.Towles, J. F.Beausang, H. G.Garcia, R. Phillips and P. C. Nelson. First-principles calculation of dna looping in tethered particle experiments. *Physical Biology*, 6(2):025001, 2009.

[68] M. Baiesi, E. Carlon, E. Orlandini and A. L.Stella. A simple model of dna denaturation and mutually avoiding walks statistics. *Eur. Phys. J. B*, 29(1):129–134, 2002.

[69] A. Y.Grosberg. Annealed lattice animal model and flory theory for the melt of non-concatenated rings: towards the physics of crumpling. *Soft Matter*, 10:560–565, 2014.

[70] N. Nahali and A. Rosa. Density effects in entangled solutions of linear and ring polymers. *J. Phys.-Condens. Matter*, 28(6):065101, 2016.

[71] J. Smrek and A. Y.Grosberg. Minimal surfaces on unconcatenated polymer rings in melt. *ACS Macro Letters*, 5(6):750–754, 2016.

[72] T. Ge, S. Panyukov and M. Rubinstein. Self-similar conformations and dynamics in entangled melts and solutions of nonconcatenated ring polymers. *Macromolecules*, 49(2):708–722, 2016.

[73] D. Michieletto. On the tree-like structure of rings in dense solutions. *Soft Matter*, 12:9485–9500, 2016.

[74] W. Kob and L. Berthier. Probing a liquid to glass transition in equilibrium. *Phys. Rev. Lett.*, 110:245702, Jun 2013.

[75] C. Cammarota and G. Biroli. Ideal glass transitions by random pinning. *Proceedings of the National Academy of Sciences*, 109(23):8850–8855, 2012.

[76] D. G.Tsalikis and V. G.Mavrantzas. Threading of ring poly(ethylene oxide) molecules by linear chains in the melt. *ACS Macro Letters*, 3(8):763–766, 2014.

[77] W. Kob et al. Dynamical Heterogeneities in a Supercooled Lennard-Jones Liquid. *Phys. Rev. Lett.*, 79(15):2827–2830, 1997.

[78] P. Chaudhuri, L. Berthier and W. Kob. Universal nature of particle displacements close to glass and jamming transitions. *Phys. Rev. Lett.*, 99:060604, Aug 2007.

[79] W. Deng and E. Barkai. Ergodic properties of fractional brownian-langevin motion. *Phys. Rev. E*, 79:011112, Jan 2009.

[80] www.wolfram.com/mathematica/.

[81] H. A.Bethe. Statistical theory of superlattices. *Proceedings of the Royal Society of London A: Mathematical, Physical and Engineering Sciences*, 150(871):552–575, 1935.

[82] Z. Q.Zhang, T. C.Li and F. C.Pu. Percolation on a bethe lattice with multineighbour bonds-exact results. *Journal of Physics A: Mathematical and General*, 16(10):2267, 1983.

[83] T. G.Mason and D. A.Weitz. Optical measurements of frequency-dependent linear viscoelastic moduli of complex fluids. *Phys. Rev. Lett.*, 74:1250–1253, Feb 1995.

[84] T. G.Mason. Estimating the viscoelastic moduli of complex fluids using the generalized stokes–einstein equation. *Rheol. Acta*, 39(4):371–378, 2000.

[85] Y. Tseng, T. P.Kole, and D. Wirtz. Micromechanical mapping of live cells by multiple-particle-tracking microrheology. *Biophys J*, 83(6):3162–3176, 12 2002.

[86] D. Wirtz. Particle-tracking microrheology of living cells: Principles and applications. *Annu. Rev. Biophys.*, 38:301–326, 2009.

[87] M. Valet and A. Rosa. Viscoelasticity of model interphase chromosomes. *J. Chem. Phys.*, 141(24):245101, 2014.

[88] R. A.Riggleman, G. Toepperwein, G. J.Papakonstantopoulos, J.-L.Barrat, and J. J. de Pablo. Entanglement network in nanoparticle reinforced polymers. *J. Chem. Phys.*, 130(24):244903, 2009.

[89] L. Cai, S. Panyukov and M. Rubinstein. Mobility of nonsticky nanoparticles in polymer liquids. *Macromolecules*, 44(19):7853–7863, 2011.

[90] T. Ge, J. T.Kalathi, J. D.Halverson, G. S.Grest and M. Rubinstein. Nanoparticle motion in entangled melts of linear and nonconcatenated ring polymers. *Macromolecules*, 50(4):1749–1754, 2017.

[91] C. A.Grabowski and A. Mukhopadhyay. Size effect of nanoparticle diffusion in a polymer melt. *Macromolecules*, 47:7238–7242, 2014.

[92] U. Yamamoto and K. S.Schweizer. Theory of nanoparticle diffusion in unentangled and entangled polymer melts. *J. Chem. Phys.*, 135:224902, 2011.

[93] U. Yamamoto and K. S.Schweizer. Microscopic theory of the long-time diffusivity and intermediate-time anomalous transport of a nanoparticle in polymer melts. *Macromolecules*, 48:152–163, 2015.

[94] F. Brochard Wyart and Pierre-Gilles de Gennes. Viscosity at small scales in polymer melts. *Eur. Phys. J. E: Soft Matter Biol. Phys.*, 1(4):93–97, 2000.

[95] G. H.Pollack and W. C.Chin. *Modern theory of polymer solutions.* Springer Netherlands, 2008.

[96] R. Poling-Skutvik, R. Krishnamoorti, and J. C.Conrad. Size-dependent dynamics of nanoparticles in unentangled polyelectrolyte solutions. *ACS Macro Letters*, 4(10):1169–1173, 2015.

[97] R. Everaers and M. R.Ejtehadi. Interaction potentials for soft and hard ellipsoids. *Phys. Rev. E*, 67:041710, 2003.

[98] I. Golding and Edward. C.Cox. Physical nature of bacterial cytoplasm. *Phys. Rev. Lett.*, 96:098102, Mar 2006.

[99] S. C.Lim and S. V.Muniandy. Self-similar gaussian processes for modeling anomalous diffusion. *Phys. Rev. E*, 66:021114, Aug 2002.

[100] C. R.Calladine, H. Drew, F. B.Luisi, and A. A.Travers. *Understanding DNA: The Molecule and how it Works.* Academic Press, Science, 1979.

[101] B. Alberts, A. Johnson, J. Lewis, M. Raff, K. Roberts and P. Walter. *Molecular Biology of the Cell, 4th edition.* New York:Garland Sience, 2002.

[102] A. Rosa and R. Everaers. *Structure and Dynamics of Interphase Chromosomes. PLOS Computational Biology*, 4:1–10, 2008.

[103] D. S.Pearson, G. Ver Strate, E. Von Meerwall and F. C.Schilling. *Viscosity and self-diffusion coefficient of linear polyethylene. Macromolecules*, 20:1133–1141, 1987.

[104] B. J.Hilley and M. F.Sykes. *Probability of initial ring closure in the restricted random-walk model of a macromolecule. J. Chem. Phys.*, 34:1531–1537, 1961.

[105] P. F.Holmes, M. Bohrer and J. Kohn. *Exploration of polymethacrylate structure-property correlations: Advances towards combinatorial and high-throughput methods for biomaterials discovery. Prog. Polym. Sci.*, 33:787–796, 2008.

[106] A. Friedman. *A statistical dynamic theory of glassy polymers.* Springer New York, NY, 1994.

[107] M. Pütz and K. Kremer and G. S.Grest. *Diffusion and fracton dimensionality on fractals and on percolation clusters. EPL (Europhysics Letters)*, 6:735–741, 2000.

[108] S. Havlin and D. Ben-Avraham. *What is the entanglement length in a polymer melt?. Journal of Physics A: Mathematical and General*, 16:L483–L487, 1983.

[109] R. Metzler and J. Klafter. *The random walk's guide to anomalous diffusion: a fractional dynamics approach. Physics Reports*, 339:1–77, 2000.

[110] J. H.Jeon and others. *Protein Crowding in Lipid Bilayers Gives Rise to Non-Gaussian Anomalous Lateral Diffusion of Phospholipids and Proteins. Phys. Rev. X*, 6:021006, 2016.